Transcriptional and post-transcriptional effects of lncRNA LINC00941 on human epidermal homeostasis

DISSERTATION

ZUR ERLANGUNG DES DOKTORGRADES DER NATURWISSENSCHAFTEN
(DR. RER. NAT.)

DER FAKULTÄT FÜR BIOLOGIE UND VORKLINISCHE MEDIZIN

DER UNIVERSITÄT REGENSBURG

vorgelegt von

Eva Morgenstern

aus

Rothenburg ob der Tauber

im Jahr

2023

Das Promotionsgesuch wurde eingereicht am:

28.09.2023

Die Arbeit wurde angeleitet von:

Prof. Dr. Markus Kretz

Unterschrift:

Publications and author contributions

Parts of this thesis derived from the following submitted manuscript:

Morgenstern, Eva; Schwartz, Uwe; Graf, Johannes; Bruckmann, Astrid; Kretz, Markus (2023): The long non-coding RNA LINC00941 modulates MTA2/NuRD occupancy to suppress premature human epidermal differentiation. *BioRxiv*. DOI: 10.1101/2023.07.25.549662.

The manuscript is currently under revision at *Review Commons* (09/2023).

Author contributions:

Johannes Graf and Astrid Bruckmann performed mass spectrometry experiments. Uwe Schwartz analyzed ChIP and RNA sequencing data. Eva Morgenstern contributed to mass spectrometry data analysis and sequencing data analysis, respectively. All other experiments and data analysis were carried out exclusively by Eva Morgenstern.

Table of Contents

1 Abstract

The epidermis is a stratified surface epithelium providing an effective barrier against environmental influences such as UV-radiation, pathogen invasion and mechanical injuries. To withstand these challenges and to maintain its functionality, respectively, the epidermis constantly renews itself. During this sophisticated process progenitor keratinocytes undergo a program of terminal differentiation resulting in flattened and annucleated cells that eventually shed from the epidermis.

As epidermal homeostasis is highly orchestrated in time and space, there is an extensive network of signaling pathways and transcriptional regulators controlling profound changes in gene expression. Furthermore, several long non-coding RNAs (lncRNAs) have been uncovered to be involved in this essential process but only few of them have been functionally characterized in human epidermal tissue. One of these lncRNAs was LINC00941 which was initially described as a negative regulator of keratinocyte differentiation, but this work sheds light on its mode of action on both transcriptional and post-transcriptional level.

We demonstrated that LINC00941 – a lncRNA with partial cytoplasmic localization – interacts with AGO2 as well as with miR-335-5p shown by Dual Luciferase Reporter assays. Correspondingly, a role of LINC00941 acting as a competitive endogenous RNA (ceRNA), which enables translation of miR-335-5p downstream mRNA targets, is suggested.

We also found that lncRNA LINC00941 regulates keratinocyte differentiation on an epigenetic level through interaction with the chromatin remodeler NuRD (Nucleosome Remodeling and Deacetylase). Chromatin immunoprecipitation (ChIP) sequencing of NuRD-associated MTA2 in LINC00941-deficient keratinocytes uncovered altered MTA2/NuRD occupancy at bivalent chromatin domains close to transcriptional regulators such as *EGR3*. EGR3 is a transcription factor that activates expression of early and late differentiation genes in human primary keratinocytes. Therefore, we could show that LINC00941/NuRD represses *EGR3* expression in non- and poorly differentiated keratinocytes preventing premature onset of differentiation in human epidermal tissue.

Additionally, LINC00941 associates with transcription factor E2F6 – a suppressor of keratinocyte differentiation – suggested to regulate similar target genes as NuRD.

This implies a pleotropic mechanism of LINC00941 regulating gene expression on a global level through various transcriptional regulators.

In conclusion, we conducted an in-depth characterization of LINC00941-mediated modes of action. First results have gained insights on its putative role as ceRNA in cytoplasm providing translational regulation. Furthermore, our studies on LINC00941 altering MTA2/NuRD chromatin binding behavior have revealed its impact as modulator of transcription. Additionally, we could show interaction between LINC00941 and E2F6, thus, further analysis of LINC00941-dependent E2F6 activity might provide insights on another mechanism of LINC00941 regulating human epidermal homeostasis.

List of abbreviations

3C	chromosome conformation capture
A	absorption
A	active
A/A	antibiotic/antimycotic
AEBSF	4-(2-aminoethyl) benzenesulfonyl fluoride hydrochloride
Amp	ampicillin
APS	ammonium persulfate
ATP	adenosine triphosphate
BCS	bovine calf serum
Biv	bivalent
bp	base pair
BRIO	BEAM RNA interaction motifs
BSA	bovine serum albumin
c	centi
cal	calorie
CC	colon cancer
cDNA	complementary DNA
CE	cornified envelope
ceRNA	competitive endogenous RNA
ChIP	chromatin immunoprecipitation
ChIRP	chromatin isolation by RNA purification
chr	chromosome
CLIP	crosslinking immunoprecipitation
cm	centimeter
CMV	cytomegalovirus
Co-IP	Co-immunoprecipitation
C_q	quantification of cycle
CRC	colorectal cancer
°C	degree Celsius
d; D	day
DAPI	4′,6-diamidino-2-phenylindole
DMEM	Dulbecco’s modified eagle medium
DMSO	dimethyl sulfoxide
DNA	deoxyribonucleic acid
dNTP	deoxy nucleoside triphosphate
DPBS	Dulbecco’s phosphate-buffered saline
ds	double stranded
DTT	dithiothreitol
dTTP	deoxythymidine triphosphate

EDC	1-ethyl-3-(3-dimethyl aminopropyl)carbodiimide
EDC	epidermal differentiation complex
EDTA	ethylenediamine-tetraacetic acid
EF	endotoxin-free
EGF	epidermal growth factor
emPAI	exponentially modified protein abundance
ENCODE	encyclopedia of DNA elements
ENCORI	encyclopedia of RNA interactomes
Enh	enhancer
ESCC	esophageal squamous cell carcinoma
ESC/E(Z)	extra sex combs/ enhancer of zeste
et al.	et alia
etc.	et cetera
FBS	fetal bovine serum
FDR	false discovery rate
Flnk	flanking
g	gram
G	genic
GEO	Gene Expression Omnibus
GFP	green fluorescent protein
GO	gene ontology
goi	gene of interest
h	hour
HCl	hydrochloride
HE	hematoxylin and eosin
HEK	human embryonic kidney
HeLa	Henrietta Lacks
HF	high fidelity
HITSCLIP	high-throughput sequencing CLIP
HKGS	human keratinocyte growth supplement
IF	immunofluorescence
IGV	Integrative Genomics Viewer
IP	Immunoprecipitation
k	kilo
KGM	keratinocyte growth medium
l	liter
LB	Luria-Bertani
LCE	late cornified envelope
IgG	Immunoglobulin G
LINC	long intergenic non-coding
lncRNA	long non-coding RNA

µ	micro
m	meter
m	milli
M	molar
Mb	megabase
MBD	methylated CpG-binding domain
min	minute
miRNA	micro RNA
MOPS	3-morpholinopropane-1-sulfonic acid
mRNA	messenger RNA
MS	mass spectrometry
MTA	metastasis-associated
MUT	mutated
n	nano
n	number (of samples)
NB	northern blot
ncRNA	non-coding RNA
NHEK	normal human epidermal keratinocytes
ns	not significant
nt	nucleotide
NuRD	nucleosome remodeling and deacetylase
NuRF	nucleosome remodeling factor
OD	optical density
ORF	open reading frame
OSCC	oral squamous cell carcinoma
PAGE	polyacrylamide gel electrophoresis
PARCLIP	photoactivable-ribonucleoside-enhanced CLIP
%	percent
PBS	phosphate-buffered saline
PC	pancreatic cancer
PC	polycomb
PCA	principal component analysis
PcG	Polycomb group
PCR	polymerase chain reaction
PDAC	pancreatic ductal adenocarcinoma
PFA	para-formaldehyde
pH	power of hydrogen
PRC	polycomb repressive complex
qRT-PCR	quantitative reverse transcription PCR
Quies	quiescent

rcf	relative centrifugal force
RIPA	radioimmunoprecipitation assay
RNA	ribonucleic acid
rpm	rounds per minute
Rpts	repeats
RT	room temperature
s	second
SDS	sodium-dodecyl-sulfate
Seq	sequencing
SFM	serum-free medium
SFTP	S100-fused type protein
siRNA	silencing RNA
sncRNA	short non-coding RNA
SSC	saline-sodium-citrate
SPRR	small proline-rich proteins
TA	transit amplifying
TAE	tris acetate EDTA
TBE	tris borate EDTA
TBS-T	tris-buffered saline with Tween 20
TE	tris EDTA
TEMED	tetramethylethylene-diamine
TG	transglutaminase
TGS	tris-glycine-SDS
T_M	melting temperature
TPM	transcript per million
Tris	tris(hydroxymethyl)amino-methane
TrxG	trithorax group
Tx	transcription
TSS; Tss	transcription start site
U	unit
UTR	untranslated region
UV	ultraviolet
v	version
V	volt
v/v	volume by volume
WB	western blot
Wk	weak
WT	wild-type
w/v	weight by volume

2 Introduction

2.1 The human skin

The human skin is essential for survival since it provides an effective barrier against environmental influences. This complex stratified organ protects the body against microbial infections, temperature extremes, radiations, injuries and other external mechanical as well as chemical hazards[1]. It also separates us from the outside world to prevent dehydration and to contribute to thermal regulation[2]. In order to accomplish these tasks, the body exerts a great effort: Adult human skin is the largest organ in terms of weight and surface area accounting up to 20% of the total body weight and approximately 2 m^2, respectively[1]. However, the basis for the skin's ability to reliably fulfill its role as a barrier lies in its sophisticated structure consisting of three layers: Hypodermis, dermis, and epidermis (Figure 1A)[3]. The innermost hypodermis mainly consists of fat tissue and therefore meets its task as thermal insulation. The dermis located above serves as a connective tissue consisting of a dense fibrous network produced by fibroblasts[1]. Furthermore, the dermis also harbors sensory receptors and blood vessels for supply of oxygen, nutrients, and immune cells important for the skin[4]. The outermost layer is the epidermis and its associated appendages including hair follicles and sweat glands[5]. Due to its exposed position, the epidermis represents the body's first and most important line of defense against the environment. Therefore, it performs all the duties of a physical, biochemical and immunological barrier simultaneously[6]. A highly specialized dermal matrix, the basement membrane, physically separates dermis and epidermis providing both a stabilizing and dynamic interface between these two skin compartments[7].

2.1.1 General architecture and regeneration of the human epidermis

The epidermis – a stratified surface epithelium – mainly consists of keratinocytes (90-95% of all epidermal cells) but other cell types which are important for a functional barrier are interspersed. These include neuroendocrine Merkel cells, pigment-producing melanocytes providing protection against UV-radiation and Langerhans cells aiding the immunological barrier of the epidermis[8,9]. Since keratinocytes occur in different stages of differentiation, the epidermis itself can be

further divided into four layers: The basal, spinous and granular layer as well as the outermost layer, the stratum corneum (Figure 1B)[10,11].

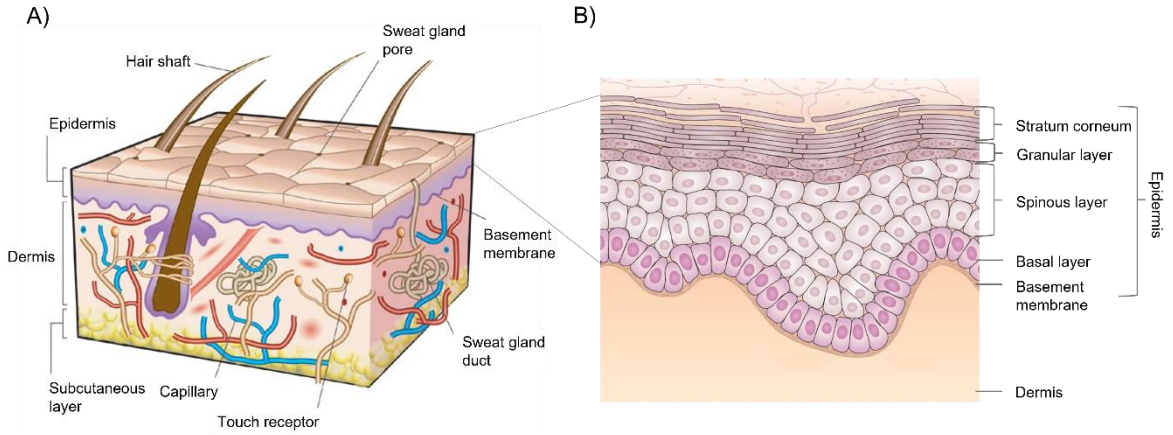

Figure 1: Schematic overview of human skin and epidermal layers.
(A) Cross section of the human skin illustrating the three layers: Hypodermis (here referred to as subcutaneous layer), dermis and epidermis. Furthermore, there are epidermal appendages extending into the dermis as well as touch receptors and blood vessels located in the dermis (modified after MacNeil)[3]. (B) Magnification of the epidermis showing the basal layer attached to the dermal basement membrane, spinous layer, granular layer, and stratum corneum (modified after Solanas and Benitah)[11].

Since the epidermis has to withstand the highest number of external influences and injuries, it must constantly renew itself to maintain a functional barrier. This occurs through the shedding of corneocytes – terminally differentiated keratinocytes of the stratum corneum – which are replaced by successive keratinocytes from below. The equilibrium (homeostasis) between new cells generated and cells lost at the surface is of great importance because excessive cell loss would cause ulceration while excessive cell division is a hallmark of cancer[12]. To ensure epidermal homeostasis, there is a sophisticated system of keratinocyte differentiation highly orchestrated in time and space. During this differentiation program undifferentiated keratinocytes of the basal layer detach and migrate to the skin surface. Leaving the basal layer, keratinocytes are no longer mitotically active. Instead, they undergo a program of terminal differentiation while they migrate through the spinous and granular layer. When the cells finally reach the stratum corneum they have undergone major structural and functional changes – including enucleation – to form an impenetrable barrier before they are shed[13]. This process of constant epidermal rejuvenation lasts 28 days on average. Over the last 60 years, there were three rival models proposing the underlying mechanism to ensure a precise balance between proliferating and differentiating keratinocytes in the basal layer as basis of epidermal homeostasis[14].

In the 1960s, it was stated that all keratinocytes of the basal layer were the same and there was a 50:50 chance of each cell to either divide or differentiate[12,15]. Later, another hypothesis – the “stem/transit amplifying (TA)” cell model was established. This model argued that a single, slow-cycling, and self-renewing stem cell can divide asymmetrically to produce both a stem cell and a TA cell. The TA daughter cell divides for a limited number of cell divisions until all its progeny finally differentiated[16]. However, as both models showed experimental and data inconsistencies, they are considered obsolete. Instead, lineage-tracing experiments led to the current hypothesis. It states that epidermal homeostasis is maintained by so-called progenitor cells. These specific cells generate other progenitors and differentiating daughter cells with equal probability. The progenitors itself are generated from rare, slow-cycling stem cells. Therefore, stem cells hardly contribute to epidermal homeostasis, but rather progenitor cells[12,17,18].

Epidermal homeostasis starts with undifferentiated keratinocytes of the basal layer characterized by the synthesis of keratin 5 and keratin 14. These main structural proteins form, along with microtubules and microfilaments, the cytoskeleton[13]. Keratinocyte differentiation program is then triggered by increasing calcium concentrations and signals form cell-cell contacts[19–21]. Consequently, keratinocytes from the basal layer migrate to the spinous layer, lose their mitotic ability but stay metabolic active, and synthesize new structural proteins. These proteins – mainly keratin 1 and keratin 10 – replace the pre-existing keratin 5 and keratin 14[13]. During keratinocyte differentiation, cells produce profilaggrin stored in keratohyalin granules. Profilaggrin is the precursor of filaggrin responsible for aggregation keratin filaments into tight bundles promoting the collapse of the cells into a flattened shape during terminal differentiation[22]. Furthermore, keratinocytes synthesize other structural proteins including involucrin, loricrin, trichohyalin, small proline-rich proteins (SPRRs) and late cornified envelope (LCE) proteins partially also stored in keratohyalin granules[10,23]. Upon increasing intracellular calcium levels, the granules release these structural proteins which are then covalently crosslinked by calcium-dependent transglutaminases (TGs) (TG1, TG3 and TG5) beneath the plasma membrane finally replacing it[21,24]. This insoluble rigid protein structure assembled by TGs is termed cornified envelope (CE)[10,13,25]. Beside keratohyalin granules, lamellar bodies are formed. These granules are enriched with glycosphingolipids,

free sterols, and phospholipids. During terminal differentiation, the lipids are secreted into the extracellular space, converted into glycerol, free fatty acids, ceramides and cholesterol which are then attached to proteins of the CE[26]. Consequentially, the outermost stratum corneum is formed of terminally differentiated, annucleated and flattened keratinocytes called corneocytes, surrounded by the CE and insoluble lipids creating a physical barrier. The cornified layer is further reinforced through corneodesmosomes – modified desmosomes – which tightly attach corneocytes to each other. However, this adhesive structure is proteolytically degraded in the outermost layer of the stratum corneum to allow desquamation, the final component to provide functional epidermal hoemsotasis[13,27]. Taken together, tightly connected, terminally differentiated keratinocytes are formed as a result of this complex process which provide an impermeable barrier against environmental challenges reinforced by the rigid protein shell and an extracellular lipid lammela[28].

2.1.2 The human epidermal differentiation complex

On chromosomes of mammalian genomes, coregulated genes are shown to be arranged in close proximity. Organizing functionally regulated genes within specific clusters enables coordinated gene regulation during cellular differentiation prcesses[29]. Many genes essential for late epidermal differentiation are consistently encoded within a region of 2 Mb on human chromosome 1q21[30–32]. This region called epidermal differentiation complex (EDC) comprises approximately 60 genes encoding for proteins mainly involved in proper CE formation indispensable for epidermal barrier formation[33]. Within the EDC, genes encoding for proteins with similar structure and functional properties are not randomly distributed but clustered together. Organizing related genes within the EDC indicates that these genes were formed by duplication of a common ancestor followed by divergence[34]. Associated genes are divided into three families that are closely clustered within the EDC: The cornified envelope precursors, the S100 and the S100-fused type proteins (SFTP) family (Figure 2)[33].

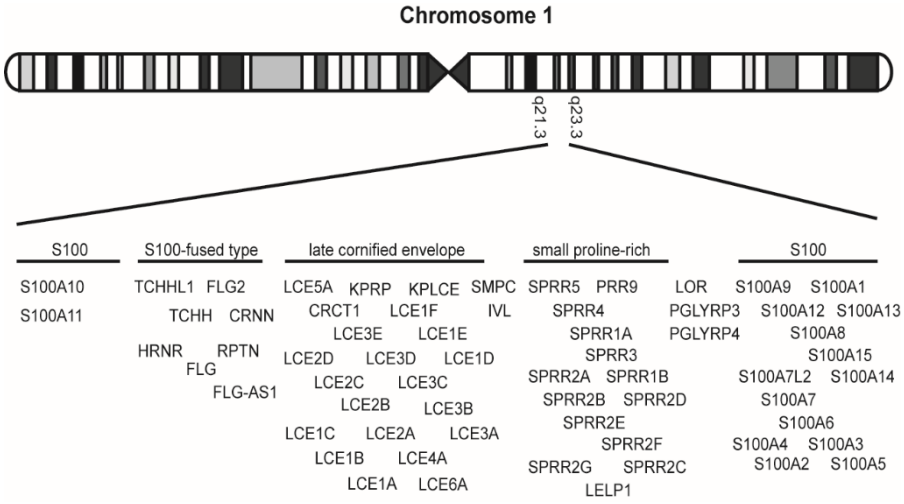

Figure 2: Schematic representation of human EDC genes on chromosome 1.
Cytogenic locations of chromosome 1 are indicated as well as the EDC locus. Its encoded genes are magnified according to the RefSeq release 2016 and subdivided into respective main gene clusters (modified after Kypriotou et al.)[35].

The family of cornified envelope precursors include other different sub-families such as the LCE and the SPRR proteins as well as involucrin and loricrin[35]. They show structural similarities, homologies in their glutamine- and lysine-rich terminal domains, as well as glutamine-, proline-, and serine-rich repeats in their internal repeats. During epidermal differentiation, the family members are expressed in the upper spinous as well as granular layer and are crosslinked by TGs to form the epidermal CE[28,35,36].

The S100 protein family includes several members of which most of them – 17 genes and 6 pseudogenes – are encoded on the EDC. While associated family members generally comprise of three exons, the first exon is not translated but only the second and third exon contain an open reading frame (ORF) coding for two calcium-binding EF-hands separated by a linker region[37]. The S100 family fulfills diverse functions in epidermal differentiation. Upon calcium-binding, they are thought to regulate the function and subcellular distribution of their target proteins. Further, they are involved in the formation of calcium-channels and they are known to be incorporated into the CE as they are substrates of TGs[38].

The SFTP family evolved by fusion of the two previously described families and comprises among others filaggrin, filaggrin-2, hornerin, repetin, trichohyalin as well as cornulin[32,33,39–43]. These proteins are major cytoplasmic matrix proteins instead

of predominant components of the CE[35]. Similar to S100 family members, they are composed of three exons, but the first exon is not translated. Instead, the second and third exon code among others for two calcium-binding EF-hand domains in the N-terminal region comparable to the S100 proteins[35].

Coordinate EDC gene expression during keratinocyte differentiation is a prerequisite for a functional epidermal barrier to emerge. This is why common regulatory elements controlling their transcription have been suggested. However, no local master regulator has been proven so far. Instead, EDC genes are regulated by several transcriptional regulators including AP1, SP1, KLF4 and GATA3[44–46]. Apart from promoter-associated transcriptional control of EDC genes, several conserved, non-coding sequences were shown to display keratinocyte differentiation-specific enhancer activities throughout the locus[47].

2.2 Long non-coding RNAs

2.2.1 Identification and definition of long non-coding RNAs

RNAs are structurally and functionally versatile molecules which inspired the “RNA world hypothesis”. Based on this hypothesis, RNAs have been the pre-stage of life billions of years ago as they had to function as enzymes and storage media for information[48]. This changed when DNA and proteins have developed and taken over most of these functions. As a consequence of the resulting dogma – DNA is transcribed into RNA which is eventually translated into a functional protein – RNAs were considered merely as an intermediate of protein production[49]. However, our center of attention has changed drastically when next generation sequencing technologies revealed that while up to 75% of the human genome is transcribed, only 2% encode for proteins[50,51]. This far-reaching discovery has brought scientific interest back to regulatory non-coding RNAs (ncRNAs). Even though some ncRNAs controlling splicing (small nuclear RNAs), RNA editing (small nucleolar RNAs) and translation (transfer RNAs and ribosomal RNAs) have been known for a long time, other so-called short ncRNAs (sncRNAs) have been identified more recently. These sncRNAs (20-30 nt in length) include microRNAs (miRNAs), endogenous small-interfering RNAs and piwi-associated RNAs acting as regulators of cellular processes[52–54]. Another class of RNAs – the long-noncoding RNAs (lncRNAs) – and

their significant impact on multitude of cellular processes, have also gained widespread attention over the last years[55–57]. LncRNAs are widely defined as RNA transcripts which are longer than 200 nucleotides with no or little coding potential[58]. In addition, many lncRNAs show significant similarities to mRNAs because most of them are also transcribed by RNA polymerase II, often spliced, 5'-capped and polyadenylated[59,60]. They can be detected in both cytoplasm and nucleus, exhibit a barely conserved primary sequence, but they can still form complex secondary structures important for their function[57,61–63].

One way to classify lncRNAs is by their genomic loci and organization, respectively. While long intergenic non-coding (LINC) RNAs are scattered all over the genome and often transcribed from their own promoters, intronic lncRNAs are transcribed from regions within protein-coding genes. Furthermore, there are bidirectional lncRNAs divergently expressed from the same promoter of a protein-coding gene as well as lncRNAs being the antisense transcript of a protein-coding gene[64–66]. Additionally, the degree of complexity in lncRNA loci is increased by the presence of different lncRNA isoforms as a result of alternative splicing, polyadenylation and transcription start sites (TSSs), respectively[56,57,67,68]. Many lncRNAs show a strict cell-type and -state specific expression pattern implying a crucial impact during different cellular processes[69]. This assumption is confirmed as they have important functions in apoptosis, cellular differentiation, cell cycle control, epigenetic imprinting, nuclear import, promoter-specific gene regulation and X-chromosome inactivation[65,69–72]. In accordance with this, several diseases including many types of cancer show strikingly deviating lncRNA expression levels highlighting their significance in cellular processes[73,74].

2.2.2 Molecular mechanisms of lncRNAs

Although there are thousands of different lncRNAs exerting various functions in cells, their specific mode of action is less clear in many cases. Since they appear to be remarkably diverse, there have always been efforts to categorize lncRNA mechanisms. Based on mechanistic similarities, there are four main archetypes called scaffolds, guides, decoys and signals interacting with RNA, DNA and proteins which mainly affect (post-)transcriptional regulation[75]. As more and more lncRNAs are being mechanistically characterized, it becomes apparent that the high diversity

of modes of action cannot broken down to only four general categories. Instead, more precise classifications and subdivisions are made today as for lncRNA-dependent transcriptional control in the nucleus.

There are lncRNAs facilitating gene expression through regulating chromatin looping (Figure 3A). Interacting with a looping-associated protein, lncRNAs can thus enhance transcription[76]. However, probably one of the most powerful tool for lncRNAs to influence transcription is through chromatin remodeling (Figure 3B)[77]. LncRNAs can associate with DNA or histone modifying enzymes including polycomb repressive complex 2 (PRC2), trithorax group (TrxG) proteins, histone demethylase LSD1, DNA methyltransferase DNMT1 and DNA demethylation regulator GADD45A[78–81]. One of the best studied examples of this category is HOTAIR. HOTAIR is capable to bind both PRC2 and LSD1 at the same time acting as a scaffold. The HOTAIR-PRC2-LSD1 complex epigenetically alters gene expression through H3K27 (PRC2) methylation and H3K4 (LSD1) demethylation. Correspondingly, the HOXD locus, one of the main HOTAIR targets, is repressed[82,83]. Binding to transcriptional regulators activating or inhibiting their activity provides another layer of lncRNA-mediated transcriptional control (Figure 3C). The zinc-finger transcription factor CNBP, for example, is a negative regulator of cardiovascular lineage commitment, specifically found to interact with lncRNA Braveheart. This lncRNA is able to functionally antagonize CNBP and therefore, Braveheart acts as positive regulator of cardiac gene expression[84].

On the post-transcriptional level, lncRNAs also affect cellular processes in both nucleus and cytoplasm through various mechanisms. They are capable to regulate splicing processes (Figure 3D) and they can influence intracellular transport and localization, respectively (Figure 3E)[85,86]. LncRNA NRON, for example, interacts with nuclear factor protein NFAT affecting its subcellular localization. In presence of NRON, the translocation of NFAT from the nucleus to the cytoplasm is regulated, while in absence of NRON, NFAT remains in the nucleus[87]. LncRNAs are also known to bind to mRNAs to protect them from degradation through exonucleases (Figure 3F). A representative of this subcategory is lncRNA BACE1-AS. BACE1-AS is transcribed from the same locus on chromosome 11 as the protein-coding *BACE1* but from the opposite strand. Therefore, BACE1-AS can form an RNA duplex with *BACE1* mRNA to increase its stability. This ultimately results in BACE1-triggered

amyloid-β 1-42 peptide production which can further enhance BACE1-AS expression via a feed-forward mechanism. Interestingly, excessive amounts of amyloid-β 1-42 are associated with Alzheimer's disease and elevated BACE1-AS level can be detected in Alzheimer's disease patients[88]. Apart from enhancing mRNA translation through increasing mRNA stability, lncRNAs can also directly affect the translational process through modulating ribosome activity (Figure 3G)[89,90]. LncRNAs are further known to act as competitive endogenous RNAs (ceRNAs) binding miRNAs (Figure 3H). The resulting inhibition of miRNA activity is therefore correlated with positive gene expression of the corresponding target mRNAs[91]. Besides, lncRNAs were also found to modulate protein stability and activity, respectively (Figure 3I). HOTAIR, for example, associates with E3 ubiquitin ligases DZIP3 and MEX3B as well as with their substrates Ataxin-1 and Snurportin-1. Providing a scaffold, HOTAIR facilitates the ubiquitination and following degradation of both substrates[92]. The opposite effect was shown for MALAT1. MALAT1 increases SREBP-1C stability in hepatic steatosis through interacting with this transcription factor thus preventing ubiquitination and degradation of SREBP-1C[93].

Apart from these widely known mechanisms, there are also more "exotic" functions of lncRNAs. Even though the term "non-coding" implies no coding potential for lncRNAs, there are a few exceptions encoding for micropeptides (Figure 3J)[94]. The lncRNA LINC00948 located on chromosome 10 and specifically expressed in skeletal muscles was found to code for a 46 amino acid micropeptide called MLN. MLN is a transmembrane α-helix modulating intracellular calcium level through inhibition of SERCA, a calcium-pump[95]. Moreover, lncRNAs such as MALAT1, HOTAIR and lincRNA-p21 may also serve as intercellular messages as they were found to be selectively loaded to exosomes[96].

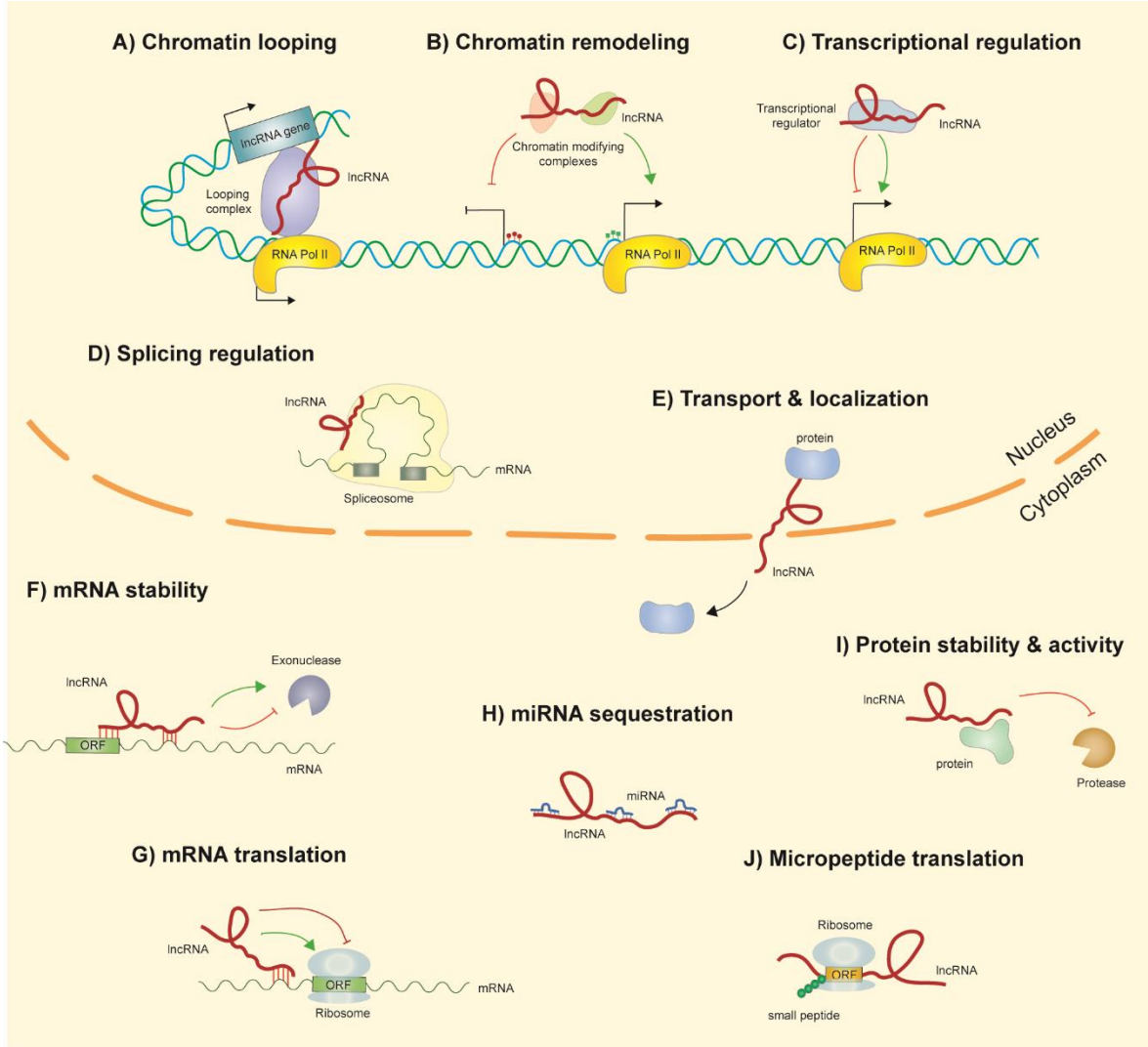

Figure 3: Overview of some representative lncRNA functions.
LncRNAs can act on transcriptional level through (A) chromatin looping, (B) modulation and recruitment of chromatin remodeler and (C) regulation of transcription factors, respectively. Furthermore, lncRNAs also have functions on the post-transcriptional level. They can influence (E) transport and (sub-)cellular localization of proteins, (F) mRNA stability and (G) mRNA translation. In some cases, lncRNAs function as (H) ceRNAs, whereas in other cases they regulate (I) protein stability and activity, respectively. Less often, lncRNAs (J) code for micropeptides (modified after Karlsson & Baccarelli)[89].

2.2.3 Roles of lncRNAs in organ development and tissue homeostasis

LncRNAs regulate various cellular processes through tightly controlled mechanisms, thus, they are intimately linked to the pathogenesis of a variety of human diseases. However, as most of them are differentiation-, state-, tissue- and cell-type specific expressed, they are first of all regulators of tissue and organ homeostasis and development, respectively[97]. Under normal physiological conditions, Braveheart, CARMEN and FENDRR, are the most popular representatives affecting cardiovascular development. LncRNA Braveheart

activates a core gene regulatory network of transcription factors in trans to orchestrate cardiovascular cell fate in mice. Since Braveheart also interacts with SUZ12, a component of PRC2, it is further hypothesized to regulate cardiomyocyte differentiation through an epigenetic mechanism[98]. Moreover, differentiation and homeostasis of human cardiac precursor cells is regulated by CARMEN acting upstream of the cardiac mesoderm-specifying gene regulatory network. Similar to Braveheart, it also interacts with SUZ12 and EZH2, respectively, another PRC2 component[99]. Furthermore, lncRNA FENDRR binds PRC2 as well as TrxG regulating their activity and thus affecting cardiovascular processes as both protein complexes are crucial for normal heart wall development[100].

Besides heart muscle-associated lncRNAs, there are lncRNAs important for differentiation, regeneration, and development of other muscles such as SENCR, MUNC and lnc-mg. Yet another muscle-specific lncRNA of importance is linc-MD1. Linc-MD1 acts as ceRNA in murine and human myoblasts through sequestration of miRNAs miR-133 and miR-135. Their downstream targets MAML1 and MEF2C, two transcription factors, can subsequently activate the expression of muscle-specific differentiation genes[101].

There are also many lncRNAs exclusively expressed in the brain regulating a variety of neuronal processes including neuronal cell differentiation and brain development[102]. These lncRNAs include DALI, Pinky and Evf2[103]. DALI, for example, facilitates *POU3F3* expression in a cis-acting manner. Furthermore, it forms a complex with POU3F3 transcription factor to finally activate neuronal-specific differentiation genes in trans[104]. Pinky, on the other hand, influences an earlier level of neurogenesis. In the embryonic and postnatal brain it affects murine neural stem cell differentiation through interaction with PTBP1, a protein involved in mRNA processing[105].

Intestinal homeostatic processes were also found to be regulated by lncRNAs such as SPRY4-IT1 and Gata6. The latter controls the maintenance of intestinal stem cell stemness through the recruitment of the nucleosome remodeling factor (NURF) complex to the promoter of the ETS transcription factor family. They eventually enable the maintenance of intestinal homeostasis via their downstream targets[106]. On the other hand, SPRY4-IT1 regulates epithelial barrier function of intestinal epithelial cells on post-transcriptional level. This lncRNA binds tight junction-

associated mRNAs to enhance their stability and thus to increase the probability of translation[107].

Apart from intestinal epithelium homeostasis, lncRNAs are also indispensable regulators in other epithelial tissues such as in the epidermis. In epidermal tissue, there must be a tightly controlled equilibrium between the number of dead corneocytes desquamated and succeeding keratinocytes to provide epidermal homeostasis. This process has also been shown to be regulated by lncRNAs including PRANCR, SMRT-2, BLNCR, ANCR and TINCR[71,108–111]. The impact of TINCR was among the first described featuring a crucial function in keratinocyte differentiation. This lncRNA is highly induced in terminal differentiation and its depletion was found to lead to reduced differentiation marker abundances on both mRNA and protein level. Mechanistically, TINCR regulates differentiation gene expression on a post-transcriptional level through the formation of short double stranded RNA duplexes with several mRNAs coding for differentiation-associated proteins. These RNA duplexes are mediated by 25 nt TINCR-box motifs which become subsequently bound by STAU1. This RNA-protein complex enables mRNA stabilization and enhanced translation[111]. Moreover, TINCR also increases *MAF* and *MAFB* mRNA stability, respectively. Thus, both transcription factors can exert their known regulatory function in keratinocyte differentiation[112].

One of the most recently identified lncRNAs also involved in epidermal homeostasis is lncRNA LINC00941[113].

2.3 The human lncRNA LINC00941

LncRNA LINC00941, sometimes also referred to as lncIAPF or lncRNA-MUF was identified by the ENCODE Project in 2012[57]. Annotated on the forward strand of chromosome 12, there are several transcript isoforms of LINC00941 including alternative splicing as well as different 3’ and 5’ end variants. Currently, LINC00941 is listed in the Ensemble Genome Browser as ENST00000650286.1 containing five exons and a total length of 1355 bp. As previously mentioned, there are some lncRNAs encoding for small peptides. In case of LINC0091, bioinformatic analysis have not predicted coding potential, indicating that it likely acts as lncRNA only[113]. While LINC00941 can be detected in most human tissues suggesting a cell type

independent function, the subcellular localization of this lncRNA is more variable[113]. Its presence can be observed in both the cytoplasm and nucleus. However, depending on cell-type and type of cancer, respectively, the distribution of LINC00941 differs. While this lncRNA was detected more frequently in the cytoplasm of pancreatic cancer (PC) cells, LINC00941 demonstrated a more prevalent occurrence in the nucleus in esophageal squamous cell carcinoma (ESCC)[114,115]. This finding revealed a dependency of LINC00941 subcellular localization on the cell state. Mechanistically, intracellular lncRNA abundance already gives a first clue as nuclear accumulation suggests a gene regulatory function, whereas cytoplasmic lncRNAs are involved in post-transcriptional processes. In line with its versatile nuclear and cytoplasmic localization, LINC00941-mediated mechanisms have been elucidated in several cancer types on both transcriptional and post-transcriptional level[116].

2.3.1 LINC00941-mediated regulation of mRNA transcription

The first research group demonstrating a mode of action of LINC00941 was Ai et al.[117]. They were studying LINC00941 as this lncRNA showed enhanced expression in oral squamous cell carcinoma (OSCC) cell lines. Interestingly, LINC00941 expression positively correlates with cell growth, colony, and tumor formation, respectively. A first indication of a putative mechanism was shown by a motif analysis revealing several binding sites of CTCF, a transcriptional regulator mediating DNA looping[118], between LINC00941 and its nearby gene *CAPRIN2*. Correspondingly, it was hypothesized that LINC00941 regulates gene expression in cis via looping to *CAPRIN2* mediated by CTCF (Figure 4A). This assumption was confirmed by quantitative chromosome conformation capture (3C) analysis conducted in OSCC cell lines. Following functional assays, a crucial role of CAPRIN2 in OSCC cell proliferation and tumor formation was shown: CAPRIN2 phosphorylates LRP6, a Wnt co-receptor, which subsequently associates with Axin[117]. This interaction led to stabilization of β-catenin and finally to activation of Wnt target gene transcription[119]. Enhanced activity of the canonical Wnt pathway – initially triggered by increased LINC00941 expression in OSCC cells – is implicated with many cancer types[120,121].

Another putative mechanism of LINC00941 was recently discovered[115]. Comparable to LINC00941 expression in OSCC, there were also increased levels of this lncRNA in ESCC resulting in enhanced cell proliferation, migration, and invasion, respectively. However, the underlying cause is different in ESCC compared to OSCC. RNA pull-down and mass spectrometry (MS) analysis identified ILF2 and YBX1, two transcriptional regulators, as interaction partners of LINC00941. Both were also found to be upregulated in OSCC. Further experiments revealed a role of the LINC00941/YBX1/ILF2 complex as positive regulator of *SOX2* expression (Figure 4B). Interestingly, SOX2 was demonstrated to regulate LINC00941 expression in ESCC. Therefore, LINC00941 not only regulates its own transcription through a feed-forward mechanism mediated by SOX2, but it also modulates ESCC cell proliferation as deregulated SOX2 is associated with various cancer types[115,122]. Apart from showing a role of LINC00941 on the transcriptional level of ESCC, Lu et al. could also reveal another LINC00941-mediated mechanism on post-transcriptional level: The LINC00941/ILF2/YBX1 complex further binds *SOX2* mRNA[115]. This association between protein, mRNA and lncRNA prolonged half-life of *SOX2*, which also causes enhanced SOX2 protein synthesis (Figure 4C). These findings demonstrated various mechanisms of LINC00941, not only between different cell types, but also within specific cells.

2.3.2 LINC00941-mediated modulation of post-transcriptional pathways

As LINC00941 is not only found in the nucleus but also in the cytoplasm, further post-transcriptional pathways regulated by LINC00941 were recently identified. Apart from LINC00941 acting as mRNA stabilizing component, this lncRNA was also identified as modulator of protein activity and stability, respectively[123]. In colorectal cancer (CRC), LINC00941 was shown to be upregulated as well as to interact with SMAD4. As LINC00941 suppression resulted in decreased SMAD4 protein levels, this led to the assumption that this lncRNA prevents SMAD4 degradation. Investigating SMAD4 poly-ubiquitination in LINC00941-overexpressing and -deficient CRC cells, respectively, it could be demonstrated that SMAD4 ubiquitination was decreased upon LINC00941 overexpression but increased after LINC00941 knockdown. These results verified that this lncRNA could stabilize SMAD4 by suppressing its ubiquitination through direct interaction in CRC. As β-

TrCP is known to be responsible for SMAD4 poly-ubiquitination and subsequent degradation, further analysis revealed a competing relationship between LINC00941 and β-TrCP[124]. Therefore, LINC00941 increases SMAD4 stability to prevent its degradation by competing with β-TrCP. Following this, the parent TGF-β1/SMAD pathway regulates transcription markers for cancer cell migration and invasion causing CRC metastases[123].

Another LINC00941-mediated mechanism enhancing protein stability was described in pancreatic ductal adenocarcinoma (PDAC)[125]. However, instead of preventing ubiquitination, LINC00941 facilitates dephosphorylation of its interaction partner MST1. MST1 is a key component of the Hippo pathway and it is also known to be dephosphorylated by PP2A to prevent phosphorylation-triggered degradation[126]. Further analysis revealed that LINC00941 knockdown in PDAC cells showed increased MST phosphorylation levels and weakened interaction between MST1 and PPA2. Taken together, LINC00941 interacts with MST1 facilitating its PP2A-mediated dephosphorylation. As a result, enhanced LINC00941 expression levels in PDAC cause excessive Hippo pathway activation leading to accelerated cancer cell proliferation[125].

Comparable to the aforementioned studies, LINC00941 shows a similar mechanism in PC cells[127]. Upregulated LINC00941 was found to interact with ANXA2 which is involved in metastasis formation in several cancer types[128,129]. Functional analysis revealed enhanced ANXA2 protein synthesis through binding of LINC00941. Co-immunoprecipitation (Co-IP) and MS analysis identified the ubiquitin ligase NEDD4L as interaction partner of ANXA2 in PC. LINC00941 and NEDD4L compete to interact with ANXA2. As LINC00941 expression levels are increased in PC, it preferentially binds ANXA2 preventing NEDD4L-mediated ubiquitination (Figure 4D). Correspondingly, stabilized ANXA2 activates the FAK/AKT signaling pathway supporting cancer cell survival and progression[130].

In addition to LINC00941-mediated stabilization of proteins and mRNAs, putative miRNA-association was also uncovered. Several studies showed interaction between LINC00941 and miR-205-5p in colon cancer (CC), miR873-3p in pancreatic adenocarcinoma, miR-335-5p in PC and miR-877-3p in ESCC cells (Figure 4E)[114,131–133]. The underlying hypothesis was the same for all studies: Elevated LINC00941 expression levels cause increased miRNA sequestration in

cancer cells. As a result of miRNAs being titrated away by ceRNA LINC00941, the respective downstream target mRNAs coding for oncogenes are not degraded but translated accelerating cancer cell proliferation.

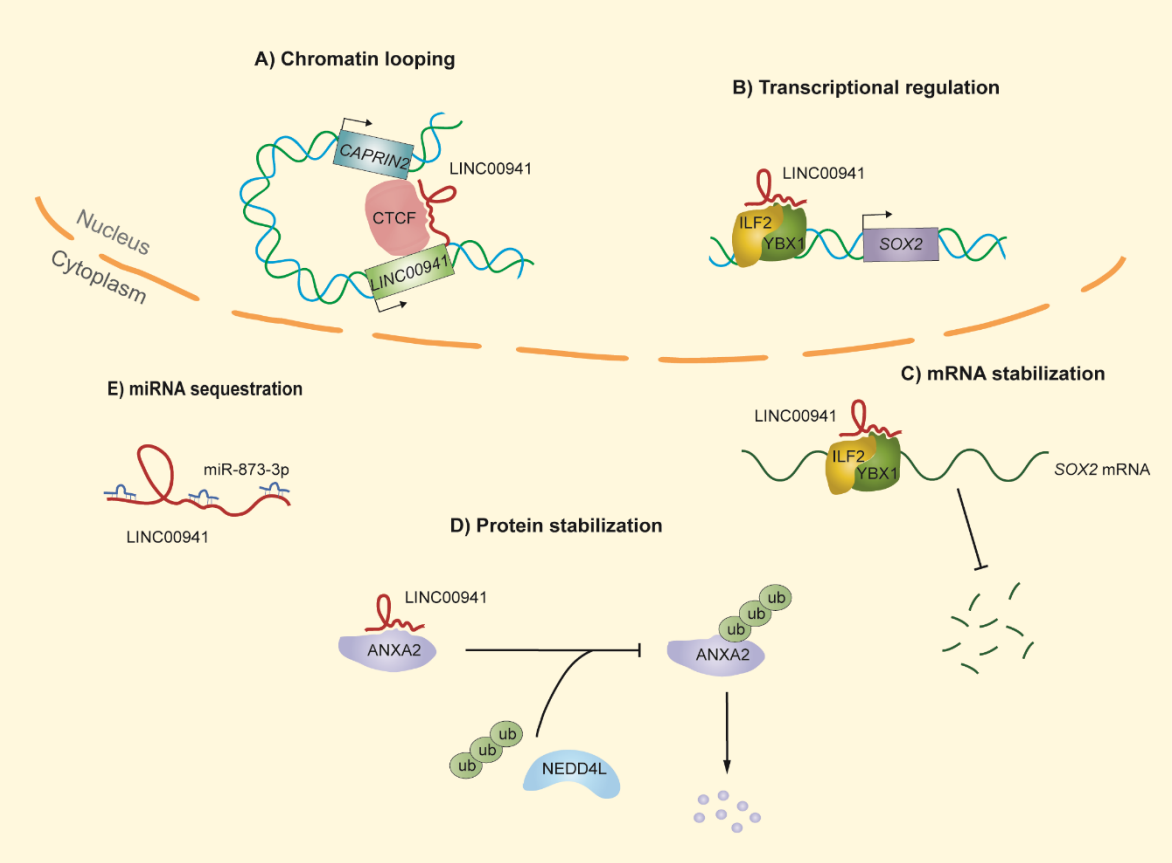

Figure 4: Schematic representation of some LINC00941-mediated modes of action in different cancer tissues.
(A) LncRNA LINC00941 can regulate nearby *CAPRIN2* expression in cis through CTCF-mediated chromatin looping. (B) LINC00941 can also modulate gene expression through interacting with transcriptional regulators in trans. On post-transcriptional level, LINC00941 was demonstrated to (C) enhance mRNA and (D) protein stability, respectively. (E) There is also some empirical evidence of LINC00941 acting as ceRNA (modified after Morgenstern and Kretz)[116].

As it is technically very challenging to determine the stoichiometric relationship between lncRNAs, their target miRNA and the affected downstream mRNA, it remains unclear whether it is stoichiometrically even possible for miRNAs to be sequestered by ceRNAs in a functionally significant manner[134–137]. Furthermore, there is currently no method available to verify direct interaction between lncRNA and miRNA *in vivo*. However, there are several experimental approaches addressing this issue. The studies mentioned above verified LINC00941/AGO2 interaction as an indirect indicator of a putative association between LINC00941 and

miRNAs as miRNAs are thought to be normally complexed by AGO2[116]. Furthermore, Dual Luciferase Reporter assays were performed to give a hint to detect direct interaction. Taken together, there is empirical evidence of LINC00941 acting as ceRNA, but some questions remain open to finally prove the ceRNA hypothesis.

2.3.3 Function of LINC00941 in keratinocytes and preliminary results

In previous studies, uncovering the mechanism of LINC00941 was of interest because it was highly upregulated in the respective cancer tissue. However, as the impact of LINC00941 might be different in healthy cells compared to cancer cells, elucidating its mode of action would also be relevant in healthy tissue. Interestingly, this has not yet been considered even though LINC00941 was demonstrated to play an important role in healthy human epidermis and epidermal homeostasis, respectively. Former members of our lab found that lncRNA LINC00941 is enriched in non- and poorly differentiated keratinocytes but repressed upon onset of differentiation (Figure 5A)[113]. Furthermore, LINC00941 is equally distributed between nucleus and cytoplasm suggesting pleiotropic mechanisms on transcriptional and post-transcriptional level in healthy human keratinocytes (Figure 5B). It could also be shown by former PhD students of our research group that LINC00941 acts as a negative regulator of keratinocyte differentiation as its knockdown resulted in increased mRNA and protein levels of early and late differentiation markers. A strong enrichment of upregulated genes upon silencing LINC00941 was observed within the EDC including filaggrin, LCE genes and SPRR4 (Figure 5C)[113]. These findings suggested a role of LINC00941 as a global regulator of mRNA transcription through an epigenetic mechanism. This hypothesis was further supported by RNA-immunoprecipitation (RNA-IP) of *in vitro* transcribed, biotinylated LINC00941 incubating with protein lysate of primary keratinocytes and subsequent MS analysis as well as by preliminary chromatin isolation by RNA purification (ChIRP) experiments. Both approaches hint towards transcriptional regulators including chromatin remodelers and towards the transcription factor E2F6 as putative interaction partners[138].

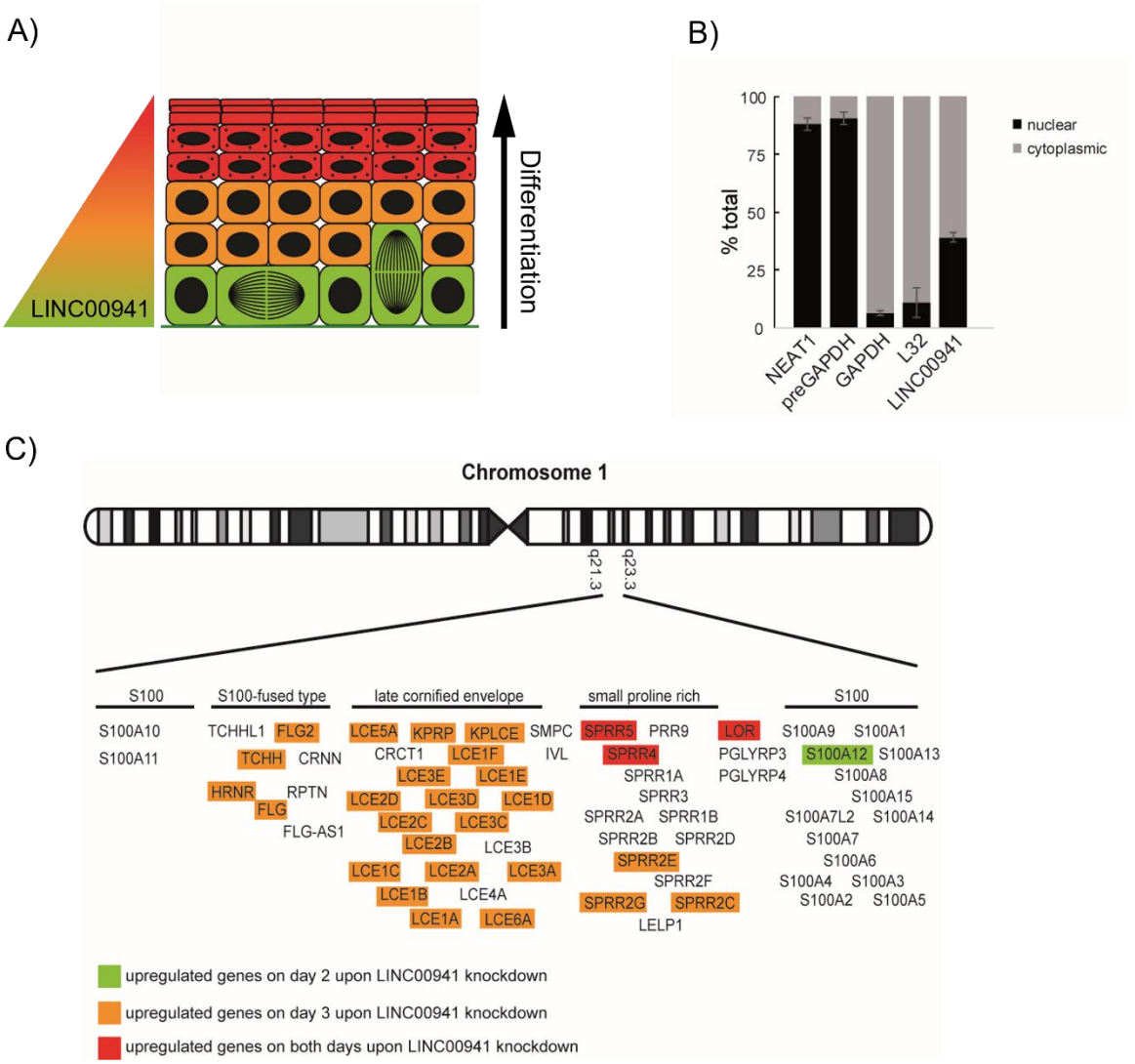

Figure 5: Overview of preliminary LINC00941 characteristics in healthy human primary keratinocytes. (A) Full transcriptome sequencing showed an enrichment of LINC00941 in undifferentiated progenitors but its repression during keratinocyte differentiation. (B) LINC00941 is equally distributed between nucleus and cytoplasm suggesting modes of action in both compartments. (C) Deregulated EDC genes upon LINC00941 knockdown on day 2 and day 3 of organotypic epidermal tissue (modified after Kypriotou et al. and Ziegler et al.)[35,113].

3 Objective

LncRNAs have been shown to be crucial regulators of many fundamental biological processes but only few of them have been mechanistically characterized. This PhD project aimed to elucidate modes of action of lncRNA LINC00941 in healthy human keratinocytes as its mechanism has only been uncovered in some cancer tissues so far. Given that LINC00941 was previously described as a negative regulator of epidermal homeostasis, the purpose of this work was to shed light on some suggested modes of action on both transcriptional and post-transcriptional level to provide an explanation for this phenotype.

To this end, the role of LINC00941 as putative ceRNA titrating away specific miRNAs and consequently enhancing target mRNA translation was elucidated. Therefore, it was examined which miRNA comes into question at all in keratinocytes. A possible interaction between LINC00941 and the respective miRNA was subsequently studied *in vitro*.

Furthermore, the role of LINC00941 as epigenetic regulator was investigated to uncover its impact on global mRNA transcription, especially on EDC gene expression. Therefore, LINC00941-associated binding to the transcription factor E2F6 and to the chromatin remodeler NuRD was examined as well as their LINC00941 dependency on chromatin binding behavior.

Overall, it was aimed to shed light on the pleiotropic modes of action of LINC00941 to fully understand its precise function as repressor of keratinocyte differentiation in healthy epidermal tissue.

4 Results

4.1 LINC00941 as putative ceRNA

4.1.1 Bioinformatics interaction analysis

In order to uncover the mechanism of LINC00941, a repressor of keratinocyte differentiation, it was crucial to first identify putative interaction partners through which this lncRNA influences cellular processes. In addition to previously performed MS analysis, we also used BRIO (BEAM RNA Interaction mOtifs). BRIO is a web tool searching for known sequence and structure protein binding motifs in RNA molecules based on crosslinking immunoprecipitation (CLIP) sequencing experiments[139]. This bioinformatic algorithm predicted interactions between LINC00941 and AGO2 based on several photoactivable-ribonucleoside-enhance CLIP (PARCLIP) and high-throughput sequencing CLIP (HITSCLIP) experiments (Table 1).

Table 1: Bioinformatics interaction analysis

Motif type	Experiment	Protein	Domain	p-value	Location [bp]	Source
Sequence	HITSCLIP	AGO2	PAZ	0.0063	1237-1244	140
Sequence	PARCLIP	AGO2	PAZ	0.0085	1242-1253	141
Structure	PARCLIP	AGO2	PAZ	0.016	1029-1061	142
Sequence	PARCLIP	AGO2	PAZ	0.02	1249-1255	141
Sequence	HITSCLIP	AGO2	PAZ	0.023	1241-1251	143
Sequence	HITSCLIP	AGO2	PAZ	0.04	1238-1244	143
Sequence	HITSCLIP	AGO2	PAZ	0.049	1122-1130	142

Correspondingly, we identified seven different AGO2-binding motifs accumulating at three different sites within exon 5 of LIN00941 (Figure 6).

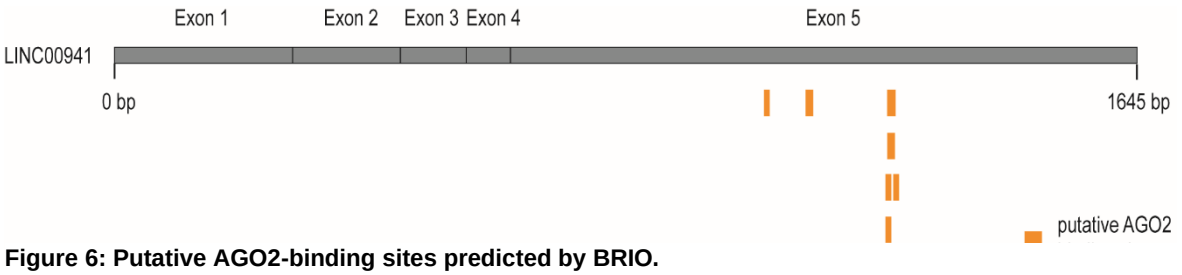

Figure 6: Putative AGO2-binding sites predicted by BRIO.
Based on CLIP sequencing experiments, BRIO predicted binding of AGO2 at seven different, partially overlapping sites within exon 5 of LINC00941 with a preference between 1237 bp and 1255 bp.

4.1.2 Interaction between LINC00941 and AGO2

To verify the results of BRIO, which predicted an interaction between AGO2 and LINC00941, we performed RNA-IP using antibodies against AGO2. After RNA-IP, qRT-PCR analysis was performed to detect LINC00941 confirming association between LINC00941 and AGO2 in primary human keratinocytes (Figure 7).

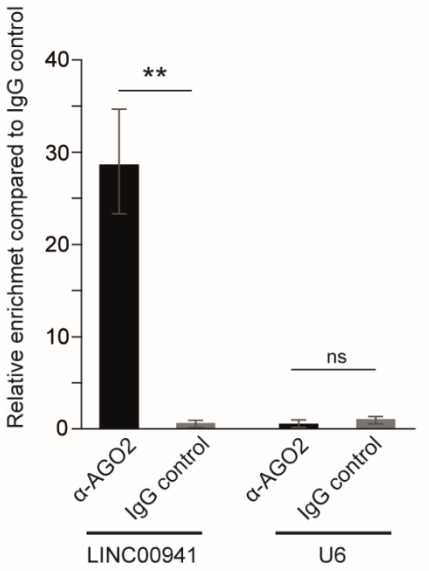

Figure 7: RNA-IP and qRT-PCR verified interaction between LINC00941 and AGO2.
Data are presented as ± standard deviation (*n* = 3). Statistical significance was tested by an unpaired *t*-test (**adj. *P*-value < 0.01, ns = not significant).

Accordingly, this experiment provided a first indirect indication of LINC00941 binding miRNAs because miRNAs are thought to be bound by AGO2 when present in the cytoplasm and because LINC00941 was further shown to interact with AGO2. Therefore, we postulated a role of LINC00941 acting as ceRNA in non- and poorly differentiated strata of the epidermis.

4.1.3 Identification of LINC00941-associated miRNAs

LncRNAs have the ability to sequester AGO2-associated miRNAs and there have already been previous reports suggesting that LINC00941 acts as ceRNA[114,131–133,144–146]. Thus, it was subsequently necessary to identify putative target miRNAs to shed further light on the hypothesized ceRNA mechanism of LINC00941. Using the web tool ENCORI (encyclopedia of RNA interactomes), which utilizes CLIP sequencing, degradome sequencing, and RNA-RNA interactome data to predict

lncRNA-miRNA interactions[147], we identified three putative target miRNAs for LINC00941: miR-526b-5p, miR-873-3p and miR-335-5p. Differing to BRIO, miR-526b-5p and miR-873-3p were predicted to bind within exon 2, while miR-335-5p binds within the previously predicted range of exon 5. As both BRIO and ENCORI lack data from epidermal tissues, we performed Northern Blot (NB) analysis with total RNA of undifferentiated and differentiated (calcium-induced; day 3) keratinocytes to determine the presence or absence of the miRNAs in keratinocytes. Our results showed that only miRNA miR-335-5p is present in keratinocytes, while the others could not be detected (Figure 8). This finding aligns with small RNA sequencing data from keratinocytes, publicly available on ENCODE.

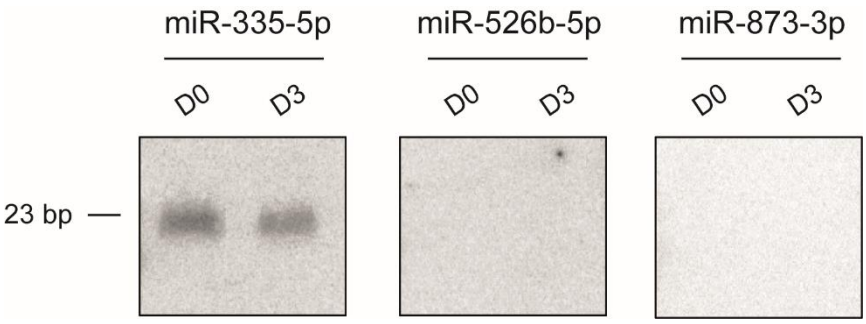

Figure 8: Northern Blot analysis detected miR-335-5p in keratinocytes.
Three different miRNAs (miR-335-5p, miR-526b-5p and miR-873-3p) were predicted to interact with LINC00941 but only miR-335-5p is expressed in undifferentiated and differentiated keratinocytes.

In summary, out of three predicted miRNAs that can potentially interact with LINC00941, only miR-335-5p is found in keratinocytes and thus putatively able to be titrated away by this lncRNA affecting cellular processes of these epidermal cells.

4.1.4 Downstream mRNA targets of miR-335-5p

In order to understand how LINC00941 affects cellular function through miR-335-5p sequestration, we needed to consider its downstream mRNA targets. Using ENCORI (based on high-throughput CLIP sequencing data) and TargetMiner (machine learning tool based on biologically verified positive and negative examples) miR-335-5p target mRNAs were predicted[147,148]. Gene ontology (GO) term analysis revealed that putative downstream mRNA targets showed strong enrichment of genes involved in proliferative processes. Specifically, miR-335-5p mRNA targets associated with epidermal homeostasis were found to be negatively regulated in terms of differentiation and positively regulated in terms of proliferative

processes (Figure 9). These findings provide further evidence for LINC00941 acting as negative regulator of epidermal homeostasis through titrating away the positive regulator of keratinocyte differentiation miR-335-5p.

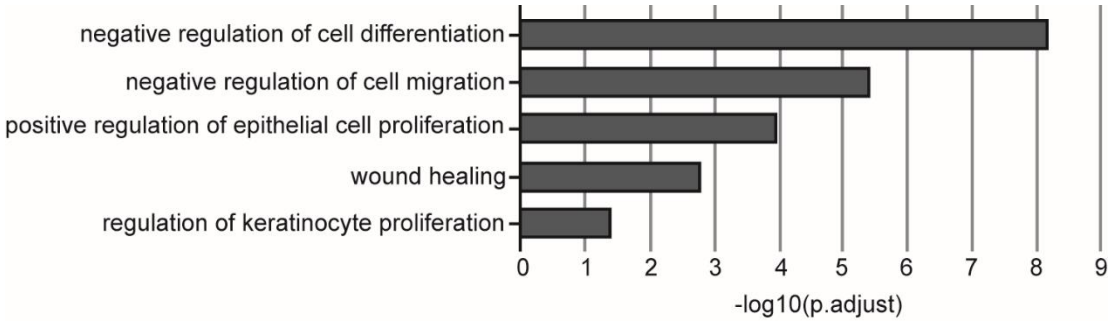

Figure 9: Epidermal homeostasis-associated GO terms of miR-335-5p downstream mRNA targets. GO term analysis revealed a role of miR-335-5p as positive regulator of keratinocyte differentiation. GO term analysis was conducted using the PANTHER Overrepresentation test. GO terms with a false discovery rate (FDR) of less than 0.05 and association with epidermal homeostasis were considered.

In order to narrow down the list of miR-335-5p regulated target mRNAs, we next considered LINC00941 knockdown RNA sequencing data (organotypic epidermal tissue; day 2). By comparing this data with miR-335-5p downstream targets, we identified 55 genes that were regulated by both miR-335-5p and LINC00941. Interestingly, 75% of these genes were found to be decreased in LINC00941 silenced keratinocytes.

This result underpinned the role of LINC00941 as ceRNA as it might act as a decoy to sequester miR-335-5p preventing it from binding to its downstream target mRNAs, and thereby enabling their translation. In absence of this lncRNA, miR-335-5p is free to bind to its target mRNAs inhibiting their translation.

4.1.5 Prediction of putative miR-335-5p binding sites within LINC00941

To effectively titrate away miRNAs, it is theoretically advantageous for lncRNAs to harbor many miRNA binding sites. Thus, we aimed determine binding sites of miR-335-5p within LINC00941 bioinformatically and manually[149,150]. Regarding manual binding site prediction, different “seed sequence types” were considered as stated by Gaidatzis et al. (2007)[151]. This not only includes perfect sequence complementarity between positions 1-8, 1-7, 2-8 and 2-7 of the miRNAs and the

respective target RNA, but also complementarity between positions 1-8 with a single G-U pair and other “imperfect” pairings.

Overall, we predicted a total of 22 putative miRNA miR-335-5p binding sites, some of which partially overlapped (Figure 10). Out of these sites, seven showed perfect complementarities in the seed sequence between LINC00941 and miR-335-5p. In comparison, lncRNAs of similar length such as ANRIL and H19 only harbor one site of perfect seed sequence complementarity with miR-335-5p. This suggests that the presence of miR-335-5p binding sites within LINC00941 is not due to random chance. Additionally, consistent with results from BRIO and ENCORI, more than half of all binding sites were located within exon 5.

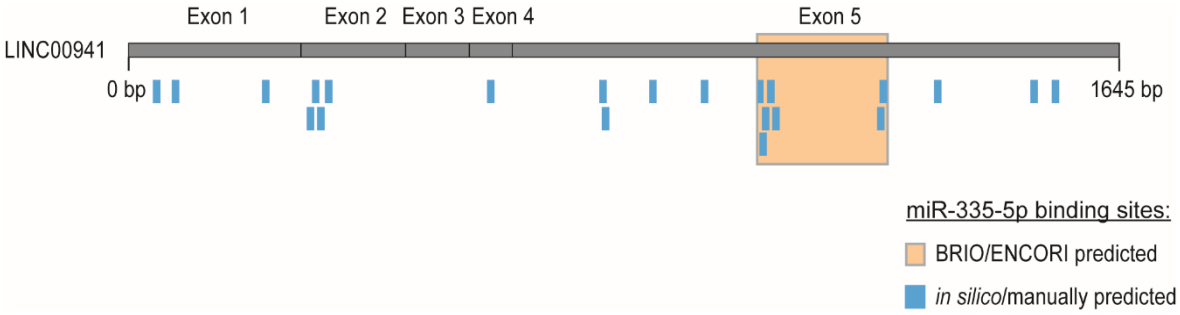

Figure 10: Putative miR-335-5p binding sites within LINC00941.

Based on this initial prediction of possible binding sites, we were able to demonstrate that LINC00941 has the ability to bind miR-335-5p through multiple binding sites, thus preventing translational inhibition of downstream mRNA targets.

4.1.6 Interaction between LINC00941 and miR-335-5p

Since the previous considerations suggested that miR-335-5p can bind multiple positions within LINC00941, we aimed to verify some of these putative binding sites in the next step. Accordingly, we performed *in vitro* Dual Luciferase Reporter assays. Similar to AGO2 RNA-IP, Dual Luciferase Reporter assays provide another indirect indication of whether lncRNAs interact with miRNAs *in vivo*.

To achieve this, we cloned either a putative wild-type (WT) miRNA-335-5p binding region or a mutated (MUT) control region of LINC00941 into the 3’ UTR of a luciferase. We selected the three most likely binding regions based on the most

favorable total free energy of binding and the accumulation of potential binding sites at these loci (Figure 11).

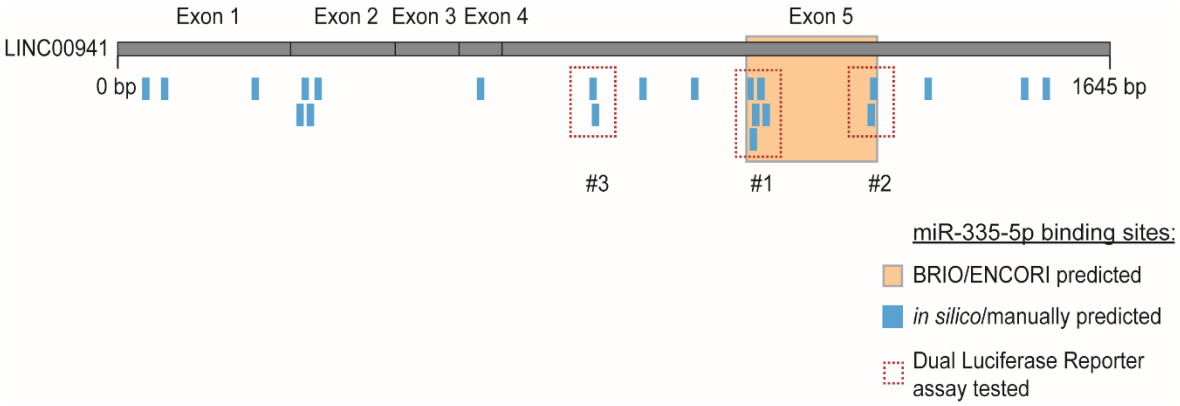

Figure 11: Binding regions tested with Dual Luciferase Reporter assays.
Three putative binding regions of miR-335-5p ("#1", "#2", "#3") with the most favorable binding energy were analyzed *in vitro* with Dual Luciferase Reporter assays. The tested WT (and MUT) regions had a total length of 23 bp correspondingly harboring up to five different putative binding sites which, for example, vary in the exact complementarity within the seed sequence.

However, it should be noted that the binding regions tested do not provide information about of the exact nature of interaction. The overlaps of the predicted binding sites, which differ in terms of perfect seed sequence complementarity between positions 1-7 or 2-7 of the miRNA, for example, make it impossible for the assay to differentiate between these modes of interaction.

Dual Luciferase Reporter assays demonstrated a significant interaction between miR-335-5p and the first putative binding region of LINC00941 ("#1"), as there is approximately 25% less relative luciferase activity in WT LINC00941 compared to MUT LINC00941 (Figure 12). One of the miR-335-5p binding sites covered by #1 was predicted to have the most favorable binding energy which was -10.04 kcal/mol. However, no interaction between LINC00941 and miR-335-5p was demonstrated in the other two putative binding regions ("#2" and "#3"). Corresponding binding sites had binding energies of approximately -7.8 kcal/mol.

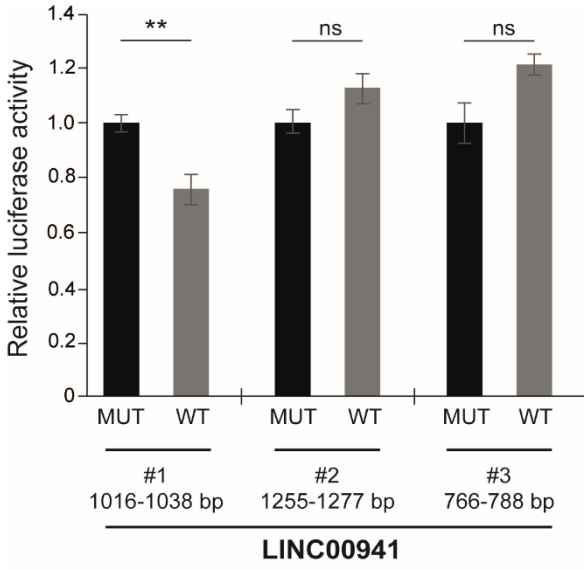

Figure 12: Results of Dual Lucifer Reporter assays.
The binding region #1 showed significant interaction between LINC00941 and miR-335-5p. Binding regions #2 and #3 showed no significant decrease of signal. Data are presented as ± standard deviation (*n* = 3). Statistical significance was tested by an unpaired *t*-test (**adj. *P*-value < 0.01, ns = not significant).

Therefore, we only detected interaction between LINC00941 and miR-335-5p at the energetically most favorable position located within exon 5 of LINC00941. This position also overlaps with the structure protein binding motif predicted by BRIO (PARCLIP, Table 1).

Taken together, we found that LINC00941 – a lncRNA with partial cytoplasmic localization – binds miR-335-5p at one binding site within exon 5. Therefore, LINC00941 is still able to act as ceRNA in non- and poorly differentiated keratinocytes enabling translation of miR-335-5p target mRNAs. These mRNAs code for proteins that are involved in the negative regulation of differentiation and in the positive regulation of proliferation, respectively. As a result, keratinocytes are kept in a proliferative state and onset of preliminary keratinocyte differentiation is prevented. As lncRNA LINC00941 abundance decreases over time, miR-335-5p can act as an inducer of keratinocyte differentiation through translational inhibition of its downstream target mRNAs, as previously described by Liew et al. (2020)[152]. However, preliminary miRNA overexpression experiments using miR-335-5p mimics did not show significant deregulation of putative downstream mRNAs. Due to time constrains, we could not continue further analysis to study the interrelationship between lncRNA LINC00941 and miR-335-5p.

4.2 Role of LINC00941 in MTA2/NuRD-mediated transcriptional regulation

4.2.1 Interaction between LINC00941 and NuRD

Apart from its localization in the cytoplasm, which strongly supports its role on the post-transcriptional level, LINC00941 is also found in the nucleus. Furthermore, previous studies of our lab have demonstrated its ability to regulate the expression of early and late differentiation genes in human keratinocytes, including genes of the EDC[113]. These two discoveries have led to the hypothesis that LINC00941 may play a role in regulating gene expression on a global level through an epigenetic mechanism.

To get a deeper insight into the mode of action of this lncRNA in human epidermis, RNA-protein interactome analysis was previously performed to identify LINC00941-associated proteins[138]. Therefore, RNA pull-down and MS analysis with *in vitro* transcribed, biotinylated LINC00941 and cell lysates from primary human keratinocytes were performed in our lab. In total, we found 627 putative interaction partners. To test the hypothesis of LINC00941 acting as transcriptional regulator in the nucleus, we only focused on chromatin-associated and related proteins for further analysis. Correspondingly, GO term analysis identified LINC00941-bound proteins attributed with nucleosomal DNA binding and histone deacetylase binding, for example, including histones H1.2, H1.3 and H1.5 (Figure 13A). LINC00941 was also found to interact with subunits of some chromatin remodeling complexes. In particular, components of the NuRD (Nucleosome Remodeling and Deacetylase) complex were enriched.

A more detailed analysis of LINC00941-bound NuRD subunits showed that MS analysis identified almost every component of the NuRD complex: CHD4, MTA2, HDAC2, GATAD2A, GATAD2B, RBBP4 and RBBP7, respectively (Figure 13B and appendix Table 26).

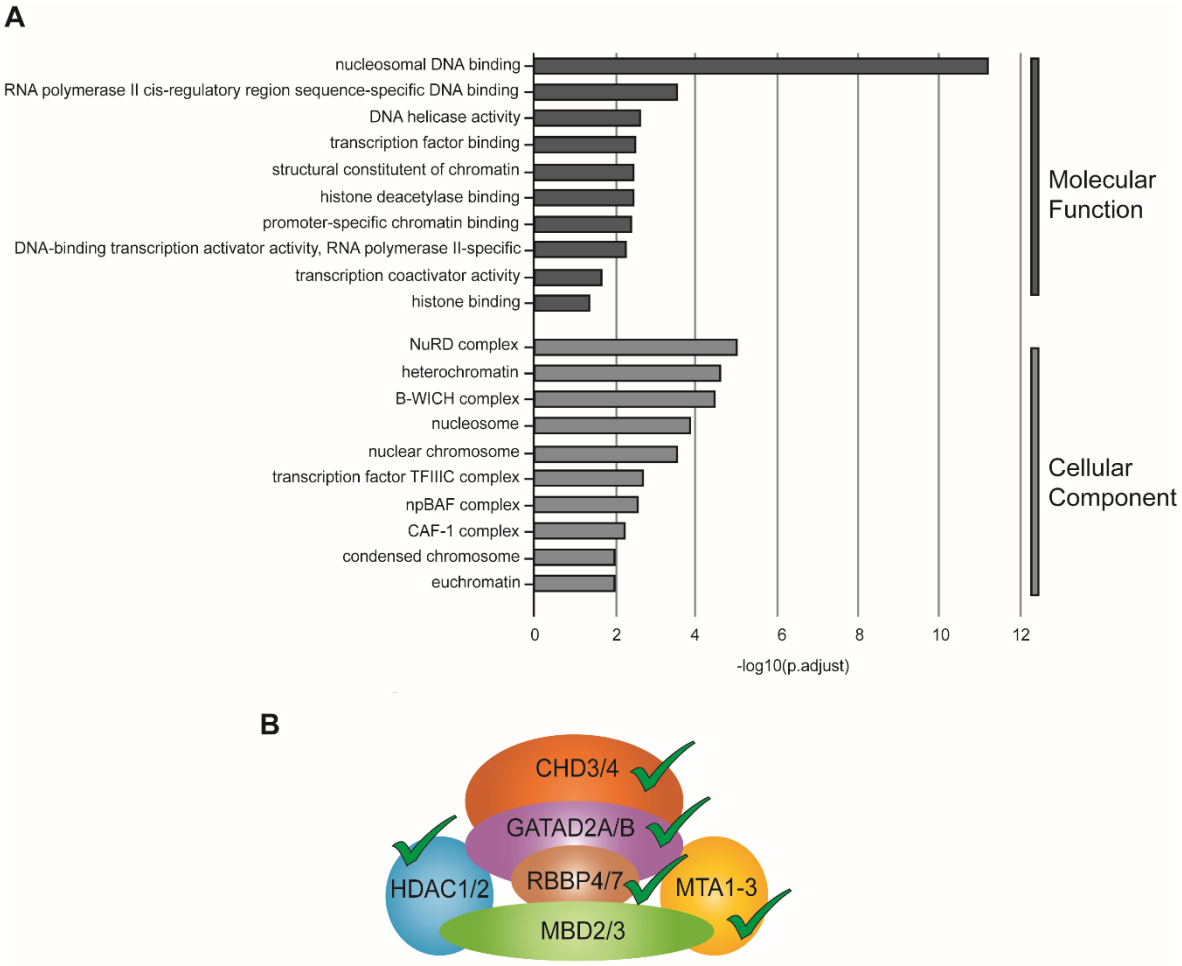

Figure 13: LINC00941 interacts with subunits of the NuRD complex.
(A) Chromatin-associated GO terms of LINC00941-associated proteins detected by MS analysis. GO term analysis was conducted using the PANTHER Overrepresentation test. GO terms with an FDR of less than 0.05 and association with chromatin were considered. (B) Schematic representation of NuRD components found to interact with LINC00941.

These findings suggested a NuRD-mediated transcriptional regulation of early and late key differentiation genes – including genes of the EDC – at least partially controlled by LINC00941. To prove this hypothesis, it was necessary to further validate interaction between LINC00941 and the NuRD complex. Since several subunits of NuRD, such as HDAC2, RBBP4, and RBBP7 also function as components of other multi-protein complexes, including NuRF complex, Sin3 and ESC/E(Z)[153–155], we focused subsequent analysis on MTA2 – a core component of the NuRD complex[156]. Johannes Graf, a former PhD student of our research group, recently demonstrated association between *in vitro* transcribed, biotinylated LINC00941 an MTA2/NuRD from cell lysate through RNA pull-down followed by Western Blot (WB) analysis[138]. In this work, RNA-IP using antibodies targeting

MTA2 and subsequent qRT-PCR analysis to detect LINC00941 also verified interaction between overexpressed LINC00941 and MTA2/NuRD in primary human keratinocytes (Figure 14).

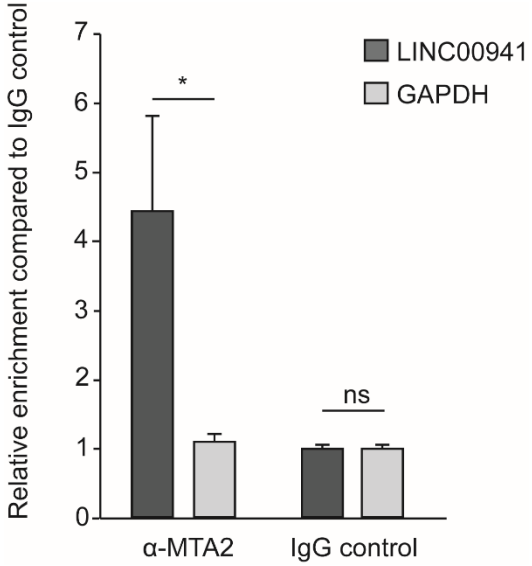

Figure 14: RNA-IP and subsequent qRT-PCR analysis verified interaction between MTA2/NuRD and overexpressed LINC00941.
Data are presented as ± standard deviation (*n* = 3). Statistical significance was tested by an unpaired *t*-test (*adj. *P*-value < 0.05, ns = not significant).

To narrow down the region of LINC00941 which interacts with the NuRD complex, truncated versions of the lncRNA were generated (overexpressed exon 1, exon 2-5, or exon 1-4) and used for RNA-IP and subsequent qRT-PCR analysis. Interestingly, we could detect no – not even weak – interaction between the different LINC00941 truncations and NuRD (data not shown) suggesting a strong sequence or structure conservation of LINC00941 necessary for its NuRD-associated functionality.

However, verified interaction between full-length LINC00941 and NuRD strongly indicated a LINC00941-mediated role regulating epidermal homeostasis through modulation of NuRD activity and recruitment, respectively.

4.2.2 MTA2/NuRD suppresses keratinocyte differentiation

It was recently reported by members of our lab that LINC00941 was highly expressed in non- and poorly differentiated keratinocytes and repressed as keratinocyte differentiation progresses[113]. Therefore, we performed qRT-PCR

analysis of NuRD-associated MTA2 throughout six time points of calcium-induced keratinocyte differentiation. This was done to see if the same expression pattern of LINC00941 could also be observed for MTA2, the interaction partner of LINC00941. *MTA2* mRNA was found to be highly induced in undifferentiated progenitor keratinocytes and reduced in abundance during keratinocyte differentiation, thus displaying a similar dynamic expression pattern as LINC00941 (Figure 15).

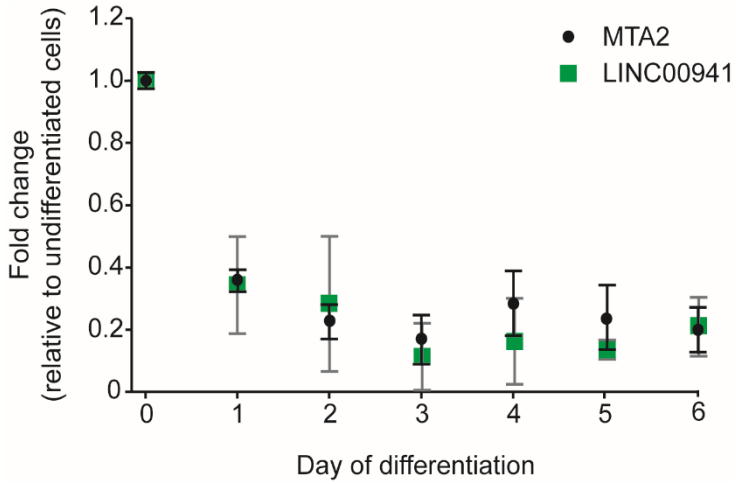

Figure 15: qRT-PCR analysis of LINC00941 and *MTA2* repression during keratinocyte differentiation. Calcium-induced, differentiated keratinocytes showed decreasing LINC00941 and *MTA2* mRNA levels compared to undifferentiated primary keratinocytes (day 0). Data are presented as mean ± standard deviation (*n* = 3-4).

Furthermore, previous research performed by Johannes Graf also confirmed declining MTA2 protein amounts in calcium-induced, differentiated keratinocytes through WB analysis[138]. Correlating expression patterns of both interaction partners thus suggested a functional relationship between LINC00941 and the NuRD complex.

Next, we conducted experiments to determine if MTA2 affects human epidermal homeostasis in a similar way as LINC00941. Therefore, siPool-mediated knockdown of MTA2 was performed. In organotypic epidermis (day 3 of differentiation), MTA2-deficient keratinocytes showed increased mRNA levels of the early differentiation gene keratin 1 and the late differentiation gene filaggrin (Figure 16A). Correspondingly, MTA2- and LINC00941-deficient keratinocytes, respectively, yielded comparable increased levels of both mRNA populations in organotypic epidermal tissue cultures (Figure 16B).

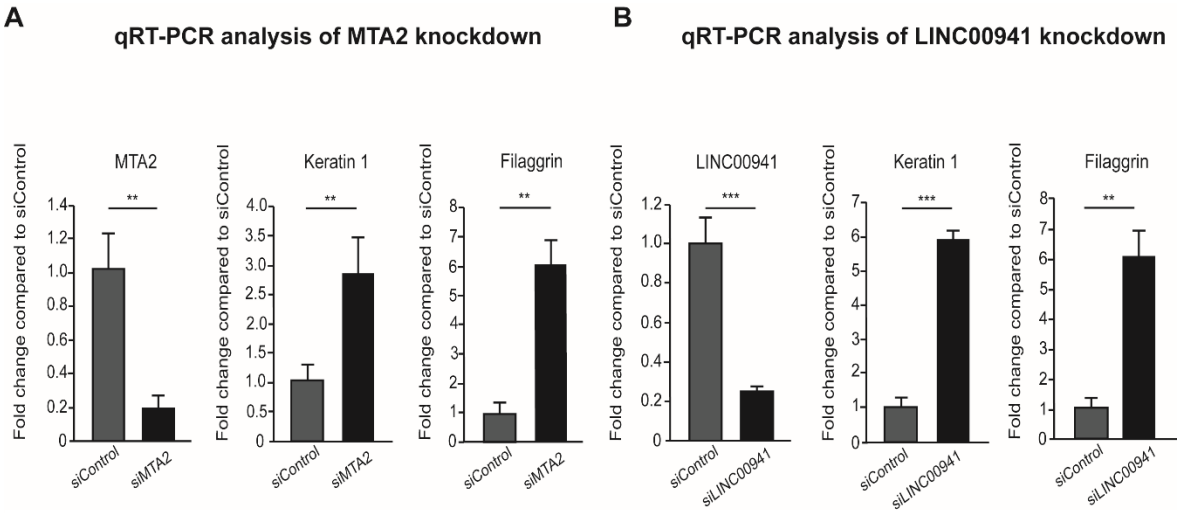

Figure 16: qRT-PCR analysis of either MTA2 or LINC00941 knockdown.
SiPool-mediated knockdown of (A) MTA2 and (B) LINC00941, respectively, resulted in increased mRNA levels of early and late differentiation markers keratin 1 and filaggrin on day 3 of differentiation in organotypic epidermis (*n* = 3-5 tissue cultures/knockdown group). Data are presented as mean ± standard deviation. Statistical significance was tested by an unpaired *t*-test and corrected for multiple testing after Bonferroni (**adj. *P*-value < 0.01, ***adj. *P*-value < 0.001).

In agreement with these findings, both MTA2 and LINC00941 knockdown tissues, respectively, were found to show more advanced differentiation compared to control-treated organotypic epidermis in immunofluorescence (IF) analysis. This was indicated by increased protein abundances of the early differentiation marker keratin 10, co-expressed with keratin 1, and the late differentiation marker filaggrin (Figure 17).

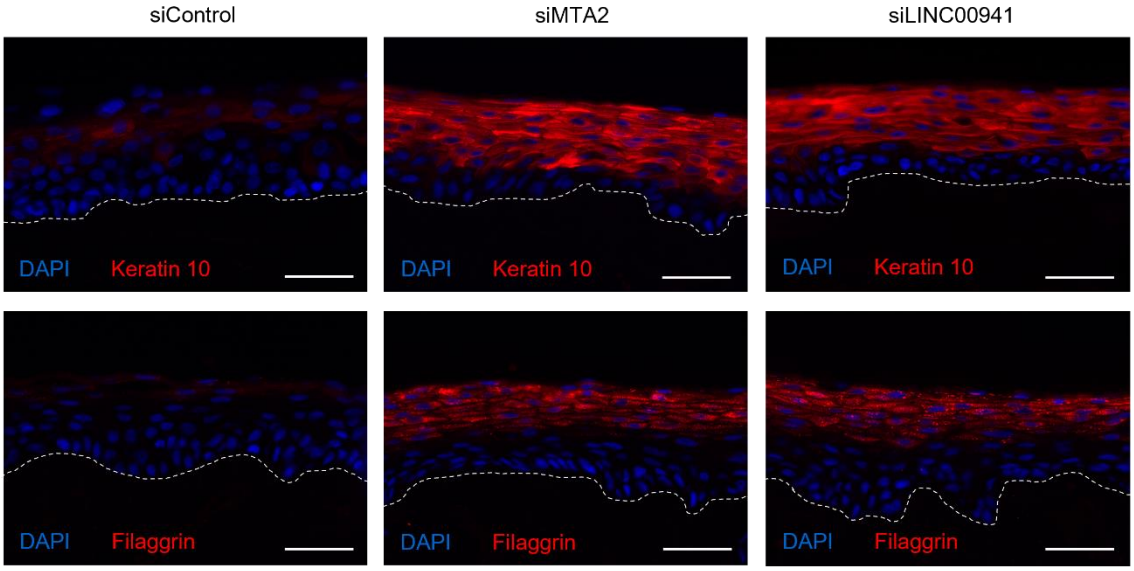

Figure 17: IF analysis showed increased levels of early and late differentiation proteins keratin 10 and filaggrin in either MTA2 or LINC00941knockdown tissue compared to control.
Dashed line indicates the basement membrane, nuclei are shown in blue, and the differentiation proteins keratin 10 and filaggrin are shown in red (*n* = 3-5 tissue cultures/knockdown group (day 3), one exemplary picture for each group is depicted). Scale bar: 100 µm.

To preclude the possibility that the increased mRNA and protein abundances of early and late differentiation markers were caused by increased proliferation rather than by premature and enhanced differentiation, we performed Ki-67 staining. However, no significant difference in Ki-67 positive cells between control, MTA2- and LINC00941-deficient cells could be detected (Figure 18).

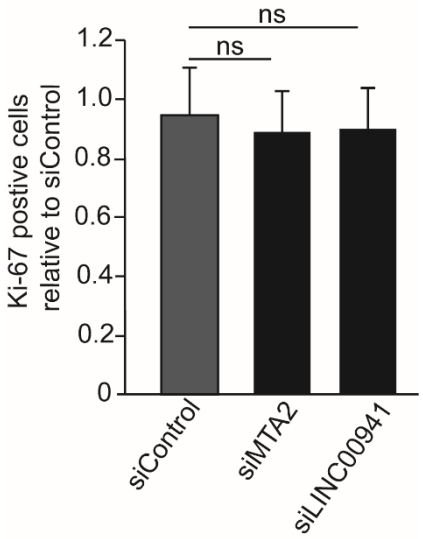

Figure 18: Proliferative potential of MTA2- and LINC00941-deficient keratinocytes. Ki-67 staining showed no significant altered proliferation of MTA2 and LINC00941 knockdown cells in comparison to control-treated keratinocytes (day 3 of organotypic epidermal tissue). Data are presented as ± standard deviation (*n* = 4-5). Statistical significance was tested by an unpaired *t*-test (ns = not significant).

Neither MTA2 nor LINC00941have an impact on the proliferative potential of keratinocytes but their role is limited to differentiation only. Therefore, a LINC00941-dependent role of MTA2/NuRD repressing premature onset of keratinocyte differentiation in human epidermal tissue was suggested as they were shown to interact.

4.2.3 Chromatin occupancy of MTA2/NuRD in human keratinocytes

To gain an overall impression of the putative impact of MTA2/NuRD in keratinocytes, chromatin immunoprecipitation (ChIP) sequencing data was of interest in this respect. However, since there was no published data on NuRD chromatin binding behavior in healthy human keratinocytes, we performed ChIP sequencing analysis using antibodies against MTA2. A total of 3,613 genome-wide MTA2/NuRD binding sites could be identified, which were highly reproducible between replicates

(appendix Figure 38A). Furthermore, an enrichment of MTA2/NuRD occupancy at promoter regions was revealed (Figure 19A and appendix Figure 38B). GO term analysis of NuRD-associated promoters revealed that corresponding genes primarily regulate cell fate commitment, as well as other morphogenic and developmental processes (Figure 19B and appendix Figure 38C). Interestingly, these terms also comprise important regulators of keratinocyte development and differentiation such as *EPHA2*, *MAFB* and *SOX9*.

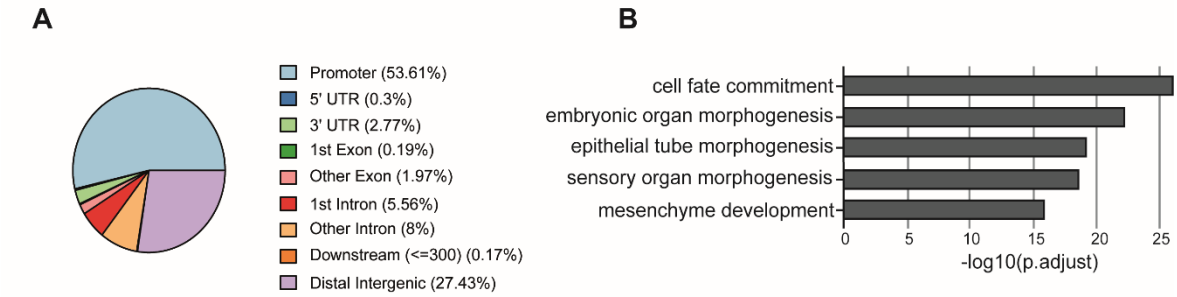

Figure 19: MTA2/NuRD occupies regulatory regions in keratinocytes.
(A) Pie chart illustrating genomic region annotation of MTA2/NuRD binding sites, preferentially binding to promoter regions. The genome annotation of protein-coding genes was used. The promoter region was defined as +/- 1000 bp distance to TSS. (B) Top GO terms at MTA2/NuRD binding sites. The respective GO terms also included genes important for keratinocyte differentiation. GO term analysis was restricted to terms ≤ 250 and ≥ 350 genes.

To get a more comprehensive understanding of the chromatin context at MTA2/NuRD occupied sites, the epigenome roadmap chromatin state mode of primary keratinocytes was used[157]. Our findings revealed that MTA2/NuRD binds to various chromatin states at regulatory elements (Figure 20A). Specifically, we observed association between MTA2/NuRD and activated chromatin states such as active TSS (TssA, TssAFlnk) and enhancers (Enh, EnhG). Furthermore, MTA2/NuRD was also found to bind to repressed chromatin states (ReprPC) and to bivalent chromatin states including bivalent TSS and enhancers as well as related flanking regions (TssBiv, BivFlnk and EnhBiv) (Figure 20B).

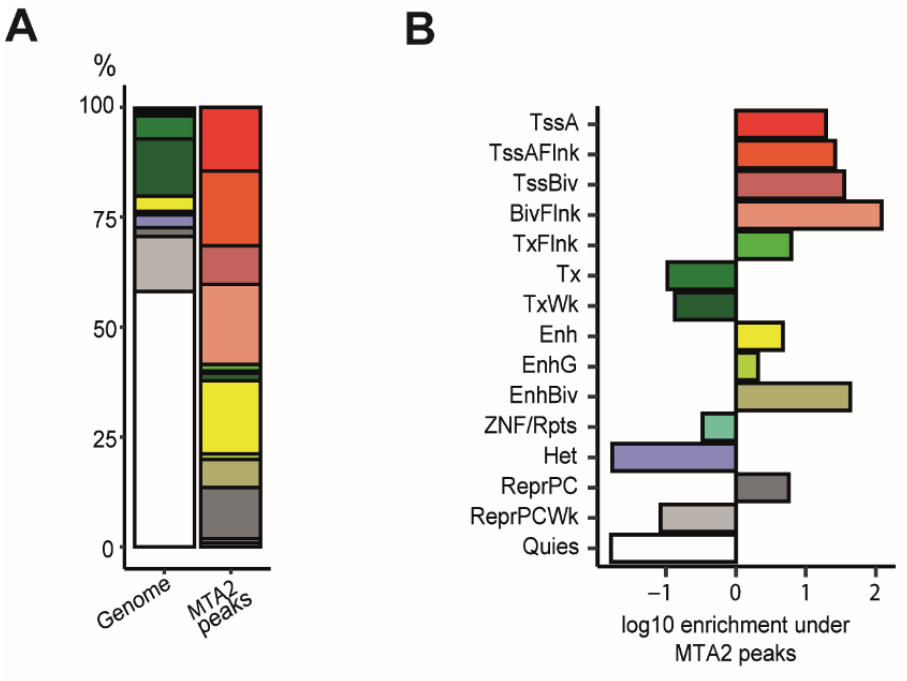

Figure 20: Chromatin states at MTA2/NuRD binding sites.
Bar plots illustrating the distribution of primary keratinocyte chromatin states at MTA2/NuRD binding sites. MTA2/NuRD showed preferred binding behavior to active, repressed, and bivalent chromatin states. (A) Distribution of chromatin states over the whole genome (left bar) and at the MTA2 binding sites (left bar). (B) Chromatin state enrichment at MTA2 binding sites shown as the log10 fold-change of the respective chromatin state against the whole genome distribution. Abbreviations: Tss = Transcription Start Site; A = Active; Flnk = Flanking; Biv = Bivalent; Tx = Transcription; Wk = Weak; Enh = Enhancer; G = Genic; Rpts = Repeats; Het = Heterochromatin; Repr = Repressed; PC = Polycomb; Quies = Quiescent.

A more detailed analysis of some representatives of those different chromatin states confirmed the versatile chromatin binding behavior of MTA2/NuRD. The membrane-associated protein *ESYT3* locus represented an example for a bivalent MTA2/NuRD occupancy. This locus harbored both active (H3K27ac, H3K4me and H3K4me3) and repressive (H3K27me3) histone marks at the MTA2-bound site, resulting in hardly any expression of *ESYT3* in undifferentiated human keratinocytes (Figure 21).

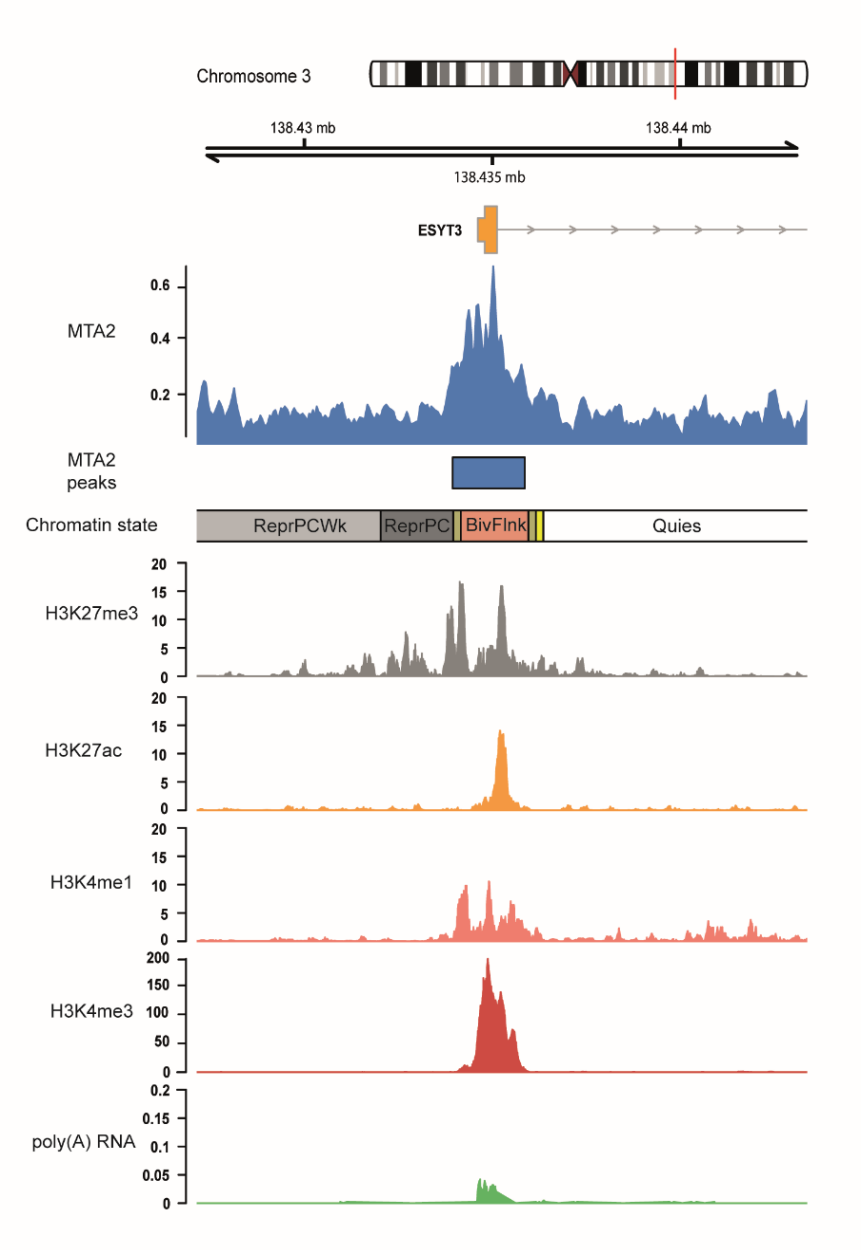

Figure 21: MTA2/NuRD binds bivalent chromatin states.
Genome browser view of *ESYT3* – a bivalent gene locus. Tracks of chromatin states, histone modifications, and transcription in primary keratinocytes obtained from roadmap (accession: E057) are shown below the MTA2 ChIP sequencing tracks.

A typical example for MTA2/NuRD occupancy within an activated chromatin site region (TssA, TssAFlnk) is observed at the *PCDHGC3* locus, which codes for an adhesion protein. In this region, only activating and no repressive histone marks were detected. This resulted in the expression of *PCDHGC3* in undifferentiated human keratinocytes (Figure 22).

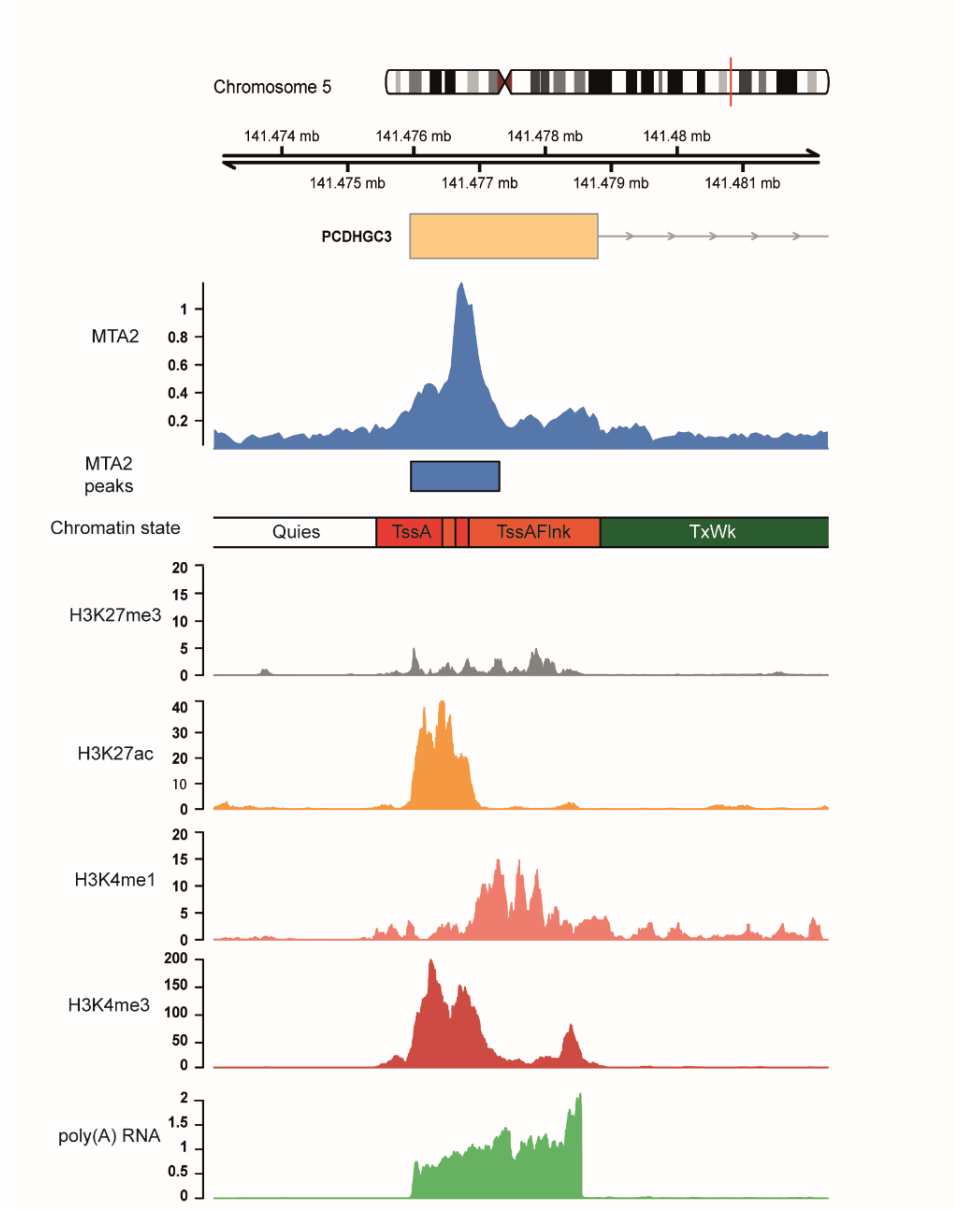

Figure 22: MTA2/NuRD binds active chromatin states.
Genome browser view of *PCDHGC3* – an active gene locus. Tracks of chromatin states, histone modifications, and transcription in primary keratinocytes obtained from roadmap (accession: E057) are shown below the MTA2 ChIP sequencing tracks.

These findings emphasized the significance of the NuRD complex as a versatile epigenetic regulator associating with various chromatin states at regulatory elements in healthy primary human keratinocytes. Accordingly, it was suggested that this binding behavior is partially influenced by LINC00941, as this lncRNA and the NuRD complex were shown to interact.

4.2.4 MTA2/NuRD-mediated regulation of LINC00941 expression

As LINC00941 was demonstrated to interact with MTA2/NuRD, it was hypothesized that NuRD might also regulate LINC00941 gene expression. A close examination of the LINC00941 locus revealed MTA2/NuRD occupancy. Similar to *PCDHGC3*, this specific locus only harbors activating histone marks (H3K27ac, H3K4me1 and H3K4me). Correspondingly, it is associated with activated chromatin sites (TssA, TssAFlnk) and the expression of LINC00941 can be detected in undifferentiated keratinocytes (Figure 23).

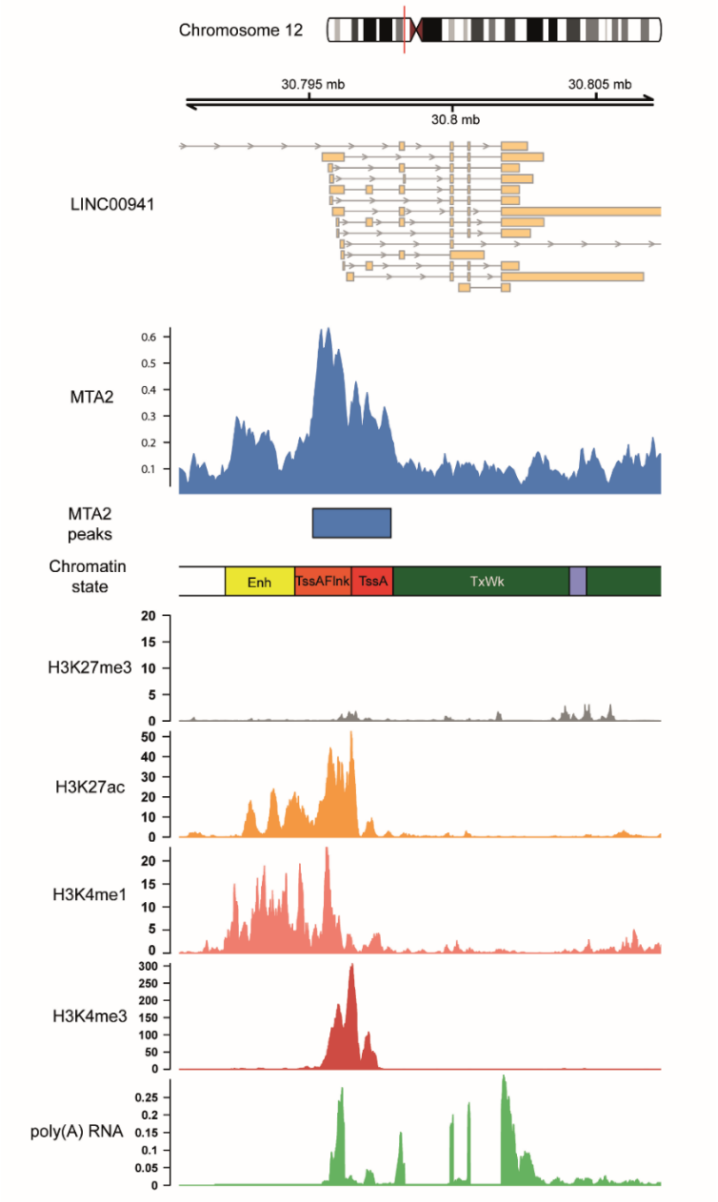

Figure 23: MTA2/NuRD binds the LINC00941 locus.
Genome browser view of LINC00941 – an active gene locus. Tracks of chromatin states, histone modifications, and transcription in primary keratinocytes obtained from roadmap (accession: E057) are shown below the MTA2 ChIP sequencing tracks.

To further investigate the impact of MTA2/NuRD on LINC00941 expression, we performed siPool-mediated MTA2 knockdown. Subsequent qRT-PCR analysis of MTA2-deficient undifferentiated keratinocytes indeed resulted in less but not significantly decreased LINC00941 levels (Figure 24A). However, in organotypic epidermal tissues (day 3 of differentiation), MTA2-deficient cells showed severely reduced LINC00941 abundances compared to control-treated cells (Figure 24B).

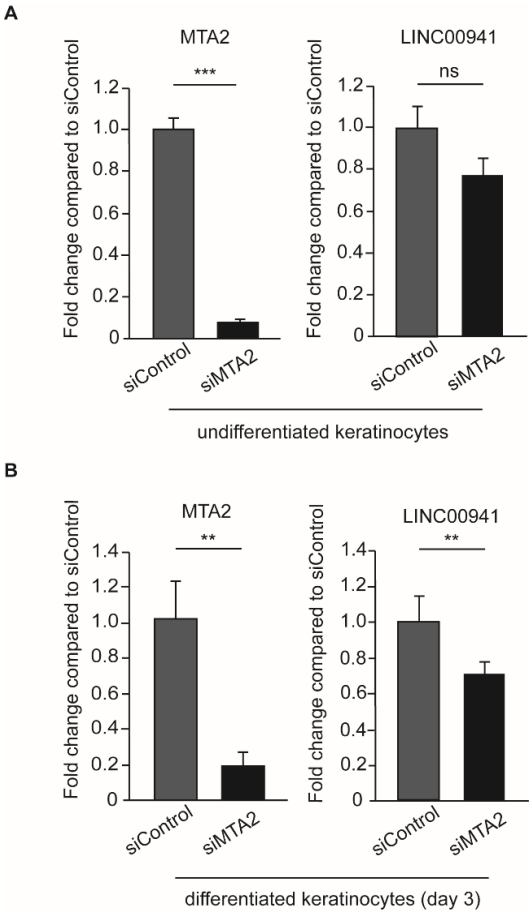

Figure 24: qRT-PCR analysis of LIN00941 levels in MTA2-deficient keratinocytes.
(A) Knockdown of MTA2 resulted in decreased abundances of LINC00941 in undifferentiated keratinocytes (day 0). (B) In differentiated keratinocytes of organotypic epidermal tissues (day 3), knockdown of MTA2 caused significantly reduced LINC00941 levels (n = 3-5 tissue cultures/knockdown group). Data are presented as mean ± standard deviation. Statistical significance was tested by an unpaired t-test and corrected for multiple testing after Bonferroni (***adj. P-value < 0.001, **adj. P-value < 0.01, ns = not significant).

Even though ChIP sequencing detected MTA2/NuRD occupancy at the promoter region of LINC00941, aforementioned qRT-PCR analysis suggested a more complex and dynamic regulatory control of LINC00941 expression. This may include, for example, the involvement of other transcriptional regulators at the *LINC00941* gene locus – at least in undifferentiated keratinocytes.

4.2.5 LINC00941 dependency of MTA2/NuRD chromatin binding

Since the interaction between NuRD and lncRNA LINC00941 has been demonstrated along with their similar functions in human primary keratinocytes, it has been hypothesized that LINC00941 influences epigenetic regulation of epidermal differentiation genes by modulating MTA2/NuRD activity. Therefore, we performed ChIP sequencing with LINC00941-deficient and control-treated, undifferentiated keratinocytes to examine the dependency of MTA2/NuRD chromatin binding on the presence of LINC00941. Analysis of differential occupancy revealed 33 significantly altered MTA2/NuRD binding sites upon LINC00941 knockdown (Figure 25A and appendix Table 28). Furthermore, most of these differential occupied chromatin sites were found to be located within promoter regions (67%) (Figure 25B). This strengthened the assumption that LINC00941 acts as regulator of transcription through MTA2/NuRD.

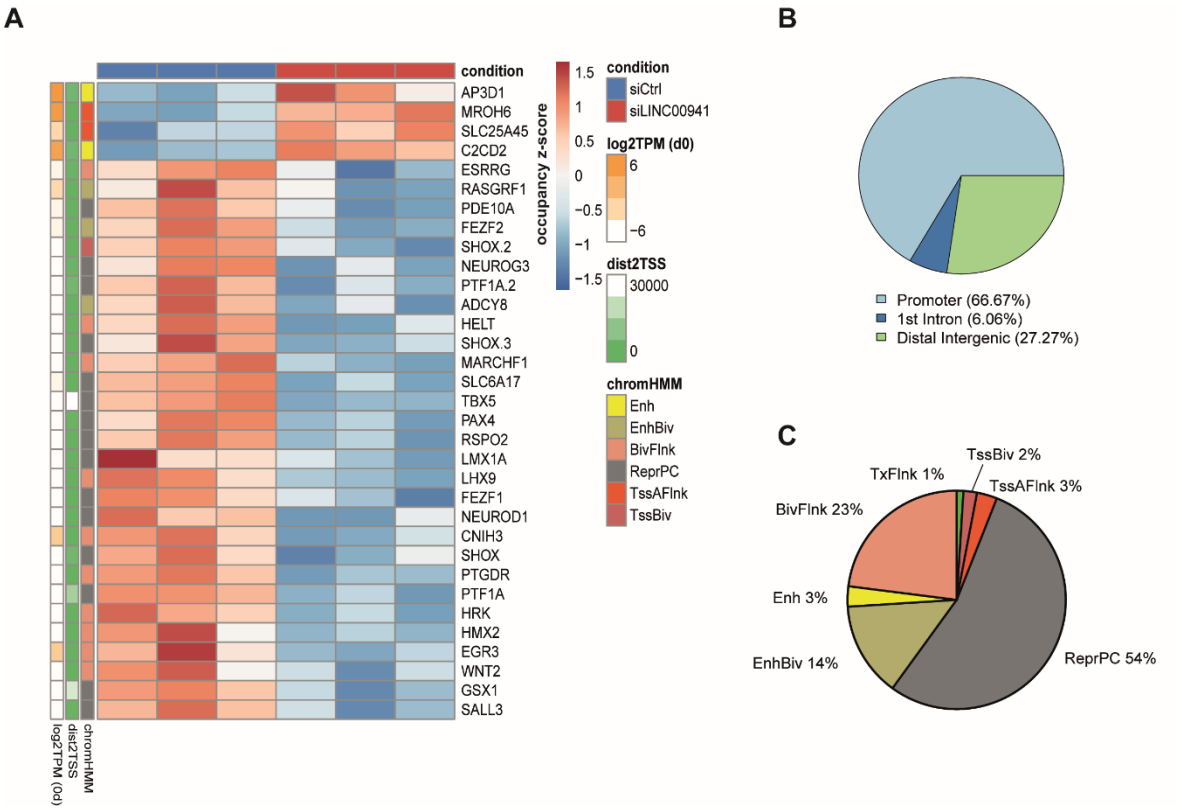

Figure 25: LINC00941 alters MTA2/NuRD chromatin occupancy.
(A) Heatmap illustrating differential MTA2/NuRD-bound sites upon LINC00941 knockdown (*n* = 33 at FDR of 5%). Z-score of normalized fragment counts under differential MTA2/NuRD binding sites are indicated by the color code. Associated chromatin state (chromHMM), distance to TSS (dist2TSS) and expression level (log2(TPM) at day 0) in primary keratinocytes of associated genes are indicated on the left site. (B) Pie charts showing the distribution of differential MTA2 peaks at genomic features or (C) chromatin states. The promoter region was defined as +/- 1000 bp distance to the TSS of protein-coding genes.

The majority of the differential MTA2/NuRD occupied sites were annotated as Polycomb repressed (ReprPC) and bivalent (EnhBiv, BivFlnk, TssBiv) chromatin states. These regions were marked with the corresponding histone modifications such as the repressive histone mark H3K27me3 (ReprPC) (Figure 25C). This finding aligns with the known function of NuRD to enhance PRC2 binding and PRC2-catalyzed H3K27 trimethylation at bivalent chromatin sides[158].

Consistent therewith, most of the 33 associated genes were either not or hardly transcribed in undifferentiated primary keratinocytes. Among these, 29 differential MTA2/NuRD occupied target sides showed severely reduced MTA2/NuRD occupancy in LINC00941-deficient cells compared to control-treated cells. This implies that LINC00941 facilitated MTA2/NuRD complex binding in these cases and promoted PRC2-mediated transcriptional repression. However, 4 out of 33 altered MTA2/NuRD binding sites were associated with active chromatin states. Correspondingly, these genes (*AP3D1*, *MROH6*, *SLC25A45* and *C2CD2*) were expressed in undifferentiated keratinocytes. This finding suggested enhanced MTA2/NuRD binding in LINC00941-deficient cells indicating that the LINC00941/MTA2/NuRD complex does not bind to these target genes and thus allows their transcription.

Interestingly, many of the genes associated with differential MTA2/NuRD occupancy were transcriptional regulators, some of which are also known to be involved in differentiation processes. Therefore, we hypothesized that the expression of transcriptional activators was suppressed in the presence of LINC00941/MTA2/NuRD in undifferentiated keratinocytes. As the levels of LINC00941 and MTA2/NuRD diminish during differentiation, their expression was subsequently initiated to enable transcription of their downstream targets suggested to be involved in epidermal differentiation processes.

4.2.6 EGR3 expression is regulated by LINC00941/MTA2/NuRD

To test the aforementioned hypothesis that LINC00941/MTA2/NuRD regulates the expression of transcriptional regulators, of which at least one was suggested to influence keratinocyte differentiation, we analyzed whether MTA2/NuRD-associated target genes exhibit dynamic expression changes during keratinocyte

differentiation. Additionally, we investigated whether the knockdown of LINC00941 affects the transcription of these genes. Apart from a carrier protein (SLC25A45) (appendix Figure 39B), the transcription factor EGR3 met both criteria and displayed the most pronounced dynamic change in expression levels during keratinocyte differentiation, compared to SLC25A45 (Figure 26).

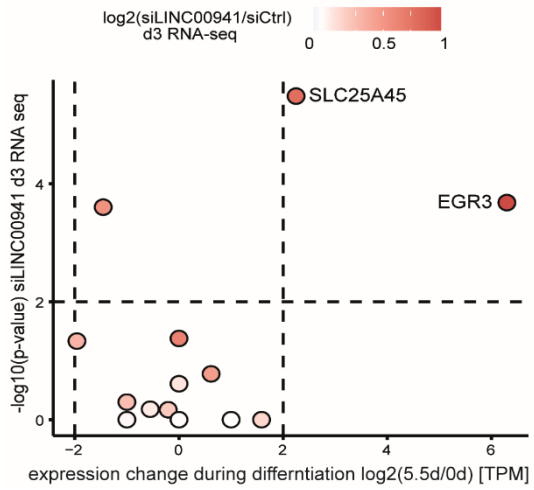

Figure 26: Scatter plot of MTA2-associated genes showing expression change upon keratinocyte differentiation and LINC00941 knockdown.
EGR3 showed the strongest changes upon both LINC00941 knockdown and keratinocyte differentiation. TPM values of undifferentiated keratinocytes and day 5.5 of calcium-treated, differentiated keratinocytes were obtained from ENCODE (day 0: ENCFF423MWU; day 5.5: ENCFF379PNP). RNA sequencing data of LINC00941-deficient cells (day 3) were obtained from Ziegler et al.[113].

To gain a deeper understanding of the *EGR3* transcriptional regulation, we conducted a more detailed analysis of the chromatin states at this gene locus (Figure 27). Interestingly, we found that *EGR3* is initially annotated as a bivalent and repressed site (ReprPC, TssBiv), respectively, up to and including day 2.5 of calcium-induced differentiated keratinocytes. However, by day 5.5, this site is associated with an active chromatin state (Enh, TssA). These findings were further supported by publicly available ChIP sequencing data of histone modifications and RNA sequencing data of calcium-treated differentiated keratinocytes from ENCODE. The repressive H3K27me3 histone modification was most prevalent in undifferentiated keratinocytes up to day 2.5 but declined as differentiation progresses. On the other hand, the activating histone mark H3K27ac increased over time. Correspondingly, RNA sequencing data revealed the presence of *EGR3* mRNA at day 5.5 of differentiation in keratinocytes. Hence, these findings suggested

that the LINC00941/MTA2/NuRD complex binds to the *EGR3* gene locus in undifferentiated keratinocytes thereby repressing its expression. However, as both MTA2 as well as LINC00941 levels decline over time, *EGR3* transcription is consequentially allowed to occur.

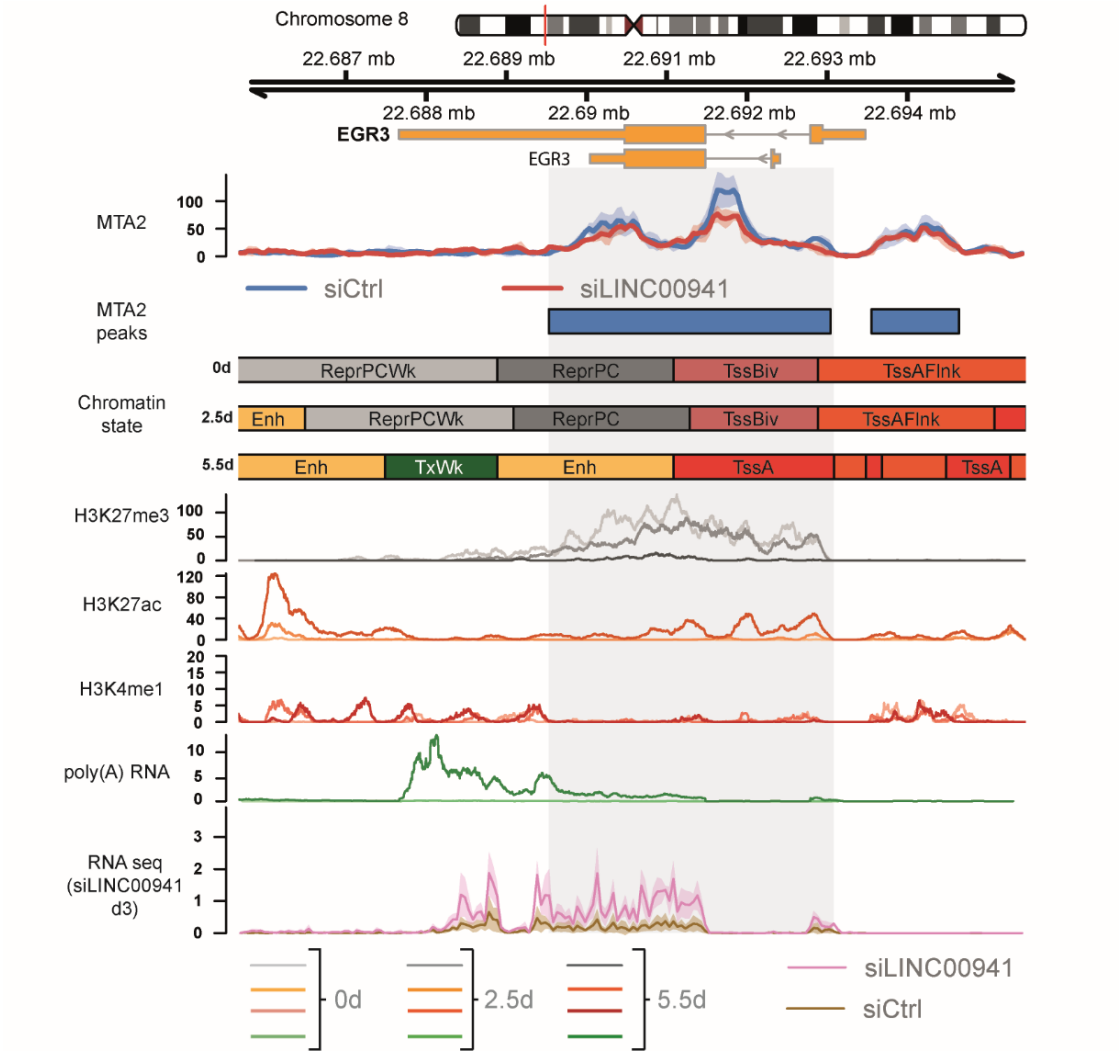

Figure 27: Genome browser view of differential MTA2 binding site at *EGR3* locus.
EGR3 showed bivalent chromatin states in non- and poorly differentiated keratinocytes but active chromatin states as differentiation progression. Correspondingly, *EGR3* is not expressed in undifferentiated keratinocytes but it is transcribed as differentiation progresses. Tracks of chromatin states, histone modifications, and transcription in primary undifferentiated (day 0) and calcium-treated differentiated (day 2.5, day 5.5) keratinocytes obtained from ENCODE portal are shown below the MTA2 ChIP sequencing tracks. Color shades of histone modifications and RNA sequencing tracks indicate the time points of differentiation (light = day 0, middle = day 2.5, dark = day 5.5). The bottom track shows the RNA sequencing coverage of siLINC00941 knockdown and control keratinocytes after 3 days of differentiation. RNA sequencing data of LINC00941-deficient cells (day 3) were obtained from Ziegler et al.[113].

Based on this finding, siPool-mediated knockdown of LINC00941 led to premature increase of *EGR3* abundance in organotypic epidermis (day 3 of differentiation) (Figure 28), which is hypothesized to accelerate keratinocyte differentiation.

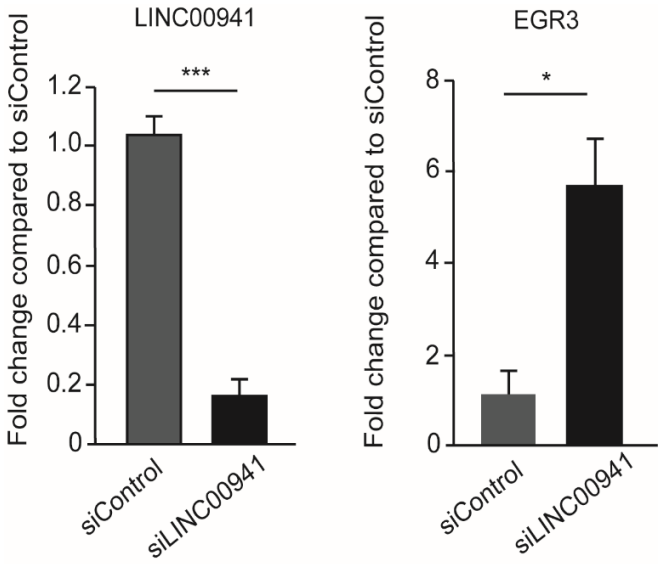

Figure 28: qRT-PCR analysis of decreased *EGR3* levels in LINC00941-deficient cells. SiPool-mediated knockdown of LINC00941 resulted in decreased abundance of *EGR3* in differentiated organotypic epidermal tissue (day 3) (*n* = 3-5 tissue cultures/knockdown group). Data are presented as mean ± standard deviation. Statistical significance was tested by an unpaired *t*-test and corrected for multiple testing after Bonferroni (***adj. *P*-value < 0.001, *adj. *P*-value < 0.05).

In conclusion, our study demonstrated that in association with MTA2/NuRD, LINC00941 acts as a repressor of the *EGR3* gene locus in undifferentiated progenitor keratinocytes. We further suggested that as LINC00941 levels decrease over time, onset of keratinocyte differentiation is triggered by EGR3 and its downstream targets.

4.2.7 EGR3 promotes keratinocyte differentiation

The aforementioned assumption regarding the involvement of EGR3 in keratinocyte differentiation was recently confirmed by Kim et al. (2019) as they studied the functional impact of EGR3 on epidermal homeostasis[159]. In addition to genes involved in late keratinocyte differentiation, Kim et al. identified 20 EGR3-regulated genes showing increased expression in calcium-induced differentiated keratinocytes, reduced abundance in EGR3 knockdown cells and co-expression with *EGR3*. To verify the hypothesis that LINC00941-dependent decrease of MTA2/NuRD binding at the *EGR3* locus affected its expression and thus its function, we performed an overlap between LINC00941 knockdown RNA sequencing data and the 20 EGR3-regulated genes identified by Kim et al. (Figure 29A). All these

genes known to be regulated by EGR3, showed increased abundance in LINC00941-deficient, organotypic epidermal tissue cultures. Interestingly, these genes were transcribed on day 2 and 3, respectively, in LINC00941 knockdown cells even though their normal expression was not observed until day 5.5 in calcium-treated differentiated keratinocytes (Figure 29B). These findings strongly indicate a transcriptional dependency of these EGR3-regulated genes on LINC00941.

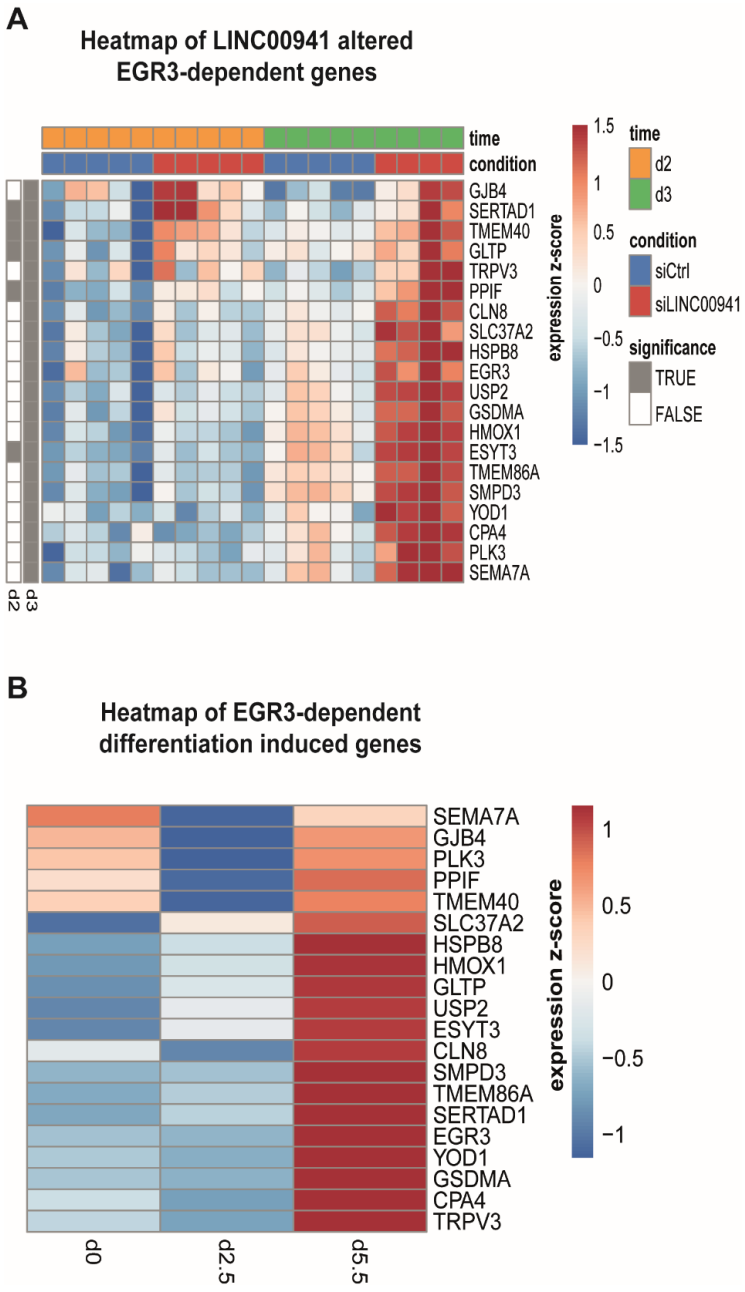

Figure 29: EGR3-regulated genes in keratinocyte differentiation.
(A) Heatmap showing transcriptional changes of *EGR3* and EGR3-regulated genes in keratinocyte differentiation upon LINC00941 knockdown. EGR3-regulated genes were selected based on the study of Kim et al. (2019)[159]. RNA sequencing data of LINC00941-deficient keratinocytes were obtained from Ziegler et al. (2019)[113]. (B) Heatmap illustrating transcriptional changes of *EGR3* and EGR3-regulated genes in calcium-induced differentiated keratinocytes. TPM expression values after day 0, day 2.5 and day 5.5 of differentiation were obtained from ENCODE. EGR3-regulated genes were selected based on the study of Kim et al. (2019)[159].

To verify the functional impact of EGR3 in our model system for epidermal homeostasis, we generated organotypic epidermal tissue either using EGR3 knockdown or control-treated keratinocytes. Consistent with Kim et al., EGR3 deficiency resulted in significantly reduced mRNA levels of keratin 1 and filaggrin (Figure 30).

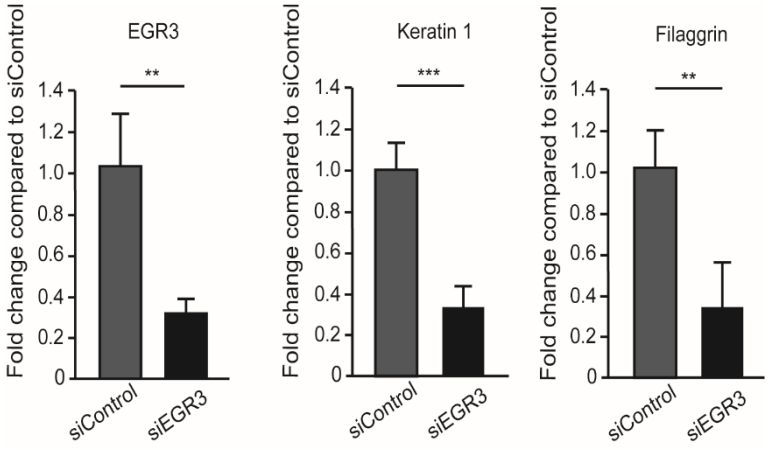

Figure 30: qRT-PCR analysis of decreased differentiation marker levels upon EGR3 knockdown. SiPool-mediated knockdown of EGR3 in primary keratinocytes resulted in decreased mRNA abundances of early and late differentiation markers keratin 1 and filaggrin on day 3 of differentiation in organotypic epidermal tissue (n = 4-6 tissue cultures/knockdown group). Data are presented as mean ± standard deviation. Statistical significance was tested by an unpaired t-test and corrected for multiple testing after Bonferroni (***adj. P-value < 0.001, **adj. P-value < 0.01).

Correspondingly, we found that the protein levels of early and late differentiation markers keratin 10 and filaggrin, respectively, were also reduced in the EGR3-deficient organotypic epidermis compared to control tissue (Figure 31).

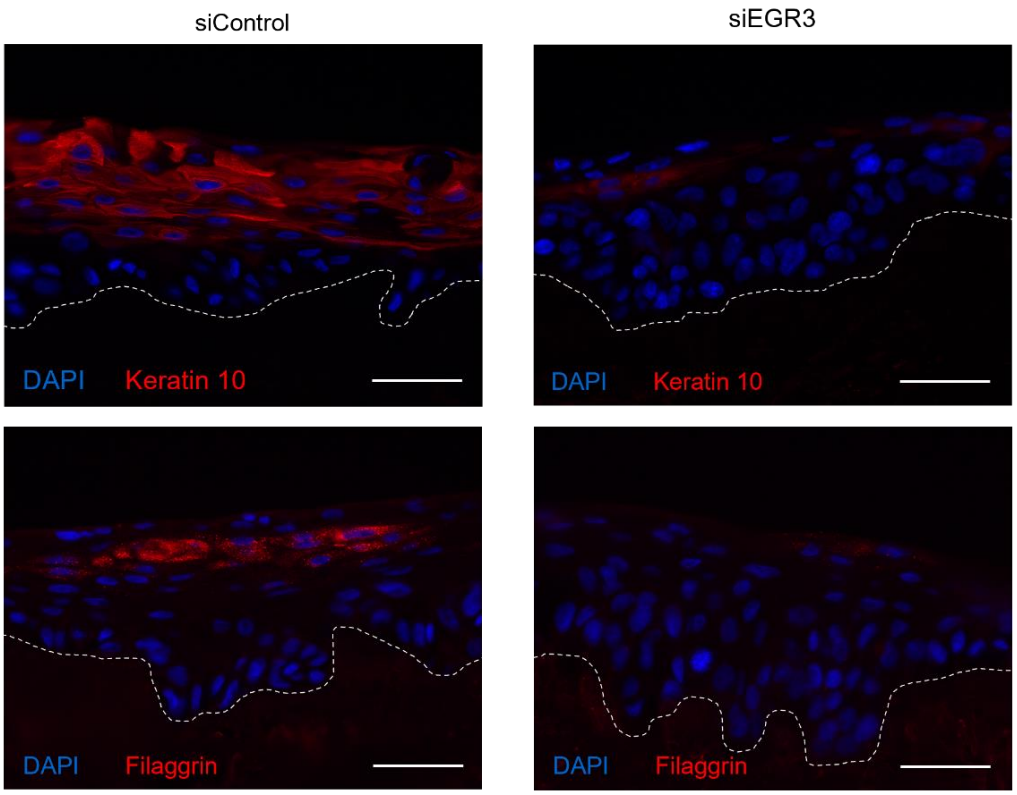

Figure 31: IF analysis showed decreased levels of early and late differentiation markers keratin 10 and filaggrin in EGR3 knockdown tissue compared to control.
Dashed line indicates the basement membrane, nuclei are shown in blue, and the differentiation proteins keratin 10 and filaggrin are shown in red (*n* = 4-6 tissue cultures/knockdown group (day 3), one exemplary picture for each group is depicted). Scale bar: 100 µm.

Furthermore, LINC00941-regulated late differentiation genes of the SPRR- and LCE-protein cluster located within the EDC showed reduced mRNA levels upon EGR3 knockdown (Figure 32). Thus, our study provides evidence of the significant role of EGR3 in promoting keratinocyte differentiation in human epidermal tissue. Additionally, EGR3 not only regulates EDC gene expression, but also affects the expression of early differentiation genes such as keratin 1 and keratin 10 which was not examined by Kim et al., who only focused on late differentiation markers.

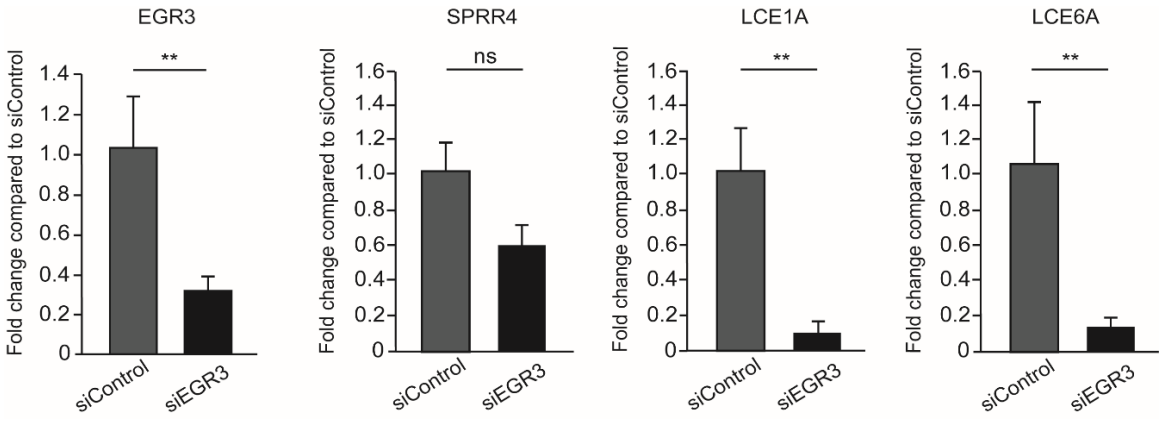

Figure 32: qRT-PCR analysis of EDC deregulated genes upon EGR3 knockdown.
SiPool-mediated knockdown of EGR3 in primary keratinocytes results in decreased abundances of EDC genes *SPRR4*, *LCE1A* and *LCE6A* on day 3 of differentiation in organotypic epidermal tissue (*n* = 3-4 tissue cultures/knockdown group). Data are presented as mean ± standard deviation. Statistical significance was tested by an unpaired *t*-test and corrected for multiple testing after Bonferroni (**adj. *P*-Value < 0.01, ns = not significant).

In conclusion, the mode of action of LINC00941 on transcriptional level can be explained as follows: Through association, LINC00941 modulates MTA2/NuRD chromatin binding behavior thereby controlling epidermal homeostasis. In non- and poorly differentiated keratinocytes, the LINC00941/MTA2/NuRD complex epigenetically represses *EGR3* transcription when bound to this gene locus. As keratinocyte differentiation progresses and LINC00941 abundances decrease, chromatin binding of NuRD is resolved and *EGR3* expression is triggered. In turn, EGR3 can thus activate transcription of its downstream targets which accelerate keratinocyte differentiation (Figure 33). These findings are supported by annotated chromatin states in keratinocytes. Including day 2.5 of keratinocyte differentiation, *EGR3* locus is annotated as bivalent and therefore, *EGR3* is repressed. As soon as bivalency is resolved (no later than day 5.5 of differentiation), supposedly because of the absence of the bivalency remodeler NuRD, *EGR3* is transcribed. However, since LINC00941 deficiency causes premature expression of *EGR3,* the bivalent state must be abolished earlier which may be due to the absence of the LINC00941-controlled NuRD complex. The results of this project, thus provide an explanation for altered histone modifications and transcriptional regulation, respectively, in LINC00941-deficient keratinocytes, as chromatin binding of NuRD (e.g. to *EGR3*) depends on the presence of LINC00941.

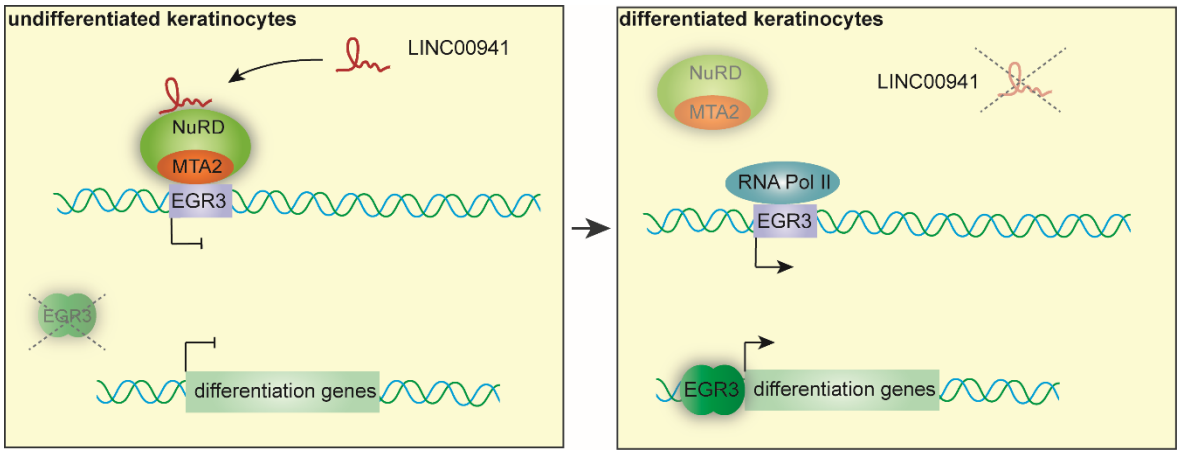

Figure 33: Scheme of predicted LINC00941 mechanism regulating NuRD.
Interaction of LINC00941 with the MTA2/NuRD complex modulates its binding to chromatin, thus repressing *EGR3* expression in non- and poorly differentiated keratinocytes. During keratinocyte differentiation, LINC00941 and MTA2 abundances decrease and *EGR3* is actively transcribed. In turn, EGR3 activates expression of its downstream differentiation genes and consequentially keratinocyte differentiation is accelerated.

4.3 Role of LINC00941 in E2F6-mediated transcriptional regulation

4.3.1 Interaction between LINC00941 and E2F6

Apart from the chromatin remodeler NuRD, LINC00941 was also suggested to interact with further transcriptional regulators as shown by Johannes Graf. Previous motif analysis of promoter-associated LINC00941 ChIRP sequencing peaks revealed the E2F6 binding motif as well as the binding motif of its heterodimeric binding partner TFDP1[138]. Based on this, we suggested that LINC00941 might also regulate gene expression through its association with E2F6. To test this hypothesis, we first verified the interaction between LINC00941 and E2F6. RNA-IP with antibodies targeting E2F6 and subsequent qRT-PCR analysis to detect LINC00941 could confirm interaction between overexpressed LINC00941 and the transcription factor E2F6 in primary human keratinocytes (Figure 34).

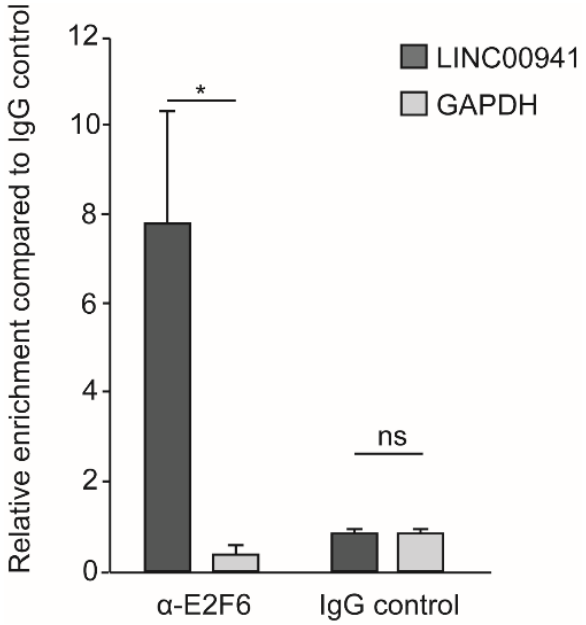

Figure 34: RNA-IP and subsequent qRT-PCR analysis verified interaction between E2F6 and overexpressed LINC00941.
Data are presented as ± standard deviation (*n* = 3). Statistical significance was tested by an unpaired *t*-test (*adj. *P*-value < 0.05, ns = not significant).

Consequently, verified interaction between LINC00941 and E2F6 indicated a LINC00941-mediated role in transcriptional regulation through modulating the activity of this transcription factor during keratinocyte differentiation.

4.3.2 E2F6 suppresses keratinocyte differentiation

As LINC00941 and E2F6 were shown to interact, a functional relevance of this association was suggested. Therefore, we proceeded to test whether E2F6 has a similar impact on human epidermal homeostasis as LINC00941. SiPool-mediated knockdown of E2F6 in organotypic epidermal tissue showed increased mRNA levels of keratin 1 and filaggrin on day 4 of differentiation (Figure 35).

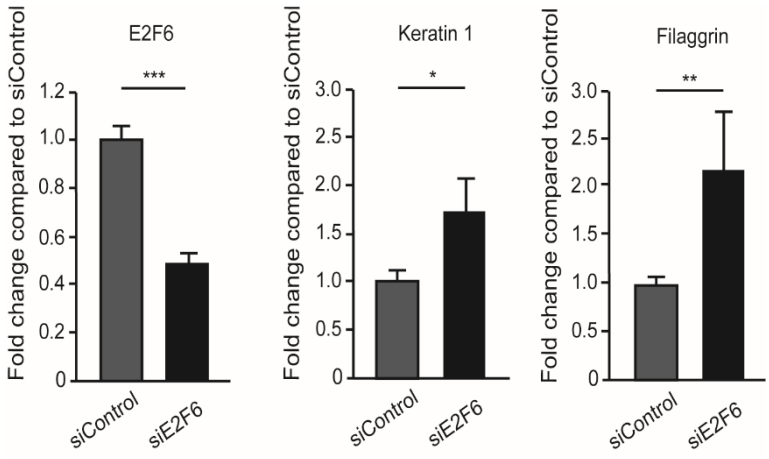

Figure 35: qRT-PCR analysis of decreased differentiation marker levels upon E2F6 knockdown. SiPool-mediated knockdown of E2F6 in primary keratinocytes resulted in decreased mRNA abundances of early and late differentiation markers keratin 1 and filaggrin on day 4 of differentiation in organotypic epidermal tissue (*n* = 3-5 tissue cultures/knockdown group). Data are presented as mean ± standard deviation. Statistical significance was tested by an unpaired *t*-test and corrected for multiple testing after Bonferroni (***adj. *P*-value < 0.001, **adj. *P*-value < 0.01, *adj. *P*-value < 0.05).

Further analysis on protein level revealed that E2F6-deficient tissues also exhibited premature and enhanced differentiation compared to control-treated keratinocytes. This was indicated by increased abundances of keratin 10 and filaggrin, representatives of early and late differentiation markers, shown in IF analysis (Figure 36).

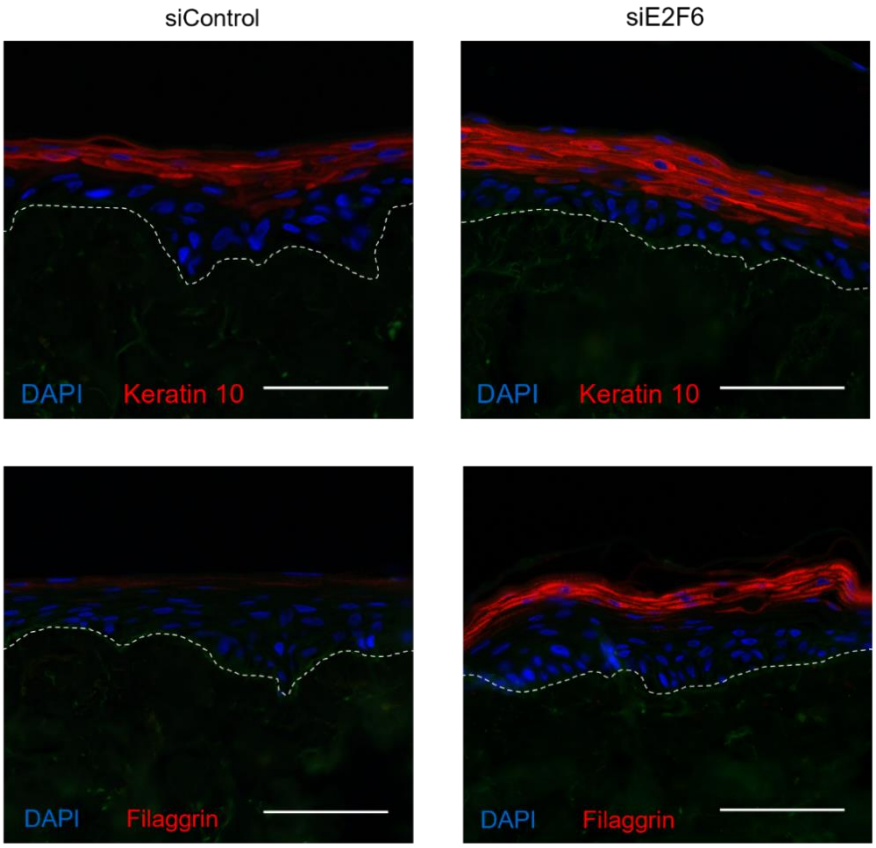

Figure 36: IF analysis showed decreased levels of early and late differentiation markers keratin 10 and filaggrin in E2F6 knockdown tissue compared to control.
Dashed line indicates the basement membrane, nuclei are shown in blue, and the differentiation proteins keratin 10 and filaggrin are shown in red (*n* = 3-5 tissue cultures/knockdown group (day 4), one exemplary picture for each group is depicted). Scale bar: 100 µm.

Correspondingly, E2F6 knockdown keratinocytes showed – similar to LINC00941 knockdown tissues (Figure 16B) – increased mRNA and protein levels of early and late differentiation markers. To analyze the impact of E2F6 on the proliferative potential of human primary keratinocytes, we performed Ki-67 staining of E2F6 knockdown cells. The results showed no significant difference in Ki-67 positive cells between E2F6 knockdown and control-treated keratinocytes (data not shown). These findings suggested a role of E2F6 acting as a negative regulator of keratinocyte differentiation similar to LINC00941. As E2F6 interacts with this lncRNA, it is further hypothesized, that this function of E2F6 is at least partially controlled by LINC00941.

4.3.3 Chromatin occupancy of E2F6 in human keratinocytes

Since LINC00941 and the transcription factor E2F6 interact and both appear to repress premature onset of keratinocyte differentiation, we suggested that LINC00941 controls the modulation E2F6 activity. Therefore, we examined the impact of LINC00941 deficiency on E2F6 binding to chromatin by performing ChIP sequencing with LINC00941-deficient and control-treated keratinocytes using antibodies targeting E2F6. In order to get a deeper understanding of the chromatin binding behavior of E2F6, we first identified genome-wide E2F6 occupancy sites (*n* = 616). Comparable to MTA2/NuRD ChIP sequencing, an enrichment of E2F6 binding within promoter regions was observed (Figure 37).

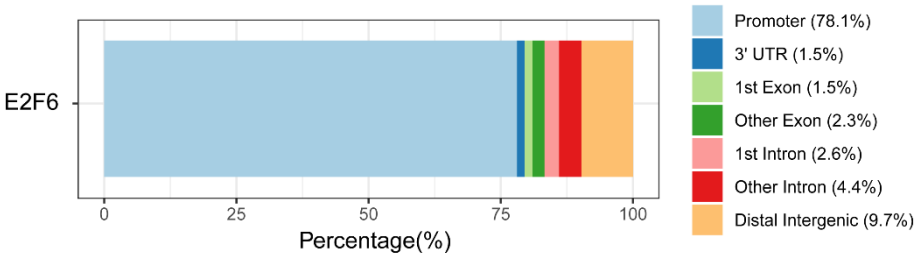

Figure 37: E2F6 preferentially occupies promoter regions in keratinocytes.
Bar plot illustrating genomic region annotation of E2F6 binding sites. The promoter region was defined as +/- 1000 bp distance to TSS.

Due to lacking sensitivity of the α-E2F6 antibodies, significant differences between LINC00941 knockdown and control-treated keratinocytes could not be observed. However, analysis of genome-wide E2F6 chromatin occupancy revealed overlapping gene loci with RNA sequencing data from LINC00941-deficient cells. These loci include genes known to be involved in keratinocyte differentiation such as *ELOVL3*, *RPSAP58*, *KRT31*, *RNF227* and the EDC gene *TCHH*. Therefore, it is suggested that E2F6 regulates transcription of genes that show altered expression upon LINC00941 knockdown.

Moreover, some of the E2F6-associated chromatin binding sites were also found to be occupied by MTA2/NuRD (*n* = 47). Interestingly, an in-depth analysis using public GeneHancer data further showed that the majority of E2F6 occupied chromatin sites are not only known to be bound by NuRD subunits but also by Polycomb group (PcG) protein components. This indicates a bivalent and repressive annotation at these gene loci. One example of this is *ESYT3*. *ESYT3* is not only found to be a bivalent and repressed chromatin-site bound by MTA2/NuRD and therefore

harboring both activating and repressive chromatin marks (Figure 21). Additionally, it is also bound by E2F6 and by PcG proteins – as shown in this project and as stated by GeneHancer, respectively.

These findings suggested a paramount interplay between E2F6 and the NuRD complex in a LINC00941-dependent manner modulating gene expression on a global level. Correspondingly, all three macromolecules might have an influence on human epidermal homeostasis. It is currently hypothesized that interactions of LINC00941 with both transcriptional regulators NuRD and E2F6, respectively, ultimately result in repression of genes which are involved in keratinocyte differentiation. While this project confirmed LINC00941-dependency of NuRD activity, evidence for E2F6 still has to be provided. However, first indications could already be shown for a LINC00941-controlled mechanism of E2F6 modulating transcription in keratinocytes.

5 Discussion and outlook

5.1 LncRNA LINC00941 as putative ceRNA

To shed light on an unknown mechanism of a given lncRNA, its cellular localization provides an initial indication. In case of LINC00941, previous work by former members of our group have demonstrated an equal distribution between nucleus and cytoplasm in healthy human keratinocytes[113]. The subcellular localization in the cytoplasm is commonly associated with functions on post-transcriptional level such as modulation of protein and mRNA stability, respectively, which have already been demonstrated to be mediated by LINC00941[123,160]. Furthermore, there is ample empirical evidence of LINC00941 acting as ceRNA sequestering miRNAs in various cancer tissues[131,132,144,145].

Based on these findings further supported by public AGO2 CLIP sequencing data suggesting interaction between LINC00941 and miRNAs, it was hypothesized that LINC00941 functions as ceRNA, titrating away miRNAs to influence keratinocyte differentiation and epidermal homeostasis, respectively. This hypothesis was strengthened by other known lncRNA-miRNA interactions that modulate differentiation processes such as muscle cell differentiation and bone marrow mesenchymal stem cell differentiation[101,161].

To this end, the respective miRNA was identified during this project. Bioinformatically predicted to bind LINC00941, miR-335-5p was demonstrated to be present in differentiated and undifferentiated human primary keratinocytes compared to other putative LINC00941-interacting miRNAs. Interestingly, miR-335-5p has recently been implicated in epidermal processes such as in diabetic wound healing and in skin barrier defects of atopic dermatitis[152,162]. Furthermore, knockdown of LINC00941 causes a phenotype comparable to atopic dermatitis. This is supported by RNA sequencing data of LINC00941-deficient keratinocytes because genes deregulated upon LINC00941 knockdown are associated with genes differentially expressed in atopic dermatitis (appendix Figure 42).

Therefore, we needed to prove binding between LINC00941 and miR-335-5p. As there are no methods to verify direct interaction *in vivo* and to clearly demonstrate downstream effects of a miRNA/lncRNA association, indirect approaches were used to examine the role of LINC00941 as ceRNA[116]. One approach involved RNA-IP

using antibodies that target AGO2, followed by qRT-PCR to detect LINC00941. This procedure was considered applicable because it its hypothesized that miRNAs are only present in cytoplasm when bound by AGO2[116]. Another method of choice to confirm direct association between a miRNA and a lncRNA, at least *in vitro*, is the Dual Luciferase Reporter assay. Both approaches, RNA-IP targeting AGO2 and Dual Luciferase Reporter assays provided evidence of an interaction between LINC00941 and miR-335-5p.

Furthermore, we examined downstream effects of LINC00941 putatively titrating away miR-335-5p by comparing the miR-335-5p target mRNAs and the genes that were deregulated upon LINC00941 knockdown. Consistent with the ceRNA hypothesis, shared genes were mostly downregulated in LINC00941-deficient cells. This finding supports the suggestion that upon LINC00941 knockdown, corresponding mRNAs were degraded through miR-335-5p binding as this miRNA is not bound by LINC00941 anymore. Taken together, the evidence indicates LINC00941/miR-335-5p association and correlating functionality but the final proof *in vivo* is still pending.

In addition to prove the direct interaction of both molecules *in vivo*, knowing the stochiometric relationship between LINC00941, miR-335-5p and the affected downstream target mRNAs would be of great importance to assess the LINC00941-mediated impact and “sequestering power”, respectively. However, as this is technically very challenging, other approaches should be considered such as miRNA knockdown and overexpression as well as rescue experiments. To accurately assess the stochiometric ratio, not only the numerical distribution of both molecules should be taken into account, but also the number of miRNA binding sites within a respective lncRNA molecule. The Dual Luciferase Reporter assay used in this study revealed only one miRNA-335-5p binding region within exon 5 of LINC00941, because it appeared to be the energetically most favorable out of three tested regions. However, it should be considered that there are many more miR-335-5p binding sites predicted in this project which could be tested. It should also be assumed that there are binding sites that have not yet been recognized. Current research suggests that miRNA/lncRNA binding behaves identical to miRNA/mRNA interaction through seed sequences, but this has not yet been examined. Considering other non-canonical seed sequence base paring patterns could

putatively reveal further miRNA binding sites within a given lncRNA. Thus, its role as ceRNA acting as an effective “sponge” would be supported. In line with this, elucidating the secondary and tertiary structure of a given lncRNA molecule is crucial as its folding affects binding of proteins and other RNA molecules, including miRNAs[163].

Furthermore, previous reports have only described LINC00941 acting as ceRNA in diseased tissue, which should also be considered for further analysis. Generally, LINC00941 has been found to be overexpressed in cancer tissue shifting the stochiometric balance towards putative enhanced miRNA sequestration. Consequentially, this has been shown to influence proliferative and invasive potential of cancer cells as well as their ability to migrate, also for LINC00941[116]. These findings led to the hypothesis that LINC00941 sequestering miR-335-5p should not only be considered in healthy human keratinocytes, but rather in epidermal diseases such as atopic dermatitis. Recapitulating the obtained insights, LINC00941 – a suppressor of keratinocyte differentiation[113] – was found to putatively interact with miR-335-5p, a miRNA proven to activate keratinocyte differentiation[152]. Moreover, RNA sequencing of LINC00941-deficient keratinocytes has been able link deregulated genes to atopic dermatitis. Therefore, it is important to assess the abundance of LINC00941 in atopic dermatitis to determine whether decreased LINC00941 levels might affect the defective epidermal barrier of atopic dermatitis through deregulated sequestering of miR-335-5p. Interestingly, the opposite effect has recently been reported in PC: LINC00941 expression levels are increased in PC cells causing enhanced LINC00941-mediated binding of miR-335-5p. This in turn leads to increased *ROCK1* mRNA populations finally promoting cancer progression[114].

The data obtained from this study and putative future projects investigating the role of LINC00941 as ceRNA binding miR-335-5p in human epidermal tissues, especially in atopic dermatitis, could offer new approaches for the development of lncRNA-based therapeutics in skin diseases. So far, intradermal injection of miR-335-5p mimics into diabetic rat wounds has been shown to accelerate wound repair as these mimics inhibited translation of target downstream mRNAs that negatively affect wound healing[162]. If deregulated LINC00941 levels were found to affect atopic dermatitis through a malfunctioning ceRNA-mediated mechanism, LINC00941

mimics could be considered as therapeutic agents titrating away enhanced miR-335-5p molecules. Correspondingly, this might result in a less pronounced defective skin barrier.

5.2 LINC00941-dependent transcriptional regulation of NuRD

Apart from a putative ceRNA mechanism of LIN00941 titrating away miR-335-5p in the cytoplasm, a LINC00941-mediated regulation at the transcriptional level was also hypothesized as this lncRNA is also present in the nucleus[113]. Moreover, previous reports have already identified LINC00941-mediated transcriptional regulation in both cis and trans, but these functions have only been identified in cancer tissues of OSCC and ESCC[115,117]. Correspondingly, it was necessary to elucidate putative interaction partners and modes of action to understand the role of LINC00941 in healthy primary human keratinocytes.

MS analysis and RNA-IP revealed that the NuRD complex is an interaction partner of LINC00941. Therefore, we suggested that NuRD-mediated epigenetic regulation of differentiation gene expression might in part be controlled by LINC00941. To test this hypothesis, we performed ChIP sequencing of undifferentiated LINC00941-deficient and control-treated keratinocytes, respectively. The results confirmed that the presence of LINC00941 is necessary for NuRD occupancy: We could show that LINC00941/NuRD binds gene loci of various transcription factors, such as *EGR3*, causing their repression. EGR3 is a transcription factor which positively regulates the transcription of genes involved in epidermal differentiation. Upon LINC00941 knockdown, EGR3 and its downstream targets showed premature expression and synthesis, respectively, inducing premature keratinocyte differentiation.

The NuRD complex, which has been shown to regulate *EGR3* expression in association with LINC00941, is a major regulator of transcription in cells. It combines both ATP-dependent chromatin remodeling and histone deacetylase activities. It consists of multiple subunits but its exact composition varies depending on cell type and state, respectively[164]. Common NuRD components include the ATP-dependent chromatin-remodeler CHD3/4, the histone deacetylases HDAC1/2, the methylated CpG-binding domain proteins 1 and 2 (MBD1/2), histone binding proteins RBBP4/7, assembly proteins GATAD2A/B as well as metastasis-associated factors 1-3 (MTA1-3)[164–166]. Since several subunits of the NuRD complex, such as HDAC2,

RBBP4 and RBBP7 can also be found in other multi-protein complexes including Extra Sex Combs/Enhancer of Zeste (ESC/E(Z)), NuRF and Sin3[153–155], this project focused on MTA2, a core subunit unique to the NuRD complex[156,167]. Even though its precise function is still unresolved so far, some functional insights can be gained from its domains, which share similarities with domains of other known proteins. The SANT domain seems to interact with unmodified histone tails and histone deacetylases through direct interaction, while the BAH domain binds histone H3 and recognized H4K20me2, respectively. Another known domain of MTA proteins is GATA which has been found to interact with specific DNA sequences. Therefore, MTA proteins are currently suggested to be responsible for recruiting and assembling of other NuRD components at chromatin binding sites[167,168]. Interestingly, MTA2 as well as other NuRD components have been shown to play crucial roles in murine epidermal development[169–171]. Especially mice deficient of MTA2 showed defective epidermal differentiation similar to the phenotype observed in LINC00941-deficient cells of human keratinocytes[113]. In this project, knockdown of MTA2 confirmed these findings in human keratinocytes as MTA2-deficient organotypic epidermal tissues also showed premature onset of keratinocyte differentiation, replicating the results seen in mice[170].

Even though its main function is to remodel chromatin, the NuRD complex is also involved in maintaining genomic stability, such as repairing DNA damages and facilitating DNA replication, respectively, providing a new layer of NuRD-mediated mechanisms[167]. Additionally, it was previously believed that NuRD solely acts as a transcriptional repressor. However, it has been discovered that the chromatin remodeling activity of NuRD goes beyond this role because it can also activate gene expression[172–174]. These findings are supported by the MTA2/NuRD ChIP sequencing data obtained from primary human keratinocytes during this project. The data showed that MTA2/NuRD can bind to active, repressed, and bivalent chromatin states in promoter regions consequentially activating or repressing gene expression of a target gene locus. Bernstein et al. (2006) were the first describing bivalent chromatin states as they discovered nucleosomes marked with repressing H3K27me3 and activating H3K4me3 at the same time in mouse embryonic stem cells. They also identified the presence of these bivalent histone modifications in close proximity to non- and poorly expressed developmental transcription factor

genes. However, these repressed or rather poised regions resolved during embryonic stem cell differentiation[175]. Correspondingly, it was proposed that developmental genes are kept silenced but poised through bivalent histone modifications, which allows rapid activation or silencing during embryonic stem cell differentiation. However, this hypothesis has been revised since bivalent domains have not only been identified in mouse and human embryonic stem cells but also in mammalian adult stem cells and adult tissues including human keratinocytes[176–178]. Therefore, bivalent chromatin states are now commonly seen as a way of transcriptional fine-tuning to prevent unscheduled gene activation or repression providing robustness and plasticity while reducing expression noise during repression. This property is especially crucial during cell fate decisions and cell development, respectively[179].

The most prominent protein complexes responsible for establishing and maintaining bivalency are PRC1 and PRC2[180]. Even though it remains largely unclear how these PcG proteins are recruited to the respective chromatin site, it is hypothesized that specific DNA elements, transcription factors and ncRNAs are involved[179]. However, it is also known by now that the NuRD complex is involved in this process, acting as a counterpart to the PcG protein complexes. NuRD deacetylates H3K27, allowing subsequent PRC2-dependent H3K27 trimethylation in cell development and differentiation processes[158,173,181,182]. As a result, NuRD controls the sensitive equilibrium between acetylation and methylation of histones influencing gene expression during cell fate decisions.

Summarizing the obtained results, it has been shown for the first time in human keratinocytes, that depending on a lncRNA – lncRNA LINC00941 – MTA2/NuRD binds at bivalent chromatin domains in close proximity to transcriptional regulators such as the transcription factor coding gene *EGR3*. This finding suggested that LINC00941 plays a role in maintaining bivalency through modulating NuRD binding behavior: *EGR3* repression is normally maintained in non- and poorly differentiated keratinocytes until bivalency is removed through unknown external factors. However, as LINC00941 and MTA2 abundances decrease upon differentiation, the bivalent *EGR3* locus is resolved. Knockdown of LINC00941 leads to premature synthesis of EGR3, a transcription factor important for keratinocyte differentiation, indicating an early removal of the bivalent status. This supports the hypothesis of

LINC00941-dependent control of bivalency at *EGR3*. It has also been verified that EGR3 influences keratinocyte differentiation through regulation of early and late differentiation marker genes, including EDC genes. Therefore, LINC00941/NuRD does not directly alter the chromatin state of EDC genes as originally suggested by the former lab member Johannes Graf but indirectly through EGR3[138]. In addition to directly regulating differentiation genes, Johannes Graf also hypothesized that LINC00941/NuRD might control EDC gene expression through binding and regulating enhancer 923[138]. Enhancer 923 was recently discovered to be located between the LCE and SPRR locus within the EDC, which is important for the onset of epidermal differentiation[183]. However, LINC00941/NuRD-dependent regulation of enhancer 923 was disproved by ChIP sequencing of LINC00941 knockdown and control-treated keratinocytes because no altered binding was demonstrated at the enhancer 923 locus. It is important to emphasize that LINC00941 does not directly regulate the expression of differentiation genes. Instead, LINC00941 acts through a higher-level mechanism involving EGR3, allowing far-reaching influence of gene expression on a global level with a limited number of LINC00941 molecules.

The precise mechanism by which LINC00941 mediates the recruitment and modulation of activity of the NuRD complex is not yet known. However, CLIP sequencing experiments have revealed CHD4 as the actual ncRNA-binding subunit of NuRD[184]. Previous reports have also observed this finding for the lncRNA PAPAS, which interacts with CHD4/NuRD. PAPAS tethers to a purine-rich region of a target enhancer region forming a DNA-RNA triplex. Furthermore, protein-RNA interaction studies as well as unraveling the secondary structure of PAPAS have demonstrated that an adenine-rich region of PAPAS recruits the N-terminal part of CHD4, thus confirming interaction between this lncRNA and CHD4[185]. A similar recruitment process for LINC00941 and NuRD could also be conceivable for *EGR3* expression regulation, but future projects will need to validate this assumption.

The MTA2 ChIP sequencing approach of LINC00941 knockdown and control-treated cells, could show that MTA2/NuRD chromatin occupancy is partially controlled by LINC00941. However, there are still some unanswered questions and additional approaches are needed to fully understand the LINC00941/NuRD mechanism. First of all, ChIP sequencing should be performed to analyze repressing and activating histone modifications, respectively, in both LINC00941-

deficient and control-treated keratinocytes. This would help to confirm the current results and to determine if there are indeed any changes in bivalency upon LINC00941 knockdown. Even though technically very challenging these experiments should not only be performed in undifferentiated keratinocytes but also with differentiated keratinocytes at various time points to confirm the dynamic and premature resolution of the bivalent state.

As the NuRD complex consist of multiple subunits, it would be beneficial to perform ChIP sequencing experiments for other NuRD components, particularly CHD4. This is because Johannes Graf showed that *CHD4* mRNA levels are also repressed during keratinocyte differentiation, similar to LINC00941 and MTA2. Additionally, since CHD4 is known to directly bind lncRNAs, obtaining comparable results with a CHD4 ChIP sequencing experiment would support the findings of this project. This approach can be further complemented by conducting CHD4 CLIP sequencing.

Another aspect that has yet to be considered is the secondary structure of LINC00941. As developing accurate methods for probing RNA secondary structure including PARS, SHAPE, LIGR and SPLASH progresses, they should be utilized to unravel the folding of LINC00941[186]. Knowing the secondary structure of LINC00941 would help to uncover the respective NuRD subunit interacting with this lncRNA, similar to PAPAS. PAPAS not only represents a lncRNA that interacts with the NuRD complex but it also demonstrates the connection between structure and function of lncRNAs[163,185].

To strengthen the presented results, additional replicates of LINC00941 ChIRP sequencing should be performed. Previous work by Johannes Graf has detected a ChIRP sequencing peak for LINC00941 at the *EGR3* locus[138]. Moreover, conducting LINC00941/EGR3 rescue experiments could provide another approach to test the connection and dependency, respectively, between LINC00941 and EGR3. This would support the mechanism proposed in this project, which suggests that LINC00941-controlled *EGR3* transcription regulates epidermal homeostasis in human keratinocytes.

5.3 LINC00941-mediated regulation of E2F6 activity

Former initial ChIRP sequencing approaches of undifferentiated keratinocytes have also revealed E2F6 and its heterodimerization partner TFDP1 as putative LINC00941-associated proteins[138]. In order to verify this interaction, we performed RNA-IP using antibodies targeting E2F6 and subsequent qRT-PCR analysis. The association between LINC00941 and E2F6 could be confirmed, and the functional interaction was further investigated by generating E2F6-deficient organotypic human epidermis. E2F6 knockdown keratinocytes showed increased mRNA and protein abundances of early and late differentiation markers similar to LINC00941- and MTA2-deficient tissue cultures, respectively. Correspondingly, these findings indicated that the LINC00941/E2F6 complex plays a role in repressing premature onset of keratinocyte differentiation in human epidermal tissue.

The LINC00941-associated interaction partner E2F6 is a member of the E2F transcription factor family. They are known as pleotropic regulators of cell proliferation, differentiation, senescence, apoptosis, autophagy and DNA repair[187–191]. This wide range of functions is possible because the E2F family consists of several members. Encoded by eight genes, there are also several E2F isoforms arising from multiple TSS and alternative splicing variants increasing the complexity of E2F transcription factors[192–194]. Due to this complexity, E2Fs are divided into three sub-categories based on transcriptional functions and sequence homology: Activators (E2F1, E2F2, E2F3A), repressors (E2F3B, E2F4, E2F5 and E2F6) and atypical repressors (E2F7 and E2F8)[194]. While all E2F family members share a distinct DNA binding domain, other domains are less conserved. E2F1-6 have a dimerization domain for association with TFDP1 or TFDP2. Apart from interacting with TFDP family members, E2F1-5 can also bind pocket proteins (RB, p107 and p130) at their transactivation domain. Interestingly, E2F7 and E2F8 both lack dimerization and transactivation domains but instead, they possess two tandem DNA binding domains. Similar to E2F7 and E2F8, E2F6 does not bind pocket proteins but instead it can be bound by PcG proteins[192,194–197]. Correspondingly, E2F6 does not bind the canonical E2F consensus sequence but rather chromatin binding sites of PcG proteins[198].

PcG proteins are transcriptional regulators essential for maintaining stem cell identity but they also control dynamics and plasticity during stem cell

differentiation[199,200]. The PcG protein family comprises two multiprotein complexes, PRC1 and PRC2, which modify histones and silence target genes, respectively. PRC2 consists of three core components: EED, SUZ12 and EZH2 (or its homologue EZH1). EZH2 is the catalytically active subunit responsible for trimethylation of H3K27, which is the characteristic PRC2 histone mark[201,202]. The H3K27me3 mark then serves as docking site for CBX (CBX2/4/6/7/8), a core component of PRC1 which is then completed by other PRC1 subunits (PCGF1-6, PHC1-3, and RING1A/B). Subsequently, PRC1 catalyzes monoubiquitination (H2AK119ub1) through its E3 ligase RING1A/B[203,204]. Consequentially, the catalytic activity of PRC1 and PRC2, respectively, leads to gene repression in numerous ways including chromatin compaction, poised RNA polymerase II or SWI/SNF exclusion form promoters[200,205–207]. Apart from the wide range of the core components described above, the diversity of PRC1 and PRC2 is even greater than anticipated, especially when non-core subunits are also considered. Furthermore, PRC1 can be divided into canonical and noncanonical complexes. Noncanonical PRC1 complexes contain RYBP instead of CBX, which means they associate with different gene loci compared to canonical PRC1, as they are independent from CBX-mediated docking to H3K27me3[208–210]. Instead, noncanonical PRC1 recruitment involves the association with sequence-specific DNA-binding proteins such as FBXL10 and E2F6[200,211,212]. Recent reports have also questioned the central dogma of canonical PRC1 recruitment depending on PRC2 and the presence of H3K27me3 mark bound by CBX, respectively. Blackledge et al. have demonstrated the reversed way – PRC1-mediated recruitment of PRC2 – but the exact process remains the subject of current research[213]. Apart from a putative PRC1-dependency of PRC2 chromatin binding, PRC2 has a preference for CpG islands close to the TSS, which is mediated by co-purified proteins JARID2 and AEBP2, both of which have a high affinity for CpG islands[214–217]. Furthermore, sequence-specific transcription factors like SNAIL and REST, as well as lncRNAs (e.g. XIST and HOTAIR) have been reported to recruit PRC2[82,218–220].

PcG proteins, however, do not function in isolation but are part of a regulatory network that involves other transcriptional regulators. Interestingly, the NuRD complex has been demonstrated to enhance PRC2 activity, as in absence of NuRD core components PRC2 recruitment and gene silencing are impaired due to the

H3K27ac mark not being removed by NuRD. As a result, PRC2 binding and activity, respectively, is blocked[221,222]. Instead, NuRD-mediated deacetylation of H3K27 facilitates PRC2 recruitment and subsequent trimethylation. Given the alternating acetylation and methylation steps also involving other proteins, these chromatin remodelers are crucial for maintaining bivalent chromatin sites, as described above, which leads to an overlap between NuRD and PcG gene loci[222]. Surprisingly, many E2F6 ChIP sequencing binding sites also overlap with bivalent MTA2/NuRD occupancy regions. Furthermore, a detailed analysis of E2F6-bound regulatory elements using GeneHancer supported this finding. It was observed that E2F6 often binds regions that are also associated with components of the NuRD and PcG protein complexes, respectively. This is significant because LINC00941 has been shown to alter the occupancy of the NuRD complex at bivalent target sites, and it has also been found to interact with E2F6. Based on these findings, it can be hypothesized that there is a common regulatory network involving LINC00941, NuRD, and E2F6 in maintaining bivalency.

The involvement of E2F6 in bivalent chromatin sites is further supported by its interaction with several components of the PcG complex. Instead of associating with pocket protein, E2F6 can act as a subunit of non-canonical PRC1, and it was also found to interact with EZH2 and SUZ12 of PRC2. This finding provides another explanation for the preferential PRC2 binding of CpG islands, as E2F6 also shows a high affinity towards these regions[198,223–226]. PcG proteins are primarily known for their role in maintaining stem cell identity. However, they have also been implicated in various mammalian differentiation processes, which supports the hypothesis of LINC00941-regulated involvement of PcG proteins, particularly those associated with E2F6, in epidermal homeostasis. In line with that, PcG proteins were not only shown to be involved in neuronal and skeletal muscle differentiation but also in epidermal differentiation processes[227–229]. Notably, studies by Ezhkova et al. and Sen et al. have shown an inverse correlation between EZH2 expression and the progress of embryonic keratinocyte differentiation. They could demonstrate a key function of EZH2 in controlling proliferative potential of undifferentiated progenitors by preventing recruitment of AP1, a transcriptional activator of genes required for epidermal differentiation[230,231]. In addition, PRC2-associated JARID2 also prevents premature onset of mammalian keratinocyte differentiation[232]. Yet another study

could prove that PRC1, like PRC2, is required for maintaining the undifferentiated state of basal epidermal cells through CBX4 regulating expression of CDKN2A, a modulator of cell cycle progress[233].

Summarizing the findings, it is suggested that LINC00941 plays a role in the regulation of bivalent chromatin sites in keratinocytes, thus controlling epidermal differentiation. This function may not only occur through NuRD, but also through PcG-associated E2F6. It is proposed that the interaction between LINC00941 and E2F6, their functional correlation as suppressors of keratinocyte differentiation, and the presence of overlapping E2F6, PcG and NuRD binding sites, suggest a pleotropic role of LINC00941 in epidermal homeostasis. Therefore, ChIP sequencing targeting E2F6-associated PcG proteins in LINC00941 knockdown and control-treated keratinocytes should be performed to verify this assumption. Furthermore, E2F6 CLIP and ChIP sequencing of both cell populations could provide insight into the potential mechanism of the LINC00941/E2F6 complex, but this is currently precluded due to the lack of suitable α-E2F6 antibodies that can detect subtle differences between LINC00941-deficient and control keratinocytes.

The obtained data about the LINC00941-mediated modes of action in epidermal differentiation revealed pleotropic functions of LINC00941 on both transcriptional and posttranscriptional level. Further analysis should focus on elucidating the secondary structure of LINC00941, as this knowledge could help to identify the specific LINC00941 interacting NuRD subunit. Understanding the role of this subunit in the LINC00941-dependent recruitment process of NuRD to chromatin, would provide valuable insights in the precise mechanism of this lncRNA acting as modulator of NuRD activity. Additionally, knowledge of the secondary structure could help to determine putative miR-335-5p binding sites. These new findings might be relevant for investigating skin diseases such as atopic dermatitis, where dysregulation of LINC00941 levels may occur. In such cases, it would be important to investigate the effects of deregulated LINC00941 levels on NuRD recruitment to chromatin and on miR-335-5p sequestration, respectively, to fully understand the impact of this lncRNA on human skin pathology.

6 Materials

6.1 Antibodies and beads

6.1.1 Antibodies

Table 2: List of primary antibodies

Name	Source	Dilution/ Amount	Application	Supplier
α-AGO2	Hybridoma 11A9	10 µg	IP	Meister Lab (Regensburg, Germany)
α-β-actin	mouse, monoclonal AC-15	1:10,000	WB	Abcam, ab6276
α-collagen VII	mouse, monoclonal LH7.2	1:800	IF staining	Merck, MAB1345
α-collagen VII	rabbit, polyclonal	1:400	IF staining	Merck, 234192
α-E2F6	rabbit, polyclonal	5 µg	ChIP/IP	Abcam, ab53061
α-Filaggrin	mouse, monoclonal	1:50	IF staining	Santa Cruz, sc-66192
α-Keratin 10	mouse, monoclonal	1:400	IF staining	Neomarkers, MS-611-P
α-Ki-67	rabbit, monoclonal	1:100	IF staining	Thermo Fisher, MA5-14520
α-MTA2	rabbit, polyclonal	5 µg	ChIP/IP	Abcam, ab8106
IgG control nonspecific	rabbit	5 µg	ChIP/IP	Santa Cruz, I5006

Table 3: List of secondary antibodies

Name	Source	Dilution	Application	Supplier
Alexa Fluor 488 goat α-rabbit IgG	goat, polyclonal	1:300	IF staining	Thermo Fisher, A11008
Alexa Fluor 488 goat α-mouse IgG	goat, polyclonal	1:300	IF staining	Thermo Fisher, A-11001
Alexa Fluor 555 goat α-rabbit IgG	goat, polyclonal	1:300	IF staining	Thermo Fisher, A21428
Alexa Fluor 555 goat α-mouse IgG	goat, polyclonal	1:300	IF staining	Thermo Fisher, A-21422
IRDye 680RD goat α-mouse IgG	goat, polyclonal	1:15,000	WB	LI-COR Biosciences, 926-68070
IRDye 800CW goat α-mouse IgG	goat, polyclonal	1:15,000	WB	LI-COR Biosciences, 926-32210
IRDye 800CW goat α-rabbit IgG	goat, polyclonal	1:15,000	WB	LI-COR Biosciences, 926-32211

6.1.2 Beads

Table 4: Overview of utilized beads

Name	Application	Supplier
Agencourt AMPure XP beads	ChIP	Beckman Coulter, A63880
Dynabeads™ Protein G	ChIP/IP	Thermo Fisher, 10004D

6.2 Buffers and solutions

All buffers and solutions mentioned were prepared with $_{dd}H_2O$ unless stated otherwise.

Table 5: Overview of utilized buffers and solutions

Buffer/Solution	Composition	
10% APS	10% (w/v)	ammonium persulfate (in $_{dd}H_2O$)

1x Demasking buffer	10 mM	sodium citrate
	0.05% (v/v)	Tween 20
		pH 6.0
2x RNA loading dye	20 mM	MOPS, pH 7.0
	5 mM	sodium acetate
	1 mM	EDTA
	5.9% (v/v)	formaldehyde
	45% (v/v)	formamide, deionized
	0.01% (w/v)	bromophenol blue
	5% (v/v)	glycerol
4x Resolving gel buffer	1.5 M	Tris
	0.4% (w/v)	SDS
		pH 8.8
4x Stacking gel buffer	0.5 M	Tris
	0.4% (w/v)	SDS
		pH 6.8
5x Laemmli Buffer	300 mM	Tris/HCl, pH 6.8
	10% (w/v)	SDS
	62.5% (v/v)	glycerol
	0.1% (w/v)	bromophenol blue
	10% (v/v)	β-mercaptoethanol, added fresh
20x SSC	3 M	sodium chloride
	0.3 M	sodium citrate
		pH 7.0
ChIP elution buffer	1% (w/v)	SDS
	50 mM	sodium bicarbonate
ChIP RIPA buffer	1% (v/v)	NP-40
	0.5% (w/v)	sodium deoxycholate
	0.1% (w/v)	SDS
	1 mM	EDTA
	1 mM	AEBSF, added fresh
	0.25%	RiboLock RNase Inhibitor (40 U/µl) (Thermo Fisher), added fresh
	1x	cOmplete, EDTA-free Protease

		Inhibitor Cocktail (Roche), added fresh filled up with PBS
ChIP swelling buffer	100 mM 10 mM 15 mM 1% (v/v) 1 mM 0.25% 1x	Tris, pH 7.5 potassium acetate magnesium acetate NP-40 AEBSF, added fresh RiboLock RNase Inhibitor (40 U/µl) (Thermo Fisher), added fresh cOmplete, EDTA-free Protease Inhibitor Cocktail (Roche), added fresh
ChIP wash buffer	100 mM 0.5 M 1% (v/v) 1% (w/v) 1 mM 0.25% 1x	Tris/HCl, pH 9.0 lithium chloride NP-40 sodium deoxycholate AEBSF, added fresh RiboLock RNase Inhibitor (40 U/µl) (Thermo Fisher), added fresh cOmplete, EDTA-free Protease Inhibitor Cocktail (Roche), added fresh
DNA loading dye	0.25% (w/v) 30% (v/v)	bromophenol blue glycerol
Firefly luciferase buffer	470 µM 530 µM 270 µM 20 mM 5.34 mM 0.1 mM 33 mM 	D-Luciferin ATP Coenzyme A Tricine magnesium sulfate-heptahydrate EDTA DTT pH 8.0
IP wash buffer	50 mM	Tris/HCl, pH 9.0

	300 mM	potassium chloride
	1 mM	magnesium chloride
	0.5%	NP-40
	0.25%	RiboLock RNase Inhibitor (40 U/µl) (Thermo Fisher), added fresh
LB medium	1% (w/v)	sodium chloride
	1% (w/v)	tryptone
	0.5% (w/v)	yeast extract
		pH 7.4, autoclaved before usage
LB-Amp	0.01% (w/v)	ampicillin
		added to LB medium after sterilization
LB-(Amp)agar	1.5% (w/v)	agar, dissolved in LB medium
	0.01% (w/v)	ampicillin
		added to LB agar after sterilization
NB 50x Denhardt's solution	1% (w/v)	albumin fraction V
	1% (w/v)	polyvinylpyrrolidone K30
	1% (w/v)	Ficoll 400
NB Hybridization solution	5x	SSC
	20 mM	sodium phosphate buffer, pH 7.2
	7% (w/v)	SDS
	1x	Denhardt's solution
NB RNA loading dye	100% (v/v)	formamide, deionized
	0.025% (w/v)	xylene cyanole
	0.025% (w/v)	bromophenol blue
NB Wash solution I	5x	SSC
	1% (w/v)	SDS
NB Wash solution II	1x	SSC
	1% (w/v)	SDS
PBS	140 mM	sodium chloride
	2.7 mM	potassium chloride
	10 mM	disodium phosphate
	1.8 mM	monopotassium phosphate
		pH 7.2
Protein lysis Buffer	25 mM	Tris/HCl, pH 7.5

	150 mM	sodium chloride
	5% (v/v)	glycerol
	2 mM	EDTA
	0.3% (w/v)	NP-40
	1 mM	DTT, added fresh
	0.25%	RiboLock RNase Inhibitor (40U/µl) (Thermo Fisher), added fresh
	1x	cOmplete, EDTA-free Protease Inhibitor Cocktail (Roche), added fresh
Renilla luciferase buffer	2 mM	EDTA
	220 mM	potassium phosphate buffer, pH 5.1
	0.44 mg/ml	BSA
	1.1 M	sodium chloride
	1.3 mM	sodium azide
		adjusted to pH 5.0 with potassium hydroxide
		filtered sterile through 0.2 µm pore filter
	0.1%	Coelenterazine (1000x)
RIPA	150 mM	potassium chloride
	25 mM	Tris, pH 7.5
	5 mM	EDTA
	0.5% (v/v)	NP-40
	0.5 mM	DTT, added fresh
	1 mM	AEBSF, added fresh
	0.25% (v/v)	RiboLock RNase Inhibitor (40U/µl) (Thermo Fisher), added fresh
	1x	cOmplete, EDTA-free Protease Inhibitor Cocktail (Roche), added fresh
RNA gel buffer	20 mM	MOPS
	5 mM	sodium acetate
	1 mM	EDTA
	1.9% (v/v)	formaldehyde
		pH 7.0

TAE buffer	8 mM	Tris
	0.2 mM	EDTA
	4 mM	acetic acid
TBS-T buffer	10 mM	Tris
	150 mM	sodium chloride
	0.02% (w/v)	Tween 20
TE buffer	10 mM	Tris
	1 mM	EDTA
		pH 8.0
TGS buffer	25 mM	Tris
	192 mM	glycine
	0.1% (w/v)	SDS
		pH 8.3
TFBI	30 mM	potassium acetate
	50 mM	manganese chloride
	100 mM	rubidium chloride
	10 mM	calcium chloride
	15% (v/v)	glycerol
		pH 5.8, filtered sterile through 0.2 µm pore filter
TFBII	10 mM	MOPS sodium salt
	75 mM	calcium chloride
	10 mM	rubidium chloride
	15% (v/v)	glycerol
		pH 7.0, filtered sterile through 0.2 µm pore filter
YT medium	0.8% (w/v)	tryptone
	0.5% (w/v)	yeast extract
	85 mM	sodium chloride
	20 mM	magnesium sulfate
	10 mM	potassium chloride
		pH 7.5, autoclaved before usage
WB transfer buffer	25 mM	Tris
	192 mM	glycine

20% (v/v)	methanol pH 8.6

6.3 Chemicals, enzymes, and peptides

Unless otherwise stated, chemicals were purchased from AppliChem (Darmstadt, Germany), Bio-Rad (Hercules, USA), Carl Roth (Karlsruhe, Germany), Merck (Darmstadt, Germany), Roche (Basel, Switzerland), Sigma-Aldrich (St. Lous, USA), Thermo Fisher (Waltham, USA) and VWR International (Radnor, USA).

Restriction enzymes, enzymes for RNA and DNA modifications (polymerases, ligases, etc.) and markers were purchased from Bio-Rad (Hercules, USA), Merck (Darmstadt, Germany), New England Biolabs (Ipswich, USA), Promega (Madison, USA), Roche (Basel, Switzerland) and Thermo Fisher (Waltham, USA). Radiochemicals were purchased from Hartmann Analytics (Braunschweig).

6.4 Commercial kits

Unless stated otherwise, commercial kits were used according to the manufacturer's manual.

Table 6: List of utilized commercial kits

Name	Supplier	Catalogue number
Agilent High Sensitivity D1000 ScreenTape and reagents	Agilent Technologies (Santa Clara, USA)	5067-5584, 5067-5585
DNase I, RNase-free	Thermo Fisher (Waltham, USA)	EN0521
Human Keratinocyte Nucleofector Kit	Lonza (Basel, Switzerland)	VVPD-1002
illustra MicroSpin G-25 Columns	GE Healthcare (Chalfont St. Giles, Great Britain)	27532501
iScript cDNA Synthesis Kit	Bio-Rad (Hercules, USA)	170-8890
Lipofectamine 3000	Thermo Fisher (Waltham, USA)	L3000015
NEBNext Multiplex Oligos for Illumina	New England Biolabs (Ipswich, USA)	E7335 (Set 1) E7500 (Set 2)

NEBNext Ultra II DNA Library Prep Kit for Illumina	New England Biolabs (Ipswich, USA)	E7645
NucleoBond Xtra Midi Kit	Macherey-Nagel (Dueren, Germany)	740410
NucleoBond Xtra Midi EF Kit	Macherey-Nagel (Dueren, Germany)	740422
NucleoSpin Gel and PCR Clean-up Kit	Macherey-Nagel (Dueren, Germany)	740609
NucleoSpin Plasmid Mini Kit (NoLid)	Macherey-Nagel (Dueren, Germany)	740499
QIAShredder	Qiagen (Hilden, Germany)	79654
QIAquick PCR Purification Kit	Qiagen (Hilden, Germany)	28106
Qubit dsDNA HS Assay Kit	Thermo Fisher (Waltham, USA)	Q32851
RNeasy Plus Mini Kit	Qiagen (Hilden, Germany)	74136
Roti-Quant	Carl Roth (Karlsruhe, Germany)	K015.1
Takyon No ROX SYBR 2x MasterMix blue dTTP	Eurogentec (Luettich, Belgium)	UF-NSMT-B0701

6.5 Consumables

Consumables were purchased from Bio-Rad (Hercules, USA), Carl Roth (Karlsruhe, Germany), Covaris (Woburn, USA) Eppendorf (Hamburg, Germany), Eurogentec (Luettich, Belgium), GE Healthcare (Chalfont St. Giles, Great Britain), Greiner Bio-One (Kremsmuenster, Austria), MP Biomedicals (Heidelberg, Germany), NeoLab (Heidelberg, Germany), Sarstedt (Nuembrecht, Germany), Thermo Fisher (Waltham, USA) or VWR International (Radnor, USA), unless otherwise stated.

6.6 Eukaryotic cell cultivation

Denucleated dermis as matrix for organotypic epidermal tissue cultures was prepared from frozen skin punches from Biopredic International (Saint-Grégoire,

France). Utilized primary cells, cell lines, media components and media composition are listed below.

Table 7: Overview of eukaryotic cell lines and primary cells

Name	Details	Supplier
HEK293T cell line	gift from Meister lab	Meister lab (Regensburg, Germany)
HeLa cell line	gift from Meister lab	Meister lab (Regensburg, Germany)
Normal Human Epidermal Keratinocytes (NHEK)	juvenile foreskin, pooled	PromoCell (Heidelberg, Germany)

Table 8: Reagents for eukaryotic cell culture

Name	Supplier	Catalogue number
3,3',5'-Triiodo-L-thyronine	Sigma-Aldrich (St. Lous, USA)	T08281
Adenine hydrochloride hydrate	Sigma-Aldrich (St. Louis, USA)	A-9795
100x Antibiotic-Antimycotic	Thermo Fisher (Waltham, USA)	15240-096
Cholera toxin from *Vibrio cholerae*	Sigma-Aldrich (St. Louis, USA)	C8052
Corning Matrigel	Thermo Fisher (Waltham, USA)	11543550
DMSO	Carl Roth (Karlsruhe, Germany)	A994.1
Dulbecco's Modified Eagle Medium, high glucose, pyruvate (DMEM)	Thermo Fisher (Waltham, USA)	41966-029
Dulbecco's Phosphate-Buffered Saline, no calcium, no magnesium (DPBS)	Thermo Fisher (Waltham, USA)	14190-094

Epidermal Growth Factor, human	Sigma-Aldrich (St. Louis, USA)	E9644
Fetal Bovine Serum	Thermo Fisher (Waltham, USA)	10270-106
Ham's F12	Lonza (Basel, Switzerland)	BE12-615F
Holo-Transferrin human	Sigma-Aldrich (St. Louis, USA)	T0665
Human Keratinocyte Growth Supplement	Thermo Fisher (Waltham, USA)	S-001-5
HyClone Bovine calf serum	Thermo Fisher (Waltham, USA)	SH3007303
HyClone Characterized Fetal Bovine serum	Thermo Fisher (Waltham, USA)	SH3007103
Hydrocortisone	Sigma-Aldrich (St. Louis, USA)	H0396
Insulin solution human	Sigma-Aldrich (St. Louis, USA)	17005-042
Keratinocyte-SFM Serum Free Medium	Thermo Fisher (Waltham, USA)	17005-042
Medium 154	Thermo Fisher (Waltham, USA)	M-154-500
Opti-MEM Reduced Serum Medium	Thermo Fisher (Waltham, USA)	31985070
Penicillin/Streptomycin (10.000 U/ml)	Thermo Fisher (Waltham, USA)	15140-122
Puromycin dihydrochloride	Carl Roth (Karlsruhe, Germany)	0240.3
Polybrene	Sigma-Aldrich (St. Louis, USA)	10768910G
Supplements for Keratinocyte-SFM	Thermo Fisher (Waltham, USA)	37000-015
Trypsin-EDTA 0.05%, phenol red	Thermo Fisher (Waltham, USA)	25000-054

Trypsin-EDTA 0.25%, phenol red	Thermo Fisher (Waltham, USA)	25200-056

Table 9: Components and composition of eukaryotic cell culture media

Medium/Solution	Composition	
50:50 medium	500 ml	Keratinocyte SFM
	500 ml	Medium 154
	5 ml	human Keratinocyte Growth Supplement
	5 ml	100x Antibiotic-Antimycotic
	1x	Supplements for Keratinocyte-SFM
Adenine Stock Solution	12 mg	adenine hydrochloride hydrate
	6.75 ml	DMEM
		adjust to pH 7.5
Basic buffer	0.2 M	sodium chloride
	3 mM	sodium azide
	1 mM	EDTA
		adjust to pH 8.0
Cholera toxin solution	1 mg	cholera toxin from *Vibrio cholera*
	1 ml	basic buffer
	99 ml	DMEM
DMEM+BCS	500 ml	DMEM
	50 ml	BCS
	5 ml	Penicillin/Streptomycin
DMEM+FBS	500 ml	DMEM
	50 ml	FBS (Thermo)
	5 ml	Penicillin/Streptomycin
EGF stock solution	100 µg	EGF
	10 ml	$_{dd}H_2O$
Hydrocortisone stock solution	5 mg	hydrocortisone
	1 ml	ethanol
	24 ml	DMEM
Insulin stock solution	5 mg	insulin solution human

	1 ml	$_{dd}H_2O$
KGM	330 ml	DMEM
	110 ml	Ham's F12
	5 ml	Penicillin/Streptomycin
	5 ml	100x Antibiotic-Antimycotic
	50 ml	FBS (HyClone)
	1 ml	adenine stock solution
	0.5 ml	cholera toxin solution
	1 ml	hydrocortisone stock solution
	0.5 ml	T/T_3 solution
	0.5 ml	EGF stock solution
	0.5 ml	Insulin stock solution
PBS+2x A/A	10 ml	100x Antibiotic-Antimycotic
	500 ml	DPBS
Polybrene solution	1 mg/ml	polybrene in PBS
T/T_3 solution	9.9 ml	Transferrin stock solution
	100 µl	Triiodo-L-thyronine stock solution
Transferrin stock solution	50 mg	holo-Transferrin human
	10 ml	DPBS
Triiodo-L-thyronine stock solution	13.6 mg	3,3',5'-Triiodo-L-thyronine
	100 ml	$_{dd}H_2O$

6.7 Instruments

General laboratory instruments and devices used were purchased from Beckman Coulter (Brea, USA), Bio-Rad (Hercules, USA), Eppendorf (Hamburg, Germany), NeoLab (Heidelberg, Germany) and Thermo Fisher (Waltham, USA). Particular instruments are listed below.

Table 10: List of instruments

Name	Supplier
2200 TapeStation System	Agilent Technologies (Santa Clara, USA)
Amersham Ultrospec 3300 pro	GE Healthcare (Chalfont St. Giles, Great Britain)

Centrifuge 5424 R	Eppendorf (Hamburg, Germany)
Centrifuge 5810	Eppendorf (Hamburg, Germany)
Centro XS^3 LB 960 Plate reader	Berthold Technologies (Bad Wildbad, German)
CO_2-Incubator HERAcell 240i	Thermo Fisher (Waltham, USA)
Concentrator SpeedVac 5301	Eppendorf (Hamburg, Germany)
Electroporation Device Nucleofector II	Lonza (Basel, Switzerland)
FastPrep-24 Instrument	MP Biomedicals (Heidelberg, Germany)
Fluorescence Microscope BZ-X800	Keyence (Osaka, Japan)
Focused Ultra-sonicator S220	Covaris (Woburn, USA)
Heraeus Megafuge 40R	Thermo Fisher (Waltham, USA)
Heraeus Multifuge 1S	Thermo Fisher (Waltham, USA)
HeraSafe KS	Thermo Fisher (Waltham, USA)
Hybridization oven type T 5042	Heraeus (Hanau, Germany)
NextSeq 2000	Illumina (San Diego, USA)
IKA MS3	Agilent Technologies (Santa Clara, USA)
Incubator Model B6200	Heraeus (Hanau, Germany)
Microtome RM 2265	Leica (Wetzlar, Germany)
MilliQ Advantage A10	Merck (Darmstadt, Germany)
NanoDrop 1000	Thermo Fisher (Waltham, USA)
New Brunswick Innova 44 Shaker	Eppendorf (Hamburg, Germany)
Odyssey Imaging System	LI-COR Biosciences (Lincoln, USA)
PMI Personal Molecular Imager FX	Bio-Rad (Hercules, USA)
Qubit 2.0 Fluorometer	Thermo Fisher (Waltham, USA)
Real-Time PCR Cycler CFX96	Bio-Rad (Hercules, USA)
Screen Eraser-K	Bio-Rad (Hercules, USA)

Shake ‘n’ Stack Hybridization Oven	Thermo Fisher (Waltham, USA)
Trans-Blot SD Semi-dry transfer cell	Bio-Rad (Hercules, Germany)
Transilluminator Quantum ST4	Peqlab (Erlangen, Germany)
UV Stratalinker 2400	Stratagene (La Jolla, USA)

6.8 Oligonucleotides

DNA and RNA oligonucleotides were ordered from Sigma-Aldrich (St. Louis, USA). SiRNA pools (mixture of 11-30 different siRNAs per target) were designed and ordered from siTools (Munich, Germany). Except from siE2F6 (0.5 nmol), 1 nmol of each siPool was used.

Table 11: Overview of utilized siRNAs

siRNA	Sequence (5’ to 3’)
siControl	siPool (exact sequences are available upon request from siTools)
siLINC00941	
siEGR3	
siE2F6	
siMTA2	

Table 12: Overview of utilized miRNAs probes

miRNA	Sequence (5’ to 3’)
miR-335-5p probe (NB)	AGTTCTCGTTATTGCTTTTTACA

Table 13: List of sequencing primers

Name	Sequence (5’ to 3’)
CMV_F	CGCAAATGGGCGGTAGGCGTG
pLARTA Ins F	CGAATCACCGACCTCTCTCC
SP6	ATTTAGGTGACACTATAG
T7	TAATACGACTCACTATAGGG

Table 14: List of primer sequences used for qRT-PCR

Name	Forward primer (5' to 3')	Reverse primer (5' to 3')
LINC00941	GACCTTTTCAGGCCAGCATT	ACAATCTGGATAGAGGGCTCA
β-actin	GGACTTCGAGCAAGAGATGG	AGGAAGGAAGGCTGGAAGAG
E2F1	CCGATCGATGTTTTCCTGTG	GATGGTGGTGGTGACACTAT
E2F2	CGCATCTATGACATCACCAAC	GGTCTTCAAACATTCCCCTG
E2F3	TCCAAAAACTCCAAAATCTCCC	CACTTCTGCTGCCTTGTTC
E2F4	ACTGCTCACCACCAAGTTC	CGATTAGCCCGATACCTTCC
E2F5	TGCTCACTACCAAGTTCGTGTC	CTCCTTTTTTGCCTCACAGCC
E2F6	CGACCTCGTTGAAAAGAAATCC	TGCTGATAAGTCAGAAAGTTCC
E2F7	TGTTGCTCCTTTCCCTGTCC	CATCCACTTGTCCATTCAGACC
E2F8	TAACCACACCTACCAAGCC	CACTTCTGTTGTCAAACAAACC
EGR3	ACGCCAAGATCCACCTCAAG	GGAAAAGTGGGGATCTGGGG
Filaggrin	AAAGAGCTGAAGGAACTTCTGG	AACCATATCTGGGTCATCTGG
GAPDH	GAAGAGAGAGACCCTCACTGCTG	ACTGTGAGGAGGGGAGATTCAGT
Keratin 1	TGAGCTGAATCGTGTGATCC	CCAGGTCATTCAGCTTGTTC
L32	AGGCATTGACAACAGGGTTC	GTTGCACATCAGCAGCACTT
LCE1A	GAAGCGGACTCTGCACCTAGAA	AGGAGACAGGTGAGGAGGAAATG
LCE6A	GTCCTGATCTCTCCTCTCGTCT	CAAGATTGCTGCTTCTGCTGT
LINC00941	GACCTTTTCAGGCCAGCATT	ACAATCTGGATAGAGGGCTCA
LINC00941 Exon 1	ACCTCCAACCCCCTTTTCTC	AAGGCAGGAAGTCTGTGCTG
SPRR4	AGCCTCCAAGAGCAAACAGA	GCAGGAGGAGATGTGAGAGG
MALAT1	TTGCTTGTCAAGCTATAACCAC	CAGTATTTTGAGATGGACATTG
U6	CACATATACTAAAATTGGAACG	CTTCACGAATTTGCGTGTCATC
MTA2	TGTACCGGGTGGGAGATTAC	GCCTCCACATTTCCATTTGC

6.9 Plasmids

Table 15: List of plasmids

Plasmid	Properties	Origin
pCMV dR8.91	Packaging plasmid for generation of lentiviral particles, encodes viral gag, rev, tat, and pol proteins under control of the CMV promotor	gift from the Khavari lab (Stanford University, USA)

pCMV-SPORT-LINC00941	-	Bought from Dharmacon
pLARTA_LINC00941	Vector for lentiviral overexpression of LINC00941	This work
pLARTA_LINC00941 _Exon 1	Vector for lentiviral overexpression of truncated LINC00941 (Exon 1)	This work
pLARTA_LINC00941 _Exon1-4	Vector for lentiviral overexpression of truncated LINC00941 (Exon 1-4)	This work
LARTA_LINC00941 _Exon 2-5	Vector for lentiviral overexpression of truncated LINC00941 (Exon 2-5)	This work
pLARTA_msGFP2	Vector for lentiviral overexpression of msGFP2	This work
pMIR-RL-TK _LINC00941_WT(#1, #2, #3)	Vectors for Dual Luciferase Reporter assay	This work; backbone: gift from the Meister lab (University of Regensburg)
pMIR-RL-TK _LINC00941_MUT (#1, #2, #3)	Vectors for Dual Luciferase Reporter assay	This work; backbone: gift from the Meister lab (University of Regensburg)
pUC-MDG	Envelope plasmid for generation of lentiviral particles, encodes the viral VSV-G envelope protein under control of the CMV promotor	gift from the Khavari lab (Stanford University, USA)

6.10 Prokaryotic cells

Table 16: Overview of utilized *Escherichia coli* strains

Strain	Genotype	Details
DH5α	F^- ϕ80*lac*ZΔM15 Δ(*lac*ZYA-*arg*F) U169 *rec*A1 *end*A1 *hsd*R17(r_k^-, m_k^+) *pho*A *sup*E44 *thi*-1 *gyr*A96 *rel*A1 ʎ$^-$	Propagation of plasmids
Stbl3	F-*mcr*B *mrrhsd*S20(r_B^-, m_B^-) *rec*A13 *sup*E44 *ara*-14 *gal*K2 *lac*Y1 *pro*A2 *rps*L20(Str^R) *xyl*-5 ʎ$^-$*leumtl*-1	Propagation of plasmids

6.11 Software

Table 17: List of utilized software

Name	Source of supply
2200 TapeStation Software	Agilent Technologies (Santa Clara, USA)
Bio-Rad CFX Manager 3.1	Bio-Rad (Hercules, USA)
BRIO	http://brio.bio.uniroma2.it/
BZ-X800 Analyzer	Keyence (Osaka, Japan)
Citavi 6	https://www.citavi.com
DisGeNET	https://www.disgenet.org/
ENCORI	https://rnasysu.com/encori/index.php
Galaxy server tools	https://usegalaxy.org/
GO term analysis	http://geneontology.org/
GraphPad t-test calculator	https://www.graphpad.com/quickcalcs/ttest1.cfm
Integrative Genomics Viewer 2.14.1 (IGV)	https://broadinstitute.org/igv/
Microsoft Office	Microsoft (Redmond, USA)
ND-1000 3.81	Thermo Fisher (Waltham, USA)
Odyssey 3.0.30	LI-COR Biosciences (Lincoln, USA)
SnapGene Viewer 6.1.1	GSL Biotech LLC (Chicago, USA)
SonoLab Software 7.2	Covaris (Woburn, USA)
UCSC Genome Browser	https://genome.ucsc.edu/

7 Methods

7.1 Bioinformatic data analysis

7.1.1 Mass spectrometry (MS) data analysis

Data analysis was carried out in collaboration with the MS facility of Biochemistry I (University of Regensburg). Raw data processing was performed in Data Analysis 4.2 (Bruker Daltonics), and Protein Scape 3.1.3 (Bruker Daltonics) in connection with Mascot 2.5.1 (Matrix Science) facilitated database searching of the Swiss-Prot Homo sapiens database (release-2020_01, 220420 entries). Search parameters were as follows: enzyme specificity trypsin with 1 missed cleavage allowed, precursor tolerance 0.02 Da, MS/MS tolerance 0.04 Da. Carbamidomethylation or propionamide modification of cysteine, oxidation of methionine, deamidation of asparagine and glutamine were set as variable modifications. Mascot peptide ion-score cut-off was set 25. Search conditions were adjusted to provide an FDR rate of less than 1%. Protein list compilation was done using the Protein Extractor function of Protein Scape. EmPAI-values (exponentially modified protein abundance index), which can be used for an approximate relative quantitation of proteins in a mixture, were extracted from Mascot. MS analysis resulted in n = 627 LINC00941 interaction partners. GO term analysis was carried out using the PANTHER Overrepresentation Test[234]. GO terms with an FDR of less than 0.05 and chromatin association were considered for further analysis.

7.1.2 Chromatin immunoprecipitation (ChIP) sequencing data analysis

ChIP sequencing data analysis of this project was carried in collaboration with Dr. Uwe Schwartz (NGS Analysis Center Biology and Pre-Clinical Medicine, University of Regensburg) as subsequently described. Initially, quality control of the raw sequence reads was conducted using FastQC (v0.11.8)[235]. Following this, reads were mapped to the reference genome (GRCh38) using bowtie2 (version v2.4.4). The following options were used to optimize the alignment process: --very-sensitive-local, --no-discordant, --no-mix, --dovetail. Aligned reads were filtered for MAPQ >= 30 using samtools[236]. Reads mapping to blacklisted genomic regions (ENCODE accession: ENCFF356LFX) were removed using bedtools[237]. Peak calling was executed on all samples relative to input samples using the MACS2 software[238]. The specific options used for this analysis were as follows: -f BAMPE, -g 2.7e9, --keep-

dup auto. Following peak calling, the resultant peaks were filtered based on a log q-value threshold > 20 for subsequent analysis. This stringent cutoff was used to ensure a high level of confidence in the identified peaks, minimizing the potential for false positives. The number of fragments in each sample falling under these peaks was quantified using the featureCounts function of the Subread package[239]. To identify changes in MTA2 binding upon LINC00941 knockdown the generated count table was processed in R using the Bioconductor package DESeq2[240]. 33 MTA2 binding sites were found to significantly change their binding abundance upon LINC00941 knockdown based on an FDR of 0.05.

7.1.3 RNA sequencing analysis

Reanalysis of publicly available RNA sequencing data of LINC00941 knockdown during keratinocyte differentiation (GSE118077) was performed in collaboration with Dr. Uwe Schwartz (NGS Analysis Center Biology and Pre-Clinical Medicine, University of Regensburg) using a nextflow RNA sequencing pipeline[241]. Initially, quality control of the raw sequence reads was conducted using FastQC (v0.11.8)[235]. Subsequently, reads were mapped to the reference genome (GRCh38) and corresponding gene annotation (Ensembl version 106) using the Spliced Transcripts Alignment to a Reference (STAR) software (version v2.7.8a)[242]. The following options were used to optimize the alignment process: --outFilterType BySJout, --outFilterMultimapNmax 20, --alignSJoverhangMin 8, --alignSJDBoverhangMin 1, --outFilterMismatchNmax 999, --alignIntronMin 10, --alignIntronMax 1000000, --outFilterMismatchNoverReadLmax 0.04, --runThreadN 12, --outSAMtype BAM SortedByCoordinate, --outSAMmultNmax 1, and --outMultimapperOrder Random. Post-mapping quality control was performed using the rnaseq mode of Qualimap (v2.2.1).[243] The level of PCR duplication was assessed using Picard MarkDuplicates (v2.21.8),[244] and dupRadar (version v1.15.0)[245]. Gene expression quantification was carried out using featureCounts (v1.6.3)[239].

Finally, differential gene expression analysis between LINC00941 knockdown and control samples was conducted using the Bioconductor DESeq2 package[240]. The normal shrinkage method was applied for scaling log2 fold changes[246]. Genes with an FDR of less than 0.05 were considered significantly differentially expressed. This

analysis resulted in the identification of 385 downregulated and 1532 upregulated genes in the LINC00941 knockdown keratinocytes at day 3.

7.1.4 Downstream analysis

In collaboration with Dr. Uwe Schwartz (NGS Analysis Center Biology and Pre-Clinical Medicine, University of Regensburg) downstream analysis was performed as subsequently described. ChIP sequence coverage tracks were generated using the bamcoverage function from deeptools package[247]. For normalization, the size factors derived from DESeq2 analysis were used. Data track visualizations were generated using the Bioconductor package Gviz[248]. The Bioconductor package ChIPseeker was used to annotate the genomic regions of the MTA2 binding sites[249]. To link the MTA2 binding sites to the next gene only protein-coding genes were considered. Gene set over-representation analysis was carried out on MTA2-associated genes with a maximum distance to the TSS of 3 kb using the Bioconductor package clusterProfiler[250].

7.1.5 Data availability

For analysis of ChIP and RNA sequencing data, external datasets were utilized by Dr. Uwe Schwartz (NGS Analysis Center Biology and Pre-Clinical Medicine, University of Regensburg). The 15-state core chromatin model of male keratinocytes (roadmap accession: E057) was obtained from the roadmap repository (https://egg2.wustl.edu/roadmap/web_portal/chr_state_learning.html)[157]. Corresponding histone modification and RNA sequencing data tracks were obtained from ENCODE repository: poly(A) RNA sequencing plus/minus strand (ENCFF283IQC, ENCFF804BRH), H3K4me3 (ENCFF517FHJ), H3K27me3 (ENCFF400FLX), H3K4me1 (ENCFF319BIJ)[251,252].

Data on *in vitro* differentiation of foreskin keratinocytes (at 0d/2.5d/5.5d) was obtained from the ENCODE Portal: ChromHMM 18-state model (ENCFF571LVQ, ENCFF385FJV, ENCFF058GJN), H3K4me1 (ENCFF539WZS, ENCFF546FWF, ENCFF821VJZ), H3K27ac (ENCFF786TBH, ENCFF870GTM, ENCFF988UOV), H3K27me3 (ENCFF492WYD, ENCFF846IJG, ENCFF902OOG), poly(A) RNA sequencing plus (ENCFF646IJP, ENCFF786AVM, ENCFF533VFT), poly(A) RNA

sequencing minus (ENCFF699EVT, ENCFF701XBY, ENCFF366JLV), poly(A) RNA sequencing quantification (ENCFF423MWU, ENCFF137YHI, ENCFF379PNP).

RNA sequencing data of LINC00941 knockdown after day 2 and 3 was obtained from Gene Expression Omnibus (GEO; GSE118077)[113].

MS data produced during this project have been deposited to the ProteomoeXchange Consortium via the PRIDE repository while MTA2 ChIP sequencing data have been deposited at GEO. Both data sets will be released upon publication of a manuscript which is currently under revision.

7.2 Cell culture methods

All cell culture methods concerning eukaryotic cells were performed in a biological safety cabinet under laminar airflow to ensure sterile conditions. With the exception of lentiviral procedures which were performed under biosafety level 2 precautions, cell culture work was carried out in accordance with biosafety level 1 regulations. Cell culture media, trypsin and DPBS (Table 9) were pre-warmed to 37 °C prior to use. The cells were cultivated in a humified incubator at 37 °C and 5% carbon dioxide.

7.2.1 Cultivation of HEK293T and HeLa cells

HEK293T and HeLa cells were cultivated in DMEM+FBS (Table 9) and passaged when a confluency of 80-90% was reached. For this purpose, the medium was aspired, and cells were washed once with DPBS. Using 0.05% trypsin, cells were subsequently detached. Fresh DMEM+FBS was used to quench the trypsin followed by a centrifugation step (200 rcf, RT, 5 min). The pelleted cells were resuspended in an appropriate volume of DMEM+FBS and equally distributed onto fresh cell culture dishes. Medium was changed every two days.

7.2.2 Cultivation of primary keratinocytes

Primary keratinocytes were cultivated in 50:50 medium until they reached a maximal confluency of 80% to prevent premature differentiation. Therefore, 50:50 medium was aspired, and cells were washed once with DPBS. To detach the cells from the

cell culture dish, 0.05% trypsin was used (4 min, 37 °C). After tapping the plate to remove the cells from the surface, DMEM+BCS was added to obtain a single cell solution. Cells were then centrifuged (200 rcf, RT, 5 min) and the resulting cell pellet was resuspended in an appropriate volume of 50:50 medium and seeded onto fresh cell culture dishes with at least 5% confluency. Medium was changed every two days. Primary keratinocytes were not passaged more than 7 times after thawing.

7.2.3 Determination of cell numbers

To determine the number of cells, Neubauer counting chambers were used. Therefore, 10 µl of cell suspension were added to both counting areas and the cells in at least four corner squares were counted. The number of cells per milliliter cell suspension was calculated using the following equation:

$$Cells\ per\ ml = \frac{Counted\ number\ of\ cells}{number\ of\ counted\ squares} * 10{,}000$$

7.2.4 Freezing and thawing of cells

For long term storage, 1.5 million keratinocytes were resuspended in 1 ml freezing medium (50:50 medium supplemented with 10% DMSO) followed by a slow cooling down (1 °C/min) to -80 °C. The next day, cryo-stocks were transferred to the vapor phase of liquid nitrogen.

Cryopreserved cells were thawed in a water bath at 37 °C and subsequently transferred to 9 ml 50:50 medium. After centrifugation (200 rcf, RT, 5 min), supernatant was aspired and the cells were resuspended in fresh cultivation media, followed by seeding the cells onto appropriate cell culture dishes.

7.2.5 Electroporation of keratinocytes

Keratinocytes were nucleofected with siRNA pools (Table 11) utilizing the Human Keratinocyte Nucleofector Kit (Lonza). After trypsinization and counting the cells (see 7.2.2 and 7.2.3), five to six million keratinocytes were pelleted (200 rcf, RT, 5 min) and resuspended in 90 µl electroporation buffer. This suspension was then

mixed with 10 µl siRNA pool of appropriate concentration and transferred to an electroporation cuvette. Nucleofection was performed with the Electroporation Device Nucleofector II (Lonza) and its preset program T-018 (Keratinocytes human, neonatal, high efficiency). Subsequently, the cells were transferred to 500 µl prewarmed (37 °C) 50:50 medium and after recovery at 37 °C for 25 min, they were seeded on a 15 cm cell culture dish and recovered for at least 24 h.

7.2.6 Keratinocyte differentiation cultures

Differentiation of monolayered keratinocytes was induced by seeding the cells after trypsinization and centrifugation (see 7.2.2) at full confluency and addition of 1.2 mM calcium chloride to the 50:50 medium. For these differentiation cultures, the medium mixed with calcium chloride was renewed every day.

7.2.7 Generation of organotypic epidermal tissue

Setups for organotypic epidermal tissue cultures consisted of an 3D-printed insert with a squared cavity (0.8 cm edge length) that was put in a 6 cm cell culture dish. Next, devitalized human dermis was cut (~ 1 cm edge length) and placed with the basement membrane side upwards over the insert cavity. After a short drying step, 90 µl Matrigel (Thermo Fisher) were applied to the bottom side of the dermis to seal holes of the dermis. Finally, KGM was added to the setups until it reached the bottom of the inserts, and thus nutrients could diffuse through the matrigel and dermis.

Keratinocytes (untreated, nucleofected with siRNA pools or transduced with lentiviral particles) were detached, counted and pelleted (see 7.2.2 and 7.2.3) and 550,000 cells were resuspended in 20 µl KGM and equally distributed onto the dermis part covering the insert cavity. Stratification and differentiation were induced by raising the keratinocytes to the air-liquid interface. KGM was exchanged every second day.

To harvest organotypic epidermal tissue cultures, the insert was lifted and the matrigel as well as excess of devitalized human dermis were carefully removed. The remaining organotypic skin tissue was taken off the insert and cut diagonally to give rise to two equal triangles. One half was transferred to an embedding cassette which

in turn was incubated in 4% PFA (60 rpm, 4 °C, overnight) (see 7.3.1), while the other half was used for RNA extraction (see 7.5.1).

7.2.8 Lentivirus production and transduction of keratinocytes

Transfection of HEK293T cells was performed according to the table below and only endotoxin free plasmid preparations (see 7.5.6) were used in combination with Lipofectamine 3000 (Thermo Fisher). The lentiviral transfer vector was pLARTA with either complete LINC00941 sequence insert, LINC00941 truncated sequences or msGFP2 (control) insert. For transfection, the required amounts of plasmids were calculated to obtain a molar ratio of 1:1:1 for all three vectors needed.

Table 18: Transfection reaction mixtures for lentiviral particle generation

	15 cm dish	Component
Plasmid dilution	3.5 ml	Opti-MEM
	17.5 µg	pCMV dR8.91
	8.68 µg	pUC-MDG
	varied	lentiviral transfer vector
	81 µl	P3000 enhancer reagent
Lipofectamine dilution	3.5 ml	Opti-MEM
	95 µl	Lipofectamine 3000 reagent

Plasmid and Lipofectamine dilution were mixed and incubated at RT for 25 min. Subsequently, the mixture was applied to the 15 cm cell culture plate and 50 million HEK293T cells resuspended in 18 ml DMEM+FBS were added for reverse transfection. 6 h and 24 h post-transfection, the medium was aspired and 27 ml of fresh DMEM+FBS was added. Lentiviral particles were harvested 48 h and 72 h post-transfection by filtering the virus containing medium through a 0.45 µm pore-sized polyethersulfone membrane. The viral particles were first frozen in dry ice but then they were stored at -80 °C.

For lentiviral transduction, 50,000 keratinocytes were seeded in wells of a 6-well plate. The next day, 2.5 ml transduction mix per well was prepared by diluting the viral particles in 50:50 medium and addition of polybrene to a final concentration of

5 µg/ml. The optimal dilution was determined beforehand in an efficiency test for each batch of lentiviral particles. In most cases, 375 µl virus particles and 2,125 µl 50:50 medium showed the best overexpression in combination with no cytotoxic effect.

Infection of keratinocytes was conducted by removing the growth medium and adding the transduction mix. Following this, the cells were centrifuged at 250 rcf for 60 min slowly heating up to 32 °C. The transduction mix was then aspirated, the cells were washed twice with DPBS and recovered in 50:50 medium for at least 24 h.

7.2.9 Preparation of human devitalized dermis

Human split-skin was washed twice in PBS+2x A/A and incubated in PBS+2x A/A at 37 °C for 3-7 days until the epidermis could be mechanically detached from the dermis. The devitalized dermis was then UV-irradiated from both sides for 3 min each. Until further use, the dermis was stored in PBS+2x A/A at 4 °C.

7.3 Histological analysis

7.3.1 Paraffin embedding of organotypic epidermal tissue

After the organotypic epidermal tissue piece were incubated in 4% PFA overnight (see 7.2.7), the embedding cassette and the skin tissue, respectively, were embedded into paraffin. Therefore, the cassette was incubated in different solutions on a shaker as described in the following table. Exceptional from steps involving paraplast which were conducted at 65 °C, remaining steps were performed at RT.

Table 19: Steps for paraffin embedding of organotypic epidermal tissues

Repetitions	Duration	Solutions
1x	30 min	$_{dd}H_2O$
1x	60 min	70% Ethanol
1x	30 min	80% Ethanol
1x	30 min	96% Ethanol
1x	45 min	96% Ethanol

2x	30 min	100% Ethanol
2x	30 min	Xylol
2x	24 h	Paraplast

After the skin sections were embedded, the paraffin cubes were cooled down to room temperature. For long-term storage of the paraffin cubes were stored at 4 °C.

By means of a microtome, paraffin cubes were cut into 7 µm sections and transferred onto Polysine slides (Carl Roth).

7.3.2 Deparaffinization, rehydration and demasking of paraffin sections

The paraffin embedded skin sections on Polysine slides (see 7.3.1) were deparaffinized and rehydrated by immersing them successively in solutions, listed in the following table.

Table 20: Sequence of deparaffinization and rehydration steps

Duration	Solution
2x 5 min	Xylol
2 min	Ethanol absolute
2 min	96% Ethanol
2 min	80% Ethanol
2 min	60% Ethanol
5 min	$_{dd}H_2O$

Demasking buffer was brought to boil, the slides were immersed and kept hot for 10 min. After repeating this step once more with fresh demasking buffer, the slides and buffer were allowed to cool down for 20 min at RT followed by washing the slides three times for 2 min each with PBS. Subsequently, IF staining followed (see 7.3.3).

7.3.3 Immunofluorescence (IF) staining

IF staining started with a blocking step. The slides were therefore blocked for 20 min at RT in PBS with 10% BCS while shaking. For primary antibody incubation, the antibodies were diluted to appropriate concentrations (Table 2) in PBS with 1% BCS. The solution was applied and incubated on the sections for 60 min at RT at humidified conditions. Next, slides were washed with 1% BCS in PBS (three times, 5 min each) and fluorescently labeled secondary antibodies (Table 3) diluted in 1% BCS in PBS were applied in a light-protected humidified chamber for 60 min at RT. The differentiation protein was generally labeled with Alexa 555 and collagen VII with Alexa 488. After one hour of incubation, the slides were washed with PBS (three times, 5 min each, in dark) and mounted in DAPI Fluoromount-G mounting medium (Thermo Fisher).

Using the Keyence fluorescence microscope, pictures from representative skin section areas were taken at 20x magnification.

7.4 Microbiological techniques

7.4.1 Cultivation of Escherichia coli

For cultivation of *Escherichia coli*, the cultures were incubated at 37 °C for DH5α bacteria and 30 °C for self-made Stbl3 bacteria. Cultures on plates were incubated on LB-agar plates and liquid cultures in appropriate volume of LB medium shaking at 180 rpm. Both, liquid cultures, and plates were containing adequate amounts of antibiotics if needed.

7.4.2 Preparation of chemically competent Escherichia coli

5 ml YT-medium were inoculated with a single colony of either Stbl3 or DH5α *Escherichia coli* strain and grown overnight at 37 °C and 220 rpm. 50 µl from this culture were mixed with 5 ml fresh YT-medium the next day, followed by an incubation step at 37 °C and 220 rpm until an OD_{600} of 0.8 was reached. Then 100 ml YT-medium were added, and the culture was grown to an OD_{600} of 0.5. Cells were spun down (2,000 rcf, 5 min, 4 °C), resuspended in 20 ml ice-cold TFBI and incubated on ice for 10 min. After a final centrifugation step (2,000 rcf, 5 min, 4 °C),

cells were resuspended in 4 ml ice-cold TFBII. Finally, 100 µl aliquots were snap-frozen in liquid nitrogen and stored at -80 °C.

7.4.3 Transformation of chemically competent Escherichia coli

The chemical competent cells (Table 16) were thawed on ice and up to 100 ng plasmid solution was added to 100 µl cell suspension. After mixing the solution carefully, the cells were incubated on ice followed by a heat shock at 42 °C. In case of DH5α, the heat shock lasted 90 s, while in case of Stbl3 it was 45 s. Next, the cells were incubated on ice for 2 min and subsequently 900 µl LB-media were added and the cell solution was incubated on a thermomixer at either 30 °C (Stbl3) or 37 °C (DH5α) for 60 min at 300 rpm.

7.5 Molecular biological methods

7.5.1 RNA extraction from organotypic epidermal tissue

The other half of the organotypic epidermal tissue (see 7.2.7) was minced and transferred into a Lysing Matrix-D tube (MP Biomedicals). This tube contained 800 µl RLT Plus buffer (RNeasy Plus Mini Kit, Qiagen) supplemented with 1% β-mercaptoethanol. Cell lysis and homogenization was performed for 45 s at 6.5 m/s in the FastPrep-24 instrument (MP Biomedicals). Following a centrifugation step (2 min, 4 °C, 13,000 rcf), the supernatant was transferred to a QIAShredder tube (Qiagen). After centrifugation (2 min, 4 °C, 13,000 rcf), the flow-through was applied for RNA purification using the RNeasy Plus Mini Kit (Qiagen) following the manufacturer's instructions apart from the centrifugation steps, which were carried out at 4 °C. At the end, RNA was eluted with 30 µl $_{dd}H_2O$. After quantification with the NanoDrop 1000 (Thermo Fisher), RNA was stored at -80 °C until further usage.

7.5.2 RNA extraction with TRIzol

Keratinocytes were washed with ice-cold DPBS and lysed in 0.3 ml TRIzol reagent (Thermo Fisher) per $1x10^5$-10^7 cells directly on the cell culture dish. The following RNA isolation and purification was performed according to the manufacturer's instructions. The RNA pellet obtained at the end was dissolved in an appropriate

amount of RNase-free $_{dd}H_2O$. Subsequently, the RNA was quantified with the NanoDrop 1000 (Thermo Fisher) and stored at -80 °C until further usage.

7.5.3 DNase I digest and cDNA synthesis

For DNase I (Thermo Fisher) digest, 500 ng of TRIzol purified RNA (see 7.5.2) was subjected according to the manufacturer's instructions with the exception that only half of the total volume (5 µl instead of 10 µl) was applied. Following this, cDNA synthesis with the iScript cDNA Synthesis Kit (Bio-Rad) was performed according to the manufacturer's instructions but correspondingly, only half the volume as indicated. RNA isolated and purified with the RNeasy Plus Mini kit was directly used for cDNA synthesis without prior DNase I digest. After cDNA synthesis, $_{dd}H_2O$ was added to give a final volume of 100 µl and the cDNA was stored at -20 °C.

7.5.4 ChIP sequencing

Undifferentiated keratinocytes were washed and harvested as described above (see 7.2.2). Formaldehyde crosslink was achieved by resuspending keratinocytes in 10 ml 1% (v/v) formaldehyde solution per 20 million cells at RT and under constant rotation for 10 min. Subsequently, the reaction was quenched by addition of 10% 1.25 M glycine (5 min, RT, rotation) and the cells were pelleted in a centrifugation step (2,000 rcf, 4 °C, 10 min). The supernatant was discarded, and the keratinocytes were washed with 10 ml ice-cold DPBS. After cells were centrifuged again (2,000 rcf, 4 °C, 10 min), they were resuspended in 1.5 ml ice-cold DPBS and transferred into a 1.5 ml reaction tube. Following centrifugation (6,000 rcf, 5 min, 4 °C), the supernatant was removed completely, and the cell pellet weight was determined. Subsequently, cells were flash frozen in liquid nitrogen and stored at -80°C.

For chromatin sonication, cells were thawed on ice and 500 µl ChIP swelling buffer per 25 million keratinocytes was added. After complete resuspension, the cells were incubated on ice for 10 min while inverting them regularly. Cell lysis was performed using a douncer and after centrifugation (1,000 rcf, 4 °C, 5 min) the resulting pellet was resuspended in 800 µl ChIP RIPA buffer minimum. Up to 95 million cells were transferred to a 2 ml milliTUBE (Covaris) and sheared to fragments between 150 bp

to 250 bp by sonication using the S220 Focused-ultrasonicator (Covaris) as indicated in the following table.

Table 21: Settings for chromatin sonication

Duty cycle	20%
Mode	Freq sweeping
Intensity	8
Cycles per burst	200
Water level	15
Time	30 min
Volume	800 µl

After centrifugation (15,000 rcf, 5 min, 4 °C), 1% (v/v) input sample was taken, flash-frozen and stored at -80 °C until further usage while the remaining supernatant was used for pulldown. Per 100 µg fragmented chromatin, 5 µg antibodies were added and incubated at 4 °C under rotation overnight. The next day, 40 µl Protein G Dynabeads (Thermo Fisher) were washed three times under rotation for 10 min each with ChIP wash buffer. The beads were then added to the antibody-chromatin mixture and incubated under rotation at RT for 45 min. Following washing steps of the beads (three times, 2 min, 400 µl ChIP wash buffer), 50 µl ChIP elution buffer was transferred to the beads and incubated on a thermomixer (15 min, RT, shaking). After centrifugation (15,000 rcf, 5 min, 4 °C), supernatant was transferred to a fresh reaction tube and stored on ice, while 50 µl ChIP elution buffer was added again to the beads (15 min, RT, shaking). The supernatant was transferred to the reaction tube on ice (total volume of the eluate: 100 µl) and a final centrifugation step (15,000 rcf, 5 min, 4 °C) provided the complete removal of remaining beads. For reverse crosslinking, 0.2 M sodium chloride were added and incubated at 67 °C for 4 h. This procedure was also applied to the input sample filled up with ChIP elution buffer to a total volume of 100 µl. To purify the chromatin, the QIAquick PCR Purification kit (Qiagen) was used. In case a pH value adjustment was necessary, sodium acetate was added beforehand. Finally, the samples were eluted in 30 µl $_{dd}H_2O$.

Library preparation for ChIP sequencing was performed using the NEBNext Ultra II DNA Library Prep Kit for Illumina (New England Biolabs), the Index Primer Set 1 and 2 of the NEBNext Multiplex Oligos for Illumina (New England Biolabs) as well as Agencourt AMPure XP beads (Beckman Coulter) for PCR clean-up. In general, the manufacturer's instructions were followed. The libraries were pooled equimolar, and the pool was quantified using the KAPA Library Quantification kit – Illumina (Roche). The libraries were sequenced on an Illumina NextSeq 2000 instrument (Illumina) controlled by the NextSeq Control Software (NCS) v1.4.1.39716, using a 100 cycles P2 Flow Cell with the single index, paired-end (PE) run parameters. Image analysis and base calling were done by the Real Time Analysis Software (RTA) v3.9.25. The resulting .cbcl files were converted into .fastq files with the bcl2fastq v2.20 software. Library pooling and ChIP sequencing were performed at the Genomics Core Facility "KFB – Center of Excellence for Fluorescent Bioanalytics" (University of Regensburg, Germany).

7.5.5 DNA agarose gel electrophoresis

Horizontal agarose gel electrophoresis was performed with 1.0 – 1.2% (w/v) agarose gels (dissolved in TAE buffer, 0.5 µg/ml ethidium bromide), depending on the expected DNA size. Samples were mixed with 6x Gel loading dye, purple (New England Biolabs) and loaded onto the gel, next to 5 µl 1 kb Plus DNA Ladder (Thermo Fisher). Separation of DNA fragments was achieved by applying 90 V in gel chambers filled with TAE buffer. For gel documentation, the Transilluminator Quantum ST4 (Peqlab) was used.

7.5.6 Plasmid purification

Depending on the required amount of vector, plasmid purification was done with NucleoSpin Plasmid Mini Kit, NucleoBond Xtra Midi Kit, or NucleoBond Xtra Midi EF Kit (for endotoxin-free plasmid purifications) (Macherey Nagel) following the manufacturer's instructions. The obtained DNA was dissolved in a suitable amount of $_{dd}H_2O$, and plasmid concentration was determined with the NanoDrop 1000 (Thermo Fisher). The correct sequence integrity was verified by either restriction enzyme digestion or colony PCR (see 7.5.10) as well as by Sanger Sequencing.

For this, up to 500 ng plasmid DNA and 5 µM sequencing primer (Table 13) was sent to and sequenced by Macrogen.

7.5.7 Polymerase chain reaction (PCR)

For PCR amplification of DNA fragments needed for the generation of new plasmids, PCR was performed in a 100 µl scale using Phusion High-Fidelity DNA Polymerase (New England Biolabs) with either 100 ng genomic or 1 ng plasmid DNA template and a final concentration of 1x HF buffer, 200 µM dNTPs, 0.5 µM of each primer and two units of Phusion DNA Polymerase. The amplification was performed in a PCR Thermocycler (Eppendorf) with the following cycling program. Denaturation, annealing, and elongation were repeated 35 times in a row.

Table 22: Cycling program for PCR with the Phusion Polymerase

	Step	Time	
	98 °C	30 s	
Denaturation	98 °C	10 s	
Annealing	55-60 °C	30 s	35x
Elongation	72 °C	30 s/kbp	
	72 °C	10 min	
	4 °C	∞	

Successful PCR amplification was verified by DNA agarose gel electrophoresis (see 7.5.5) and the PCR product of interest was purified by either PCR clean-up or gel extraction (both NucleoSpin Gel and PCR Clean-up kit, Macherey-Nagel) according to the manufacturer's instructions.

7.5.8 Restriction enzyme digest

For preparative restriction enzyme digests, 2 µg DNA vector or the complete amount of purified PCR product resulting after using the PCR Clean-up kit (see 7.5.7) were digested with suitable restriction enzymes in the designated buffer provided by New England Biolabs. Duration and temperature were generally – depending on the

digestion enzyme – 4 h at 37 °C. The obtained DNA fragments were analyzed with the help of DNA agarose gel electrophoresis (see 7.5.5) and desired fragments for molecular cloning were purified via the NucleoSpin Gel and PCR Clean-up kit (Macherey-Nagel) according to the manufacturer's instructions.

7.5.9 Generation of plasmids

After the purification of restricted inserts and plasmids (see 7.5.8), their concentration was determined using the NanoDrop 1000 device (Thermo Fisher). 50 ng vector were mixed with the insert of interest in a 1:3 or 1:5 molar ratio, 1x TE DNA ligase buffer and 400 units T4 DNA ligase (both from New England Biolabs) in a 20 µl reaction. Ligation was achieved by incubation at RT for 1 h or overnight at 4 °C. The generated plasmid was used for transformation of competent *Escherichia coli* cells (see 7.4.3).

7.5.10 Colony PCR

To verify the integrity of the generated plasmid a colony PCR was performed. Up to 1,000 ng template DNA was mixed with 1x ThermoPol reaction buffer (New England Biolabs), 200 µM dNTPs, 0.2 µM of each primer and 0.75 units Taq DNA Polymerase (New England Biolabs) in a total volume of 25 µl. The amplification was performed in a PCR Thermocycler (Eppendorf) with the following cycling program. Denaturation, annealing, and elongation were repeated 30 times in a row.

Table 23: Cycling program for PCR with Taq Polymerase

	Step	Time	
	86 °C	5 min	
Denaturation	95 °C	30 s	
Annealing	46-68 °C	45 s	30x
Elongation	68 °C	1 min/kbp	
	68 °C	5 min	
	4 °C	∞	

Successful PCR amplification was verified by DNA agarose gel electrophoresis (see 7.5.5) followed by Sanger sequencing (see 7.5.6).

7.5.11 qRT-PCR analysis

For qRT-PCR analysis, 7.5 µl Takyon Mix (Eurogentech) were mixed with 1 µl Primermix (5 µM each primer, Table 14), 4.5 µl $_{dd}H_2O$ and 2 µl cDNA (see 7.5.3). The reaction was analyzed in a 96-well format using the Real-Time PCR Cycler CFX96 (Bio-Rad) and its corresponding software Bio-Rad CFX Manager 3.1 (Bio-Rad). Samples were normally run in triplicates and specificity of each reaction was monitored using a melt curve analysis for each PCR product. The linear amplification for each Primermix was ensured by testing their amplification range with cDNA dilution series in preliminary experiments.

Table 24: Cycle conditions of qRT-PCR

Step	Time	
95 °C	3 min	
95 °C	15 s	
60 °C	30 s	40x
72 °C	30 s	
95 °C	10 s	
65 °C to 95 °C; +0.5 °C/step	5 s	melt curve

Fold changes of the samples were calculated for each gene of interest (goi) in reference to a control sample from the C_q-values (determined by the Bio-Rad CFX Manager 3.1, Bio-Rad) according to the $2^{-\Delta\Delta Cq}$ method[253]. L32 (housekeeping gene) was used for normalization according to the following formula:

$$Fold\ change = 2^{-[(Cq\ sample\ (goi) - Cq\ control\ (goi)) - (Cq\ sample\ (L32) - Cq\ control\ (L32))]}$$

7.5.12 RNA immunoprecipitation (RNA-IP)

Keratinocytes were washed with ice-cold DPBS on the cell culture dishes. After adding an appropriate volume of RIPA buffer to the cells, they were scraped off, transferred to a reaction tube an incubated on ice for 20 min. After lysing the cells using a douncer, the cells were centrifuged (15,000 rcf, 4 °C, 10 min) and 10% input control was taken for RNA isolation using TRIzol (see 7.5.2). The remaining volume was split in two halves. To one half antibodies against the target of interest were added and to the other IgG control (Table 2). The mixture incubated at 4 °C for 2 h while rotating. Next, 40 µl Protein G Dynabeads per approach were washed twice with 0.2 ml RIPA buffer. The antibody-supernatant mix were then added to the beads and incubated for 1 h at 4 °C under rotation. Subsequently, the supernatant was removed, and the beads were washed three times with 500 µl RIPA buffer. The beads were finally resuspended in TRIzol, and RNA isolation was carried out. DNase I digestion and cDNA synthesis were carried out for both, input control and samples (see 7.5.3). After cDNA synthesis $_{dd}H_2O$ was added to a total volume of 40 µl and RT-qPCR was performed subsequently to calculate the relative enrichment over IgG control by determining percent input beforehand.

7.5.13 Northern blot (NB) analysis of miRNAs

15 µg TRIzol purified RNA from keratinocytes solved in 10 µl $_{dd}H_2O$ were mixed with 10 µl 1x RNA loading dye. For gel preparation, a 12% denaturing polyacrylamide gel was prepared mixing 28.8 ml Concentrate and 25.2 ml Dilutent (both from the Rotiophorese Sequencing Gel System, Carl Roth) with 6 ml 10x TBE. Finally, 500 µl 10% APS and 50 µl TEMED were added, and the gel was poured in the corresponding system. After the gel was polymerized, the gel was run in 1x TBE at 400 V with a metal plate attached from behind for approximately 20 min. When the pre-run was finished, the RNA samples were heated up for 1 min at 95 °C and loaded onto the gel. The gel was run for about 60 min at 400 V. For ethidium bromide staining, the gel was disassembled and incubated in 1:20,000 ethidium bromide in 1x TBE for 10 min on a shaker. After taking a picture, the gel was washed in water. To blot the gel, a Trans-Blot SD Semi-dry transfer cell system (Bio-Rad) was prepared with Amersham Hybond-N^+ membrane (GE) and Whatman papers and run for 30 min at 20 V.

Preparing for the hybridization steps, 61.25 µl 1-methylimidazol, 2.25 ml $_{dd}H_2O$ and 75 µl 1 M hydrochloric acid were mixed and shortly before use, 188 mg EDC-hydrochloride acid were added and filled up with $_{dd}H_2O$ to 6 ml to get the EDC crosslinking solution. Subsequently, the EDC solution was distributed equally onto a Whatman paper, and the membrane was – with RNA side faced up – put on top of the Whatman paper. Both, Whatman paper and membrane were wrapped in cling film and incubated at 50 °C for 1 h in a hybridization oven. To remove crosslinking solution, the membrane was washed three times with $_{dd}H_2O$ and was ready for hybridization. Preparatory to this 1 µl 20 µM antisense-oligos, 2 µl 10x T4 polynucleotide kinase buffer A, 1 µl T4 polynucleotide kinase (10 U/µl) (both from Thermo Fisher) and 14 µl water were mixed. Finally, 2 µl g-32^P-ATP were added. The mix incubated at 37 °C for 60 min. To stop the reaction, 30 µl 30 mM EDTA were added, and the mixture was purified with G25 columns (GE) to get remove free g-32^P-ATP following the manufacturer's instructions. For hybridization, the membrane was transferred to a respective flask. 15 ml hybridization buffer and the labeled probe were added and incubated overnight at the corresponding T_M of the oligo under rotation. The next day, the membrane was washed twice with 30 ml Wash solution I for 10 min each followed by one washing step with 30 ml Wash solution II for 10 min. The membrane was wrapped in cling film and exposed using the PMI Personal Molecular Imager FX (Bio-Rad).

7.5.14 Dual Luciferase Reporter assay

One day prior to HeLa cell transfection, cells were seeded onto a 48 well plates (18,000 cells/well). The next day, they were transfected with the pMIR-TK-RL vector using Lipofectamine 3000 according to the manufacturer's instruction. 48 hours post-transfection, medium was removed, and HeLa cells were lysed in 100 µl passive lysis buffer (Promega) incubating for 15 min at RT while shaking at 500 rpm on a thermomixer. 20 µl were then transferred to a 96 well plate appropriate to the Centro XS^3 LB960 plate reader. The plate reader was prepared and primed, respectively, with washing steps (99 cycles of 75% ethanol and 99 cycles of $_{dd}H_2O$). Subsequently, the 96 well plate was measured using the "dual luciferase jan.par" program.

7.6 Protein biochemistry

7.6.1 Bradford assay for protein quantification

To quantify protein, 5x Roti-Quant (Carl Roth) was diluted 1:5 with $_{dd}H_2O$ and 900 µl of this dilution was mixed with 100 µl prepared bovine serum albumin standards with known concentrations between 0 and 150 µg/ml. 1 to 10 µl of protein sample were brought to a final volume of 10 µl with protein lysis buffer and mixed with 990 µl 1x Roti-Quant. After 5 min incubation at RT, the absorption at 595 nm was measured with a nanophotometer, and the total protein amount for each sample was determined using the standard curve obtained by plotting blank-corrected A_{595} for the protein standards against their total protein amount.

7.6.2 Preparation of protein lysates from keratinocytes

Protein lysates were prepared by harvesting keratinocytes in an appropriate amount of RIPA buffer. After 15 min of incubation on ice the cells were lysed with a douncer and subsequently centrifuged (15,000 rcf, 4 °C, 15 min). The supernatant was transferred into a new tube and immediately used, or flash frozen in liquid nitrogen and stored at -80 °C until further use.

7.6.3 SDS-PAGE analysis

For SDS-Page analysis, protein samples were mixed with 1x Laemmli buffer and denaturated at 95 °C for 5 min. Depending on the size of the proteins of interest, a 10% or 15% resolving SDS-PAGE gel was made as well as a stacking gel as described in the following table.

Table 25: Composition of SDS-PAGE gels

Component	Stacking gel (4%)	Resolving gel (10%)	Resolving gel (15%)
$_{dd}H_2O$	2.25 ml	3.2 ml	1.9 ml
4x Resolving gel buffer	-	1.9 ml	1.9 ml
4x Stacking gel buffer	0.95 ml	-	-

Acrylamide/Bis-solution 30% (37.5:1)	0.5 ml	2.6 ml	3.9 ml
TEMED	5 µl	4.5 µl	4.5 µl
10% APS	22.5 µl	45 µl	45 µl

To determine protein size, 5 µl pre-stained Precision Plus Protein Standard Dual Color (Bio-Rad) was used and electrophoresis was performed in TGS buffer at 90 V for 30 min and subsequently at 120 V until the dye front reached the bottom of the gel.

7.6.4 Western Blot (WB) analysis

7.5 to 30 µg total protein from keratinocytes which was separated by terms of SDS-PAGE (see 7.6.2 and 7.6.3) was transferred to an Amersham Hybond-ECL membrane (GE) via semi-dry blotting (Bio-Rad system). Therefore, WB transfer buffer and 13 V for 60 min was used. Blocking was subsequently performed with 5% milk powder solved in TBS-T at room temperature for 60 min. Primary antibodies (Table 2) were diluted in 5% milk powder in TBS-T and transferred to the membrane at room temperature for 1 h or overnight at 4 °C. After washing the membrane with TBS-T (three times, RT, 5 min each), secondary antibodies (Table 3) were also diluted in TBS-T supplemented with 5% milk powder and applied to the membrane for 60 min at room temperature. After three washing steps with TBS-T (RT, 5 min), the fluorescence signal was captured with the Odyssey Imaging System (LI-COR biosciences) and analyzed with the Odyssey software (LI-COR Biosciences).

8 Appendix

8.1 Supplementary figures

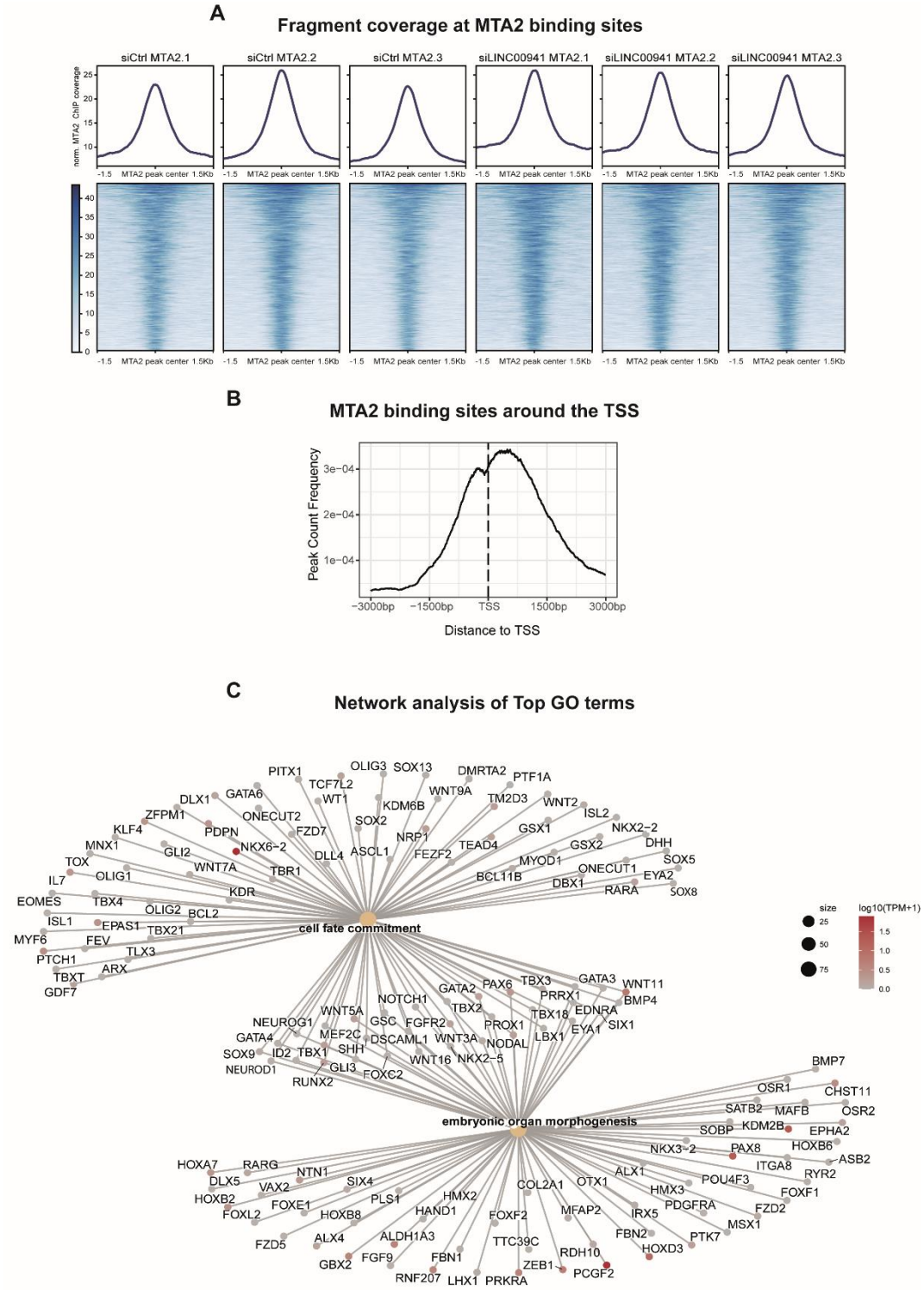

Figure 38: MTA2/NuRD occupies regulatory regions in keratinocytes
(A) MTA2 ChIP sequencing fragment coverage at MTA2 binding sites of all replicates. The top panel shows the average fragment coverage of each sample across all called MTA2 peaks (*n* = 3,617). The bottom panel depicts the fragment coverage over the MTA2-bound sites as heatmap. (B) Average profile of MTA2 binding sites around the TSS. (C) Gene network plot of Top 2 GO terms of MTA2 ChIP sequencing including keratinocyte differentiation- and development-associated genes. The color of the gene nodes signifies the expression levels in undifferentiated keratinocytes.

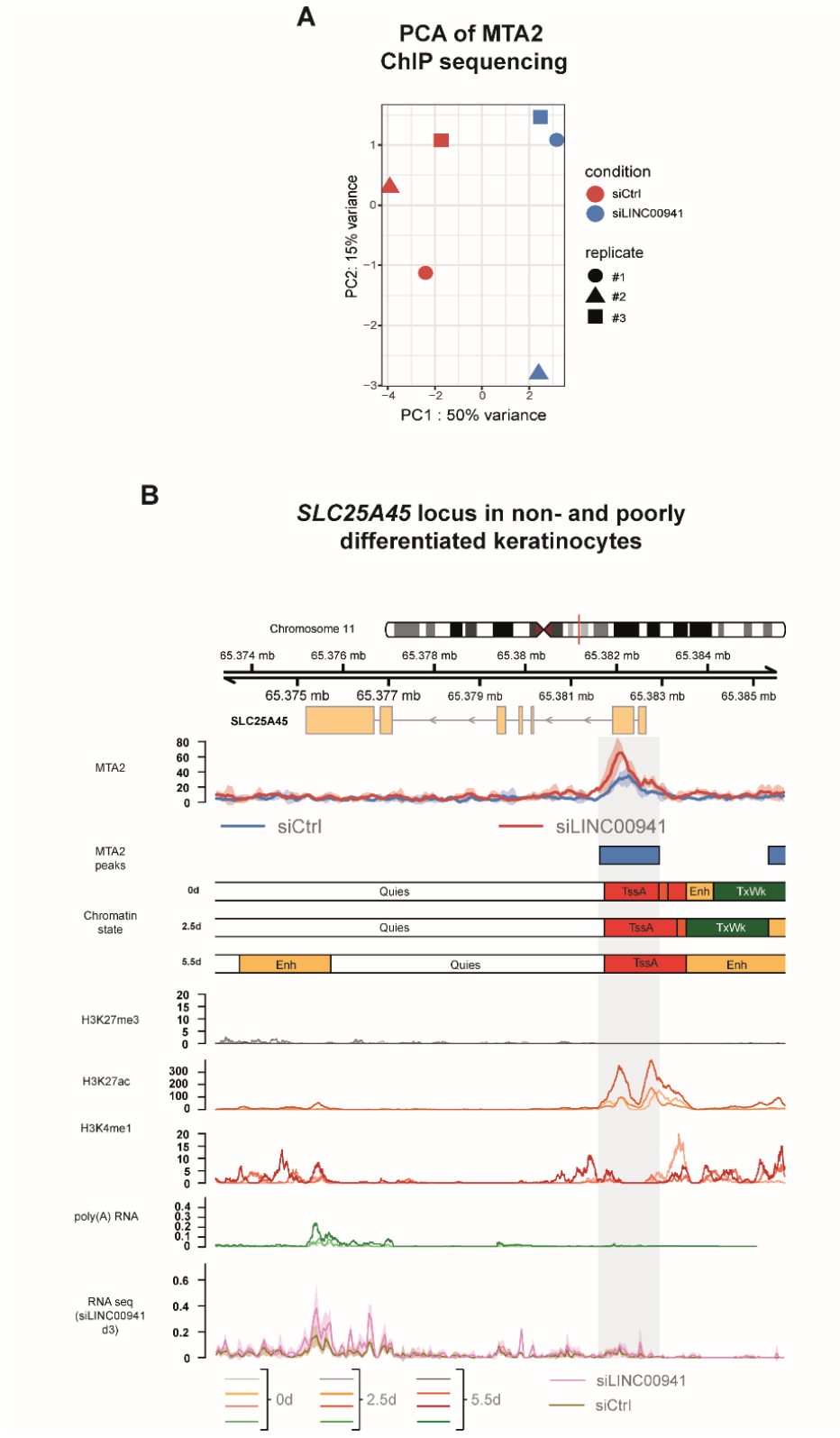

Figure 39: LINC00941 dependency of NuRD-associated MTA2 binding.
(A) Principal Component Analysis (PCA) of MTA2 ChIP sequencing experiments upon LINC00941 knockdown. (B) Genome browser view of differential binding site at *SLC25A45* locus. Tracks of chromatin states, histone modifications, and transcription in primary undifferentiated (day 0) and calcium-treated differentiated (day 2.5, day 5.5) keratinocytes obtained from ENCODE portal are shown below the MTA2 ChIP sequencing tracks. Color shades of histone modifications and RNA sequencing tracks indicate the time points of differentiation. The bottom track shows the RNA sequencing coverage of siLINC00941 knockdown and control keratinocytes after 3 days of differentiation.

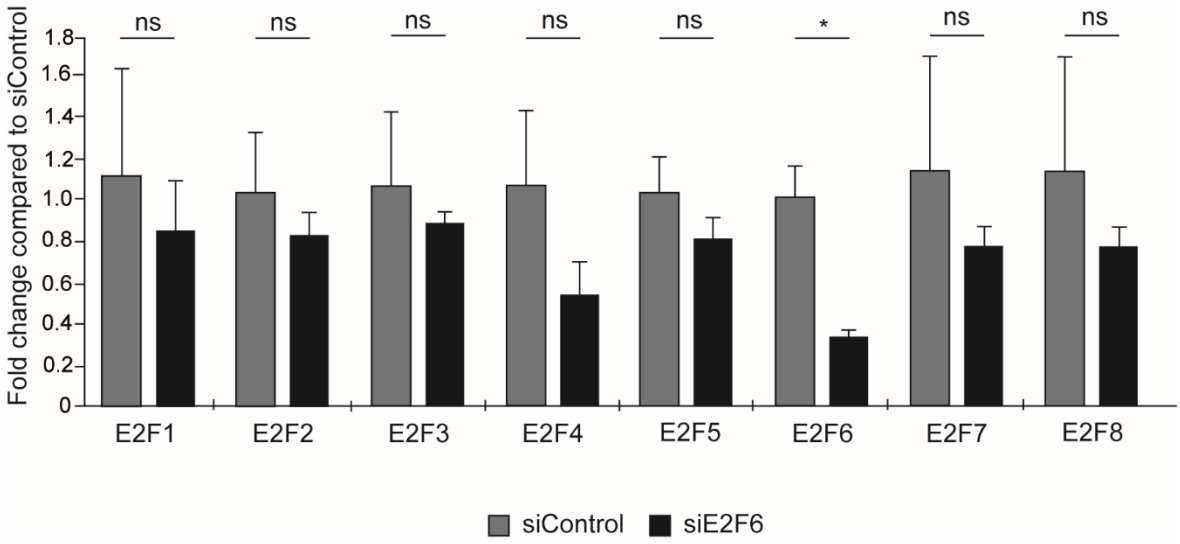

Figure 40: qRT-PCR analysis of E2F6 knockdown.
SiPool-mediated knockdown of E2F6 did not significantly alter expression levels of other E2F family members in calcium-treated differentiated keratinocytes (day 3 of differentiation). Data are presented as mean ± standard deviation. Statistical significance was tested by an unpaired *t*-test and corrected for multiple testing after Bonferroni (*adj. *P*-value < 0.05, ns = not significant).

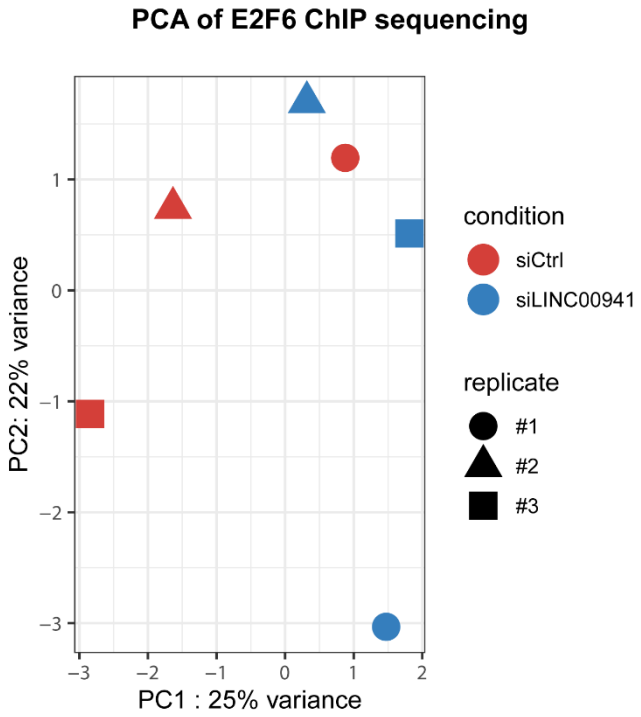

Figure 41: PCA analysis of E2F6 ChIP sequencing upon LINC00941 knockdown.
No clear separation of LINC00941-deficient and control-treated keratinocytes could be shown.

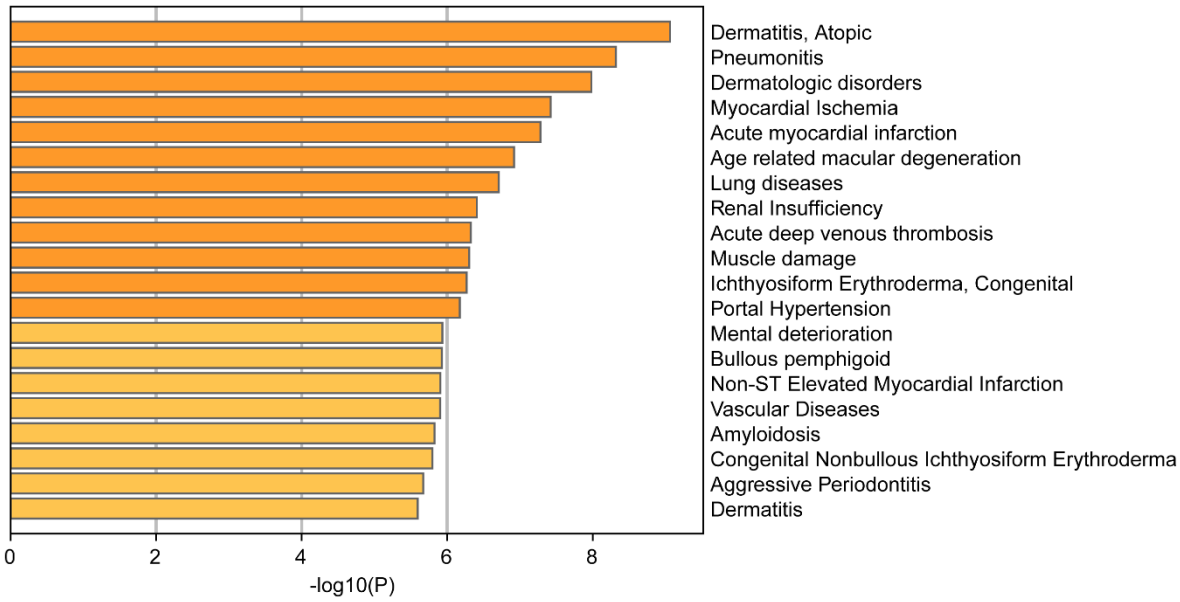

Figure 42: LINC00941-associated diseases.
Summary of enrichment analysis in DisGeNET. All genes in the genome have been used as enrichment background. Terms with a *p*-value < 0.01, a minimum count of 3, and an enrichment factor > 1.5 (ratio between observed counts and the counts expected by chance) are collected and grouped into clusters.

8.2 LINC00941 transcript sequence

The LINC00941 transcript used for cloning purposes was the isoform annotated as ENST00000547804.1. It has 5 exons, a total length of 1645 bp and is located on chromosome 12:30,948,865-30,955,645 (forward strand).

5’-GCCCTGCTGGCTGTCCCGCAGGACCCAGCGCCGCGGTAGCCTTCTCTGA
ACTGCGGCTCAGGCGGAGGTGTCACTCCTGCCTCCAGCCCAGGAGGGCAG
GTCAGGTTATGCAACGCGTGCCGCGCGATCTCCCCCCACCTCCAACCCCCTT
TTCTCCCGGGTCCACACCGCAGTTCCCACCGCTCCGGGTGTCCTCCCCAGT
GCGCCGCGATTTTTGTGTCCAAGCCCCAGAGTCCCTCTGAGACCAACCCCCA
GCCAGCACAGACTTCCTGCCTTCCCAGCTCGGGGATGTGGTCTCATTAGGTT
GCCCAAGCTGGACTTGTACTCTTGGCCTCAAGAGGTCCTTCCATCTCAGTCT
CCCAAGTAGCTGGGACTACAAGCATGCACCACTACACTCAGCCAAATACTTT
CAATAATTTGCCAGCTGACAACTTGATTGGGTTCTCCTTCAGGTTTGAAGCGC
CCTCGAGAAGTGTCTAAAGGAGACAGTTGATAGCCAAACAACAGTTTTGGATT
CACTGACTGATTATGAAAGAAGCAGTAGACTGGTATCAAGAATCAGTCAGCAA
GGAGGCCCTCACCAGACGCCAGTGCCATGTTCTTGGACTTCTCAGCCTCCAT
ATTCATGAACTAAGTTTTTGGAATCCTTAGGCTTCCACGTGTGGAAAGCCTGA

GCTAACCTACTGGAGGATGAGCCATCACCTGGAGCAGATTCAGGCCATCCTA
GTTGAAGCCTCCCTAGGCCAAGCAACCGTCCAACTACCAGACATTGACCATT
CAGCCTTGAACATTCAGCACAAAGACAAAACAGACCAGACCAGAAGAGTCCC
ACAGAATAGGGGAAACTATTCAGAGAAAACTTAAGCCACTAAGTTTTATGGTG
TTTTGTTCTGTAGCAGAAGCATAGGCATACTGACAATACAAACCGAAATCCTT
CTAACGTAGTGGACCTTTTCAGGCCAGCATTTTTTCCTTGAAAACCTGGAGCA
TGTATCCATCTTATAGCAGAGATCACTTTCACAATGTTTGGGCTCTTGATTTGA
ATTGATGATGTAATGAGCCCTCTATCCAGATTGTAACTAATTACTCTGCGAATT
GACTGGATTCCACACCCTTCTAATATTTTACTTTTCCTCTTTTATCAACTCTCAT
TCTTGCTGCCATGATCAATGGACCAACTATGCTTATAACCACAAATTTTGATAT
GCTTAAACAAATGAACAAATATATTTAATAATTTCTTTTTTTTTTTTGAAATAGTA
TCTTGCTCTGTCACCCAGGCTGCAGTGCAGCAGCGTGATCTCAGCTCACTAT
AACCTCCACCTCCCGGGTTCAAGTGATTCTCCTGCCTCAGCCTCCCAAGTAG
CTGGGACTACAGGCGCCCACCACCATACCTGGCTAATTTTTTGTATTTTTAGT
AGAGACAGGGTTTATCCATGTTGGCCAGGCTGGTCTCAAACTCCTGACCTCA
AGTGATCCTCCTGCCTCGGCCTCCCAAAGTGCTGGGATTACAGGTGTGAGCC
ACCATGCCCAGCCAATAATTTCCTGATATAATAAAAATGCCAATACTATACAAT
TAAATAGTAAAGTGATAAAAAATAGGATAACATGATAACCACTAATTAATATAT
ACTACATAATCATC-3’

8.3 miR-335-5p sequence

The miRNA hsa-miR-335-5p has a total length of 23 bp and is annotated at chr7:130,496,126-130,496,148 (forward strand).

5’-TGTAAAAAGCAATAACGAGAACT -3’

8.4 Quantitative NuRD component analysis detected in MS

Table 26: NuRD components detected in MS analysis upon RNA-IP of biotinylated LINC00941

	Protein score	emPAI	Sequence coverage (%)	Peptides detected
HDAC1	50	0.11	6	2
HDAC2	83	0.23	18	4

MTA2	100	0.17	16	4
CHD4	195	0.08	13	6
GATAD2A	52	0.,09	17	2
GATAD2B	77	0.09	20	2
RBBP4	205	0.35	15	5
RBBP7	45	0.27	11	4

8.5 ChIP sequencing statistics

Table 27: Statistics of ChIP sequencing reads

Sample	Number of reads	% >=Q30 bases
siControl_Input_E2F6	28,229,760	90.49
siControl_E2F6-1	32,279,967	90.27
siControl_E2F6-2	33,503,171	90.56
siControl_E2F6-3	29,449,913	90.44
siLINC00941_Input_E2F6	28,469,579	90.43
siLINC00941_E2F6-1	27,403,649	90.40
siLINC00941_E2F6-2	27,661,751	90.40
siLINC00941_E2F6-3	29,409,826	90.23
siControl_Input_MTA2	32,227,556	90.54
siControl_MTA2-1	27,708,264	90.17
siControl_MTA2-2	30,829,270	90.10
siControl_MTA2-3	28,499,421	90.27
siLINC00941_Input_MTA2	32,910,780	90.34
siLINC00941_MTA2-1	28,775,397	90.18
siLINC00941_MTA2-2	28,099,527	90.16
siLINC00941_MTA2-3	30,340,452	90.14

8.6 List of significantly altered MTA2/NuRD binding sites upon LINC00941 knockdown

Table 28: Statistically significant altered MTA/NuRD occupancy sites of LINC00941 knockdown

Gene	Peak-p-adj	Regulatory element	Distance to TSS [bp]	Chromatin state
SLC6A17	190.815	Promoter	542	ReprPC
LMX1A	101.955	Promoter	0	ReprPC
LHX9	60.0128	Promoter	0	BivFlnk
ESRRG	464.874	Intron	1493	BivFlnk
CNIH3	137.65	Promoter	0	BivFlnk
PTF1A	113.384	Distal Intergenic	-16769	ReprPC
PTF1A	209.221	Distal Intergenic	3765	ReprPC
NEUROG3	306.444	Distal Intergenic	-2257	ReprPC
HMX2	250.533	Promoter	0	BivFlnk
SLC25A45	44.9782	Promoter	0	TssAFlnk
TBX5	581.042	Distal Intergenic	-34845	ReprPC
HRK	205.711	Promoter	0	BivFlnk
GSX1	294.122	Distal Intergenic	27218	ReprPC
PTGDR	183.055	Promoter	0	BivFlnk
RASGRF1	183.055	Promoter	0	EnhBiv
SALL3	35.2363	Distal Intergenic	-1266	ReprPC
AP3D1	38.1301	Intron	-3900	Enh
NEUROD1	24.4842	Promoter	0	ReprPC
C2CD2	25.182	Distal Intergenic	-3988	Enh
FEZF2	125.899	Promoter	0	EnhBiv
MARCHF1	64.7869	Promoter	0	BivFlnk
HELT	348.844	Promoter	0	BivFlnk
PDE10A	30.2694	Promoter	0	ReprPC
WNT2	182.543	Promoter	0	BivFlnk

FEZF1	52.5661	Promoter	0	ReprPC
PAX4	460.328	Distal Intergenic	-1295	ReprPC
EGR3	238.226	Promoter	0	BivFlnk
RSPO2	74.4105	Promoter	0	ReprPC
ADCY8	47.781	Promoter	0	EnhBiv
MROH6	23.6808	Promoter	0	TssAFlnk
SHOX	76.4688	Distal Intergenic	-3580	ReprPC
SHOX	159.625	Promoter	0	TssBiv
SHOX	57.9792	Promoter	0	ReprPC

8.7 List of figures

8.8 List of tables

9 References

1. Martin, M. T., Vulin, A. & Hendry, J. H. Human epidermal stem cells: Role in adverse skin reactions and carcinogenesis from radiation. *Mutation research. Reviews in mutation research* **770,** 349–368; 10.1016/j.mrrev.2016.08.004 (2016).
2. Blanpain, C. & Fuchs, E. Epidermal homeostasis: a balancing act of stem cells in the skin. *Nature reviews. Molecular cell biology* **10,** 207–217; 10.1038/nrm2636 (2009).
3. MacNeil, S. Progress and opportunities for tissue-engineered skin. *Nature* **445,** 874–880; 10.1038/nature05664 (2007).
4. Kanitakis, J. Anatomy, histology and immunohistochemistry of normal human skin. *European journal of dermatology : EJD* **12,** 390-9; quiz 400-1 (2002).
5. Gonzales, K. A. U. & Fuchs, E. Skin and Its Regenerative Powers: An Alliance between Stem Cells and Their Niche. *Developmental cell* **43,** 387–401; 10.1016/j.devcel.2017.10.001 (2017).
6. Proksch, E., Brandner, J. M. & Jensen, J.-M. The skin: an indispensable barrier. *Experimental dermatology* **17,** 1063–1072; 10.1111/j.1600-0625.2008.00786.x (2008).
7. Breitkreutz, D., Mirancea, N. & Nischt, R. Basement membranes in skin: unique matrix structures with diverse functions? *Histochemistry and cell biology* **132,** 1–10; 10.1007/s00418-009-0586-0 (2009).
8. Freinkel, R. K. & Woodley, D. T. (eds.). *The biology of the skin* (Parthenon, New York, London, 2001).
9. White, S. D. & Yager, J. A. Resident Dendritic Cells in the Epidermis: Langerhans Cells, Merkel Cells and Melanocytes. *Veterinary dermatology* **6,** 1–8; 10.1111/j.1365-3164.1995.tb00034.x (1995).
10. Fuchs, E. Epidermal differentiation: the bare essentials. *The Journal of cell biology* **111,** 2807–2814; 10.1083/jcb.111.6.2807 (1990).

11. Solanas, G. & Benitah, S. A. Regenerating the skin: a task for the heterogeneous stem cell pool and surrounding niche. *Nature reviews. Molecular cell biology* **14,** 737–748; 10.1038/nrm3675 (2013).

12. Doupé, D. P. & Jones, P. H. Interfollicular epidermal homeostasis: dicing with differentiation. *Experimental dermatology* **21,** 249–253; 10.1111/j.1600-0625.2012.01447.x (2012).

13. Candi, E., Schmidt, R. & Melino, G. The cornified envelope: a model of cell death in the skin. *Nature reviews. Molecular cell biology* **6,** 328–340; 10.1038/nrm1619 (2005).

14. Baroni, A. *et al.* Structure and function of the epidermis related to barrier properties. *Clinics in Dermatology* **30,** 257–262; 10.1016/j.clindermatol.2011.08.007 (2012).

15. Marques-Pereira, J. P. & Leblond, C. P. Mitosis and differentiation in the stratified squamous epithelium of the rat esophagus. *The American journal of anatomy* **117,** 73–87; 10.1002/aja.1001170106 (1965).

16. Potten, C. S. & Morris, R. J. Epithelial stem cells in vivo. *Journal of cell science. Supplement* **10,** 45–62; 10.1242/jcs.1988.Supplement_10.4 (1988).

17. Clayton, E. *et al.* A single type of progenitor cell maintains normal epidermis. *Nature* **446,** 185–189; 10.1038/nature05574 (2007).

18. Alcolea, M. P. & Jones, P. H. Lineage analysis of epidermal stem cells. *Cold Spring Harbor perspectives in medicine* **4,** a015206; 10.1101/cshperspect.a015206 (2014).

19. Hennings, H. & Holbrook, K. A. Calcium regulation of cell-cell contact and differentiation of epidermal cells in culture. An ultrastructural study. *Experimental cell research* **143,** 127–142; 10.1016/0014-4827(83)90115-5 (1983).

20. Hennings, H. *et al.* Calcium regulation of growth and differentiation of mouse epidermal cells in culture. *Cell* **19,** 245–254; 10.1016/0092-8674(80)90406-7 (1980).

21. Steven, A. C. & Steinert, P. M. Protein composition of cornified cell envelopes of epidermal keratinocytes. *Journal of cell science* **107,** 693–700; 10.1242/jcs.107.2.693 (1994).

22. McGrath, J. A. & Uitto, J. The filaggrin story: novel insights into skin-barrier function and disease. *Trends in molecular medicine* **14,** 20–27; 10.1016/j.molmed.2007.10.006 (2008).

23. Fuchs, E. Epidermal differentiation and keratin gene expression. *Journal of cell science. Supplement* **17,** 197–208; 10.1242/jcs.1993.Supplement_17.28 (1993).

24. Hitomi, K. Transglutaminases in skin epidermis. *European journal of dermatology: EJD* **15,** 313–319 (2005).

25. Kalinin, A., Marekov, L. N. & Steinert, P. M. Assembly of the epidermal cornified cell envelope. *Journal of cell science* **114,** 3069–3070; 10.1242/jcs.114.17.3069 (2001).

26. Sahle, F. F., Gebre-Mariam, T., Dobner, B., Wohlrab, J. & Neubert, R. H. H. Skin diseases associated with the depletion of stratum corneum lipids and stratum corneum lipid substitution therapy. *Skin pharmacology and physiology* **28,** 42–55; 10.1159/000360009 (2015).

27. Serre, G. *et al.* Identification of late differentiation antigens of human cornified epithelia, expressed in re-organized desmosomes and bound to cross-linked envelope. *Journal of Investigative Dermatology* **97,** 1061–1072; 10.1111/1523-1747.ep12492589 (1991).

28. Nemes, Z. & Steinert, P. M. Bricks and mortar of the epidermal barrier. *Experimental & molecular medicine* **31,** 5–19; 10.1038/emm.1999.2 (1999).

29. Kosak, S. T. *et al.* Coordinate gene regulation during hematopoiesis is related to genomic organization. *PLoS biology* **5,** e309; 10.1371/journal.pbio.0050309 (2007).

30. Engelkamp, D., Schäfer, B. W., Mattei, M. G., Erne, P. & Heizmann, C. W. Six S100 genes are clustered on human chromosome 1q21: identification of two genes coding for the two previously unreported calcium-binding proteins S100D and S100E. *Proceedings of the National Academy of Sciences of the United States of America* **90,** 6547–6551; 10.1073/pnas.90.14.6547 (1993).

31. Hardas, B. D. *et al.* Assignment of psoriasin to human chromosomal band 1q21: coordinate overexpression of clustered genes in psoriasis. *Journal of*

Investigative Dermatology **106,** 753–758; 10.1111/1523-1747.ep12345807 (1996).

32. Mischke, D., Korge, B. P., Marenholz, I., Volz, A. & Ziegler, A. Genes encoding structural proteins of epidermal cornification and S100 calcium-binding proteins form a gene complex ("epidermal differentiation complex") on human chromosome 1q21. *Journal of Investigative Dermatology* **106,** 989–992; 10.1111/1523-1747.ep12338501 (1996).

33. Henry, J. *et al.* Update on the epidermal differentiation complex. *Frontiers in bioscience (Landmark edition)* **17,** 1517–1532; 10.2741/4001 (2012).

34. Backendorf, C. & Hohl, D. A common origin for cornified envelope proteins? *Nature genetics* **2,** 91; 10.1038/ng1092-91 (1992).

35. Kypriotou, M., Huber, M. & Hohl, D. The human epidermal differentiation complex: cornified envelope precursors, S100 proteins and the 'fused genes' family. *Experimental dermatology* **21,** 643–649; 10.1111/j.1600-0625.2012.01472.x (2012).

36. Gibbs, S. *et al.* Molecular characterization and evolution of the SPRR family of keratinocyte differentiation markers encoding small proline-rich proteins. *Genomics* **16,** 630–637; 10.1006/geno.1993.1240 (1993).

37. Zimmer, D. B., Cornwall, E. H., Landar, A. & Song, W. The S100 protein family: history, function, and expression. *Brain research bulletin* **37,** 417–429; 10.1016/0361-9230(95)00040-2 (1995).

38. Eckert, R. L. *et al.* S100 proteins in the epidermis. *Journal of Investigative Dermatology* **123,** 23–33; 10.1111/j.0022-202X.2004.22719.x (2004).

39. Krieg, P. *et al.* Repetin (Rptn), a new member of the "fused gene" subgroup within the S100 gene family encoding a murine epidermal differentiation protein. *Genomics* **43,** 339–348; 10.1006/geno.1997.4818 (1997).

40. Contzler, R., Favre, B., Huber, M. & Hohl, D. Cornulin, a new member of the "fused gene" family, is expressed during epidermal differentiation. *Journal of Investigative Dermatology* **124,** 990–997; 10.1111/j.0022-202X.2005.23694.x (2005).

41. Takaishi, M., Makino, T., Morohashi, M. & Huh, N.-H. Identification of human hornerin and its expression in regenerating and psoriatic skin. *The Journal of biological chemistry* **280,** 4696–4703; 10.1074/jbc.M409026200 (2005).

42. Wu, Z., Hansmann, B., Meyer-Hoffert, U., Gläser, R. & Schröder, J.-M. Molecular identification and expression analysis of filaggrin-2, a member of the S100 fused-type protein family. *PloS one* **4,** e5227; 10.1371/journal.pone.0005227 (2009).

43. Lee, S. C. *et al.* Human trichohyalin gene is clustered with the genes for other epidermal structural proteins and calcium-binding proteins at chromosomal locus 1q21. *Journal of Investigative Dermatology* **100,** 65–68; 10.1111/1523-1747.ep12354504 (1993).

44. Andreoli, J. M. *et al.* The expression of a novel, epithelium-specific ets transcription factor is restricted to the most differentiated layers in the epidermis. *Nucleic acids research* **25,** 4287–4295; 10.1093/nar/25.21.4287 (1997).

45. Segre, J. A., Bauer, C. & Fuchs, E. Klf4 is a transcription factor required for establishing the barrier function of the skin. *Nature genetics* **22,** 356–360; 10.1038/11926 (1999).

46. Guzman Strong, C. de *et al.* Lipid defect underlies selective skin barrier impairment of an epidermal-specific deletion of Gata-3. *The Journal of cell biology* **175,** 661–670; 10.1083/jcb.200605057 (2006).

47. Guzman Strong, C. de *et al.* A milieu of regulatory elements in the epidermal differentiation complex syntenic block: implications for atopic dermatitis and psoriasis. *Human molecular genetics* **19,** 1453–1460; 10.1093/hmg/ddq019 (2010).

48. Geisler, S. & Coller, J. RNA in unexpected places: long non-coding RNA functions in diverse cellular contexts. *Nature reviews. Molecular cell biology* **14,** 699–712; 10.1038/nrm3679 (2013).

49. Crick, F. Central dogma of molecular biology. *Nature* **227,** 561–563; 10.1038/227561a0 (1970).

50. International Human Genome Sequencing Consortium. Finishing the euchromatic sequence of the human genome. *Nature* **431,** 931–945; 10.1038/nature03001 (2004).

51. Djebali, S. *et al.* Landscape of transcription in human cells. *Nature* **489,** 101–108; 10.1038/nature11233 (2012).

52. Farazi, T. A., Juranek, S. A. & Tuschl, T. The growing catalog of small RNAs and their association with distinct Argonaute/Piwi family members. *Development (Cambridge, England)* **135,** 1201–1214; 10.1242/dev.005629 (2008).

53. Matera, A. G., Terns, R. M. & Terns, M. P. Non-coding RNAs: lessons from the small nuclear and small nucleolar RNAs. *Nature reviews. Molecular cell biology* **8,** 209–220; 10.1038/nrm2124 (2007).

54. Okamura, K. & Lai, E. C. Endogenous small interfering RNAs in animals. *Nature reviews. Molecular cell biology* **9,** 673–678; 10.1038/nrm2479 (2008).

55. Jia, H. *et al.* Genome-wide computational identification and manual annotation of human long noncoding RNA genes. *RNA (New York, N.Y.)* **16,** 1478–1487; 10.1261/rna.1951310 (2010).

56. Cabili, M. N. *et al.* Integrative annotation of human large intergenic noncoding RNAs reveals global properties and specific subclasses. *Genes & development* **25,** 1915–1927; 10.1101/gad.17446611 (2011).

57. Derrien, T. *et al.* The GENCODE v7 catalog of human long noncoding RNAs: analysis of their gene structure, evolution, and expression. *Genome research* **22,** 1775–1789; 10.1101/gr.132159.111 (2012).

58. Quinn, J. J. & Chang, H. Y. Unique features of long non-coding RNA biogenesis and function. *Nature reviews. Genetics* **17,** 47–62; 10.1038/nrg.2015.10 (2016).

59. Guttman, M. *et al.* lincRNAs act in the circuitry controlling pluripotency and differentiation. *Nature* **477,** 295–300; 10.1038/nature10398 (2011).

60. Ransohoff, J. D., Wei, Y. & Khavari, P. A. The functions and unique features of long intergenic non-coding RNA. *Nature reviews. Molecular cell biology* **19,** 143–157; 10.1038/nrm.2017.104 (2018).

61. Pang, K. C., Frith, M. C. & Mattick, J. S. Rapid evolution of noncoding RNAs: lack of conservation does not mean lack of function. *Trends in Genetics* **22,** 1–5; 10.1016/j.tig.2005.10.003 (2006).

62. Lai, W.-J. C. *et al.* mRNAs and lncRNAs intrinsically form secondary structures with short end-to-end distances. *Nature communications* **9,** 4328; 10.1038/s41467-018-06792-z (2018).

63. Guo, X. *et al.* Advances in long noncoding RNAs: identification, structure prediction and function annotation. *Briefings in functional genomics* **15,** 38–46; 10.1093/bfgp/elv022 (2016).

64. Ma, L., Bajic, V. B. & Zhang, Z. On the classification of long non-coding RNAs. *RNA biology* **10,** 925–933; 10.4161/rna.24604 (2013).

65. Rinn, J. L. & Chang, H. Y. Genome regulation by long noncoding RNAs. *Annual review of biochemistry* **81,** 145–166; 10.1146/annurev-biochem-051410-092902 (2012).

66. Ziegler, C. & Kretz, M. The More the Merrier-Complexity in Long Non-Coding RNA Loci. *Frontiers in endocrinology* **8,** 90; 10.3389/fendo.2017.00090 (2017).

67. Kornienko, A. E. *et al.* Long non-coding RNAs display higher natural expression variation than protein-coding genes in healthy humans. *Genome biology* **17,** 14; 10.1186/s13059-016-0873-8 (2016).

68. Niemczyk, M. *et al.* Imprinted chromatin around DIRAS3 regulates alternative splicing of GNG12-AS1, a long noncoding RNA. *American journal of human genetics* **93,** 224–235; 10.1016/j.ajhg.2013.06.010 (2013).

69. Schmitt, A. M. & Chang, H. Y. Long Noncoding RNAs in Cancer Pathways. *Cancer cell* **29,** 452–463; 10.1016/j.ccell.2016.03.010 (2016).

70. Sleutels, F., Zwart, R. & Barlow, D. P. The non-coding Air RNA is required for silencing autosomal imprinted genes. *Nature* **415,** 810–813; 10.1038/415810a (2002).

71. Kretz, M. *et al.* Suppression of progenitor differentiation requires the long noncoding RNA ANCR. *Genes & development* **26,** 338–343; 10.1101/gad.182121.111 (2012).

72. Nagano, T. & Fraser, P. No-nonsense functions for long noncoding RNAs. *Cell* **145,** 178–181; 10.1016/j.cell.2011.03.014 (2011).

73. Fatica, A. & Bozzoni, I. Long non-coding RNAs: new players in cell differentiation and development. *Nature reviews. Genetics* **15,** 7–21; 10.1038/nrg3606 (2014).

74. Flynn, R. A. & Chang, H. Y. Long noncoding RNAs in cell-fate programming and reprogramming. *Cell stem cell* **14,** 752–761; 10.1016/j.stem.2014.05.014 (2014).

75. Wang, K. C. & Chang, H. Y. Molecular mechanisms of long noncoding RNAs. *Molecular cell* **43,** 904–914; 10.1016/j.molcel.2011.08.018 (2011).

76. Shibayama, Y., Fanucchi, S., Magagula, L. & Mhlanga, M. M. lncRNA and gene looping: what's the connection? *Transcription* **5,** e28658; 10.4161/trns.28658 (2014).

77. Han, P. & Chang, C.-P. Long non-coding RNA and chromatin remodeling. *RNA biology* **12,** 1094–1098; 10.1080/15476286.2015.1063770 (2015).

78. Brockdorff, N. Noncoding RNA and Polycomb recruitment. *RNA (New York, N.Y.)* **19,** 429–442; 10.1261/rna.037598.112 (2013).

79. Wang, K. C. *et al.* A long noncoding RNA maintains active chromatin to coordinate homeotic gene expression. *Nature* **472,** 120–124; 10.1038/nature09819 (2011).

80. Di Ruscio, A. *et al.* DNMT1-interacting RNAs block gene-specific DNA methylation. *Nature* **503,** 371–376; 10.1038/nature12598 (2013).

81. Arab, K. *et al.* Long noncoding RNA TARID directs demethylation and activation of the tumor suppressor TCF21 via GADD45A. *Molecular cell* **55,** 604–614; 10.1016/j.molcel.2014.06.031 (2014).

82. Rinn, J. L. *et al.* Functional demarcation of active and silent chromatin domains in human HOX loci by noncoding RNAs. *Cell* **129,** 1311–1323; 10.1016/j.cell.2007.05.022 (2007).

83. Chu, C., Qu, K., Zhong, F. L., Artandi, S. E. & Chang, H. Y. Genomic maps of long noncoding RNA occupancy reveal principles of RNA-chromatin interactions. *Molecular cell* **44,** 667–678; 10.1016/j.molcel.2011.08.027 (2011).

84. Xue, Z. *et al.* A G-Rich Motif in the lncRNA Braveheart Interacts with a Zinc-Finger Transcription Factor to Specify the Cardiovascular Lineage. *Molecular cell* **64,** 37–50; 10.1016/j.molcel.2016.08.010 (2016).

85. Beltran, M. *et al.* A natural antisense transcript regulates Zeb2/Sip1 gene expression during Snail1-induced epithelial-mesenchymal transition. *Genes & development* **22,** 756–769; 10.1101/gad.455708 (2008).

86. Clemson, C. M. *et al.* An architectural role for a nuclear noncoding RNA: NEAT1 RNA is essential for the structure of paraspeckles. *Molecular cell* **33,** 717–726; 10.1016/j.molcel.2009.01.026 (2009).

87. Willingham, A. T. *et al.* A strategy for probing the function of noncoding RNAs finds a repressor of NFAT. *Science (New York, N.Y.)* **309,** 1570–1573; 10.1126/science.1115901 (2005).

88. Faghihi, M. A. *et al.* Expression of a noncoding RNA is elevated in Alzheimer's disease and drives rapid feed-forward regulation of beta-secretase. *Nature medicine* **14,** 723–730; 10.1038/nm1784 (2008).

89. Karlsson, O. & Baccarelli, A. A. Environmental Health and Long Non-coding RNAs. *Current environmental health reports* **3,** 178–187; 10.1007/s40572-016-0092-1 (2016).

90. Bazin, J. *et al.* Global analysis of ribosome-associated noncoding RNAs unveils new modes of translational regulation. *Proceedings of the National Academy of Sciences of the United States of America* **114,** E10018-E10027; 10.1073/pnas.1708433114 (2017).

91. Salmena, L., Poliseno, L., Tay, Y., Kats, L. & Pandolfi, P. P. A ceRNA hypothesis: the Rosetta Stone of a hidden RNA language? *Cell* **146,** 353–358; 10.1016/j.cell.2011.07.014 (2011).

92. Yoon, J.-H. *et al.* Scaffold function of long non-coding RNA HOTAIR in protein ubiquitination. *Nature communications* **4,** 2939; 10.1038/ncomms3939 (2013).

93. Yan, C., Chen, J. & Chen, N. Long noncoding RNA MALAT1 promotes hepatic steatosis and insulin resistance by increasing nuclear SREBP-1c protein stability. *Scientific reports* **6,** 22640; 10.1038/srep22640 (2016).

94. Nelson, B. R. *et al.* A peptide encoded by a transcript annotated as long noncoding RNA enhances SERCA activity in muscle. *Science (New York, N.Y.)* **351,** 271–275; 10.1126/science.aad4076 (2016).

95. Anderson, D. M. *et al.* A micropeptide encoded by a putative long noncoding RNA regulates muscle performance. *Cell* **160,** 595–606; 10.1016/j.cell.2015.01.009 (2015).

96. Gezer, U., Özgür, E., Cetinkaya, M., Isin, M. & Dalay, N. Long non-coding RNAs with low expression levels in cells are enriched in secreted exosomes. *Cell biology international* **38,** 1076–1079; 10.1002/cbin.10301 (2014).

97. Xiao, L., Gorospe, M. & Wang, J.-Y. Long noncoding RNAs in intestinal epithelium homeostasis. *American journal of physiology. Cell physiology* **317,** C93-C100; 10.1152/ajpcell.00092.2019 (2019).

98. Klattenhoff, C. A. *et al.* Braveheart, a long noncoding RNA required for cardiovascular lineage commitment. *Cell* **152,** 570–583; 10.1016/j.cell.2013.01.003 (2013).

99. Ounzain, S. *et al.* CARMEN, a human super enhancer-associated long noncoding RNA controlling cardiac specification, differentiation and homeostasis. *Journal of molecular and cellular cardiology* **89,** 98–112; 10.1016/j.yjmcc.2015.09.016 (2015).

100. Grote, P. *et al.* The tissue-specific lncRNA Fendrr is an essential regulator of heart and body wall development in the mouse. *Developmental cell* **24,** 206–214; 10.1016/j.devcel.2012.12.012 (2013).

101. Cesana, M. *et al.* A long noncoding RNA controls muscle differentiation by functioning as a competing endogenous RNA. *Cell* **147,** 358–369; 10.1016/j.cell.2011.09.028 (2011).

102. Qureshi, I. A. & Mehler, M. F. Emerging roles of non-coding RNAs in brain evolution, development, plasticity and disease. *Nature reviews. Neuroscience* **13,** 528–541; 10.1038/nrn3234 (2012).

103. Salviano-Silva, A., Lobo-Alves, S. C., Almeida, R. C. de, Malheiros, D. & Petzl-Erler, M. L. Besides Pathology: Long Non-Coding RNA in Cell and Tissue Homeostasis. *Non-coding RNA* **4**; 10.3390/ncrna4010003 (2018).

104. Chalei, V. *et al.* The long non-coding RNA Dali is an epigenetic regulator of neural differentiation. *eLife* **3,** e04530; 10.7554/eLife.04530 (2014).

105. Ramos, A. D. *et al.* The long noncoding RNA Pnky regulates neuronal differentiation of embryonic and postnatal neural stem cells. *Cell stem cell* **16,** 439–447; 10.1016/j.stem.2015.02.007 (2015).

106. Zhu, P. *et al.* LncGata6 maintains stemness of intestinal stem cells and promotes intestinal tumorigenesis. *Nature cell biology* **20,** 1134–1144; 10.1038/s41556-018-0194-0 (2018).

107. Xiao, L. *et al.* Long noncoding RNA SPRY4-IT1 regulates intestinal epithelial barrier function by modulating the expression levels of tight junction proteins. *Molecular biology of the cell* **27,** 617–626; 10.1091/mbc.E15-10-0703 (2016).

108. Cai, P. *et al.* A genome-wide long noncoding RNA CRISPRi screen identifies PRANCR as a novel regulator of epidermal homeostasis. *Genome research* **30,** 22–34; 10.1101/gr.251561.119 (2020).

109. Lee, C. S. *et al.* Cancer-Associated Long Noncoding RNA SMRT-2 Controls Epidermal Differentiation. *The Journal of investigative dermatology* **138,** 1445–1449; 10.1016/j.jid.2018.01.003 (2018).

110. Tanis, S. E. J., Köksal, E. S., van Buggenum, J. A. G. L. & Mulder, K. W. BLNCR is a long non-coding RNA adjacent to integrin beta-1 that is rapidly lost during epidermal progenitor cell differentiation. *Scientific reports* **9,** 31; 10.1038/s41598-018-37251-w (2019).

111. Kretz, M. *et al.* Control of somatic tissue differentiation by the long non-coding RNA TINCR. *Nature* **493,** 231–235; 10.1038/nature11661 (2013).

112. Lopez-Pajares, V. *et al.* A LncRNA-MAF:MAFB transcription factor network regulates epidermal differentiation. *Developmental cell* **32,** 693–706; 10.1016/j.devcel.2015.01.028 (2015).

113. Ziegler, C. *et al.* The long non-coding RNA LINC00941 and SPRR5 are novel regulators of human epidermal homeostasis. *EMBO reports* **20**; 10.15252/embr.201846612 (2019).

114. Wang, J., He, Z., Xu, J., Chen, P. & Jiang, J. Long noncoding RNA LINC00941 promotes pancreatic cancer progression by competitively binding miR-335-5p to regulate ROCK1-mediated LIMK1/Cofilin-1 signaling. *Cell death & disease* **12,** 36; 10.1038/s41419-020-03316-w (2021).

115. Lu, J.-T. *et al.* Reciprocal regulation of LINC00941 and SOX2 promotes progression of esophageal squamous cell carcinoma. *Cell death & disease* **14,** 72; 10.1038/s41419-023-05605-6 (2023).

116. Morgenstern, E. & Kretz, M. The human long non-coding RNA LINC00941 and its modes of action in health and disease. *Biological chemistry*; 10.1515/hsz-2023-0183 (2023).

117. Ai, Y., Wu, S., Zou, C. & Wei, H. LINC00941 promotes oral squamous cell carcinoma progression via activating CAPRIN2 and canonical WNT/β-catenin signaling pathway. *Journal of cellular and molecular medicine* **24,** 10512–10524; 10.1111/jcmm.15667 (2020).

118. Eagen, K. P. Principles of Chromosome Architecture Revealed by Hi-C. *Trends in Biochemical Sciences* **43,** 469–478; 10.1016/j.tibs.2018.03.006 (2018).

119. Jeong, W. & Jho, E.-H. Regulation of the Low-Density Lipoprotein Receptor-Related Protein LRP6 and Its Association With Disease: Wnt/β-Catenin Signaling and Beyond. *Frontiers in cell and developmental biology* **9,** 714330; 10.3389/fcell.2021.714330 (2021).

120. Ding, Y. *et al.* Caprin-2 enhances canonical Wnt signaling through regulating LRP5/6 phosphorylation. *The Journal of cell biology* **182,** 865–872; 10.1083/jcb.200803147 (2008).

121. Duchartre, Y., Kim, Y.-M. & Kahn, M. The Wnt signaling pathway in cancer. *Critical reviews in oncology/hematology* **99,** 141–149; 10.1016/j.critrevonc.2015.12.005 (2016).

122. Novak, D. *et al.* SOX2 in development and cancer biology. *Seminars in cancer biology* **67,** 74–82; 10.1016/j.semcancer.2019.08.007 (2020).

123. Wu, N. *et al.* LINC00941 promotes CRC metastasis through preventing SMAD4 protein degradation and activating the TGF-β/SMAD2/3 signaling pathway. *Cell death and differentiation* **28,** 219–232; 10.1038/s41418-020-0596-y (2021).

124. Wan, M. *et al.* SCF(beta-TrCP1) controls Smad4 protein stability in pancreatic cancer cells. *The American journal of pathology* **166,** 1379–1392; 10.1016/S0002-9440(10)62356-5 (2005).

125. Xu, M. *et al.* LINC00941 promotes glycolysis in pancreatic cancer by modulating the Hippo pathway. *Molecular therapy. Nucleic acids* **26,** 280–294; 10.1016/j.omtn.2021.07.004 (2021).

126. Tang, Y. *et al.* Selective Inhibition of STRN3-Containing PP2A Phosphatase Restores Hippo Tumor-Suppressor Activity in Gastric Cancer. *Cancer cell* **38,** 115-128.e9; 10.1016/j.ccell.2020.05.019 (2020).

127. Wang, J. *et al.* LINC00941 promotes pancreatic cancer malignancy by interacting with ANXA2 and suppressing NEDD4L-mediated degradation of ANXA2. *Cell death & disease* **13,** 718; 10.1038/s41419-022-05172-2 (2022).

128. Anselmino, N. *et al.* HO-1 Interactors Involved in the Colonization of the Bone Niche: Role of ANXA2 in Prostate Cancer Progression. *Biomolecules* **10**; 10.3390/biom10030467 (2020).

129. Mao, L. *et al.* EphA2-YES1-ANXA2 pathway promotes gastric cancer progression and metastasis. *Oncogene* **40,** 3610–3623; 10.1038/s41388-021-01786-6 (2021).

130. Paul, R. *et al.* FAK activates AKT-mTOR signaling to promote the growth and progression of MMTV-Wnt1-driven basal-like mammary tumors. *Breast cancer research: BCR* **22,** 59; 10.1186/s13058-020-01298-3 (2020).

131. Chang, L., Zhou, D. & Luo, S. Novel lncRNA LINC00941 Promotes Proliferation and Invasion of Colon Cancer Through Activation of MYC. *OncoTargets and therapy* **14,** 1173–1186; 10.2147/OTT.S293519 (2021).

132. Fang, L., Wang, S.-H., Cui, Y.-G. & Huang, L. LINC00941 promotes proliferation and metastasis of pancreatic adenocarcinoma by competitively binding miR-873-3p and thus upregulates ATXN2. *European review for medical and pharmacological sciences* **25,** 1861–1868; 10.26355/eurrev_202102_25081 (2021).

133. Zhang, Y. *et al.* Linc00941 regulates esophageal squamous cell carcinoma via functioning as a competing endogenous RNA for miR-877-3p to modulate PMEPA1 expression. *Aging* **13,** 17830–17846; 10.18632/aging.203286 (2021).

134. Denzler, R., Agarwal, V., Stefano, J., Bartel, D. P. & Stoffel, M. Assessing the ceRNA hypothesis with quantitative measurements of miRNA and target abundance. *Molecular cell* **54,** 766–776; 10.1016/j.molcel.2014.03.045 (2014).

135. Denzler, R. *et al.* Impact of MicroRNA Levels, Target-Site Complementarity, and Cooperativity on Competing Endogenous RNA-Regulated Gene Expression. *Molecular cell* **64,** 565–579; 10.1016/j.molcel.2016.09.027 (2016).

136. Bosson, A. D., Zamudio, J. R. & Sharp, P. A. Endogenous miRNA and target concentrations determine susceptibility to potential ceRNA competition. *Molecular cell* **56,** 347–359; 10.1016/j.molcel.2014.09.018 (2014).

137. Smillie, C. L., Sirey, T. & Ponting, C. P. Complexities of post-transcriptional regulation and the modeling of ceRNA crosstalk. *Critical reviews in biochemistry and molecular biology* **53,** 231–245; 10.1080/10409238.2018.1447542 (2018).

138. Graf, J. Functional characterization of the novel lncRNA LINC00941 in tissue homeostasis and disease. *Universität Regensburg*; 10.5283/epub.45236 (2020).

139. Adinolfi, M. *et al.* Discovering sequence and structure landscapes in RNA interaction motifs. *Nucleic acids research* **47,** 4958–4969; 10.1093/nar/gkz250 (2019).

140. Haecker, I. *et al.* Ago HITS-CLIP expands understanding of Kaposi's sarcoma-associated herpesvirus miRNA function in primary effusion lymphomas. *PLoS pathogens* **8,** e1002884; 10.1371/journal.ppat.1002884 (2012).

141. Gottwein, E. *et al.* Viral microRNA targetome of KSHV-infected primary effusion lymphoma cell lines. *Cell host & microbe* **10,** 515–526; 10.1016/j.chom.2011.09.012 (2011).

142. Skalsky, R. L. *et al.* The viral and cellular microRNA targetome in lymphoblastoid cell lines. *PLoS pathogens* **8,** e1002484; 10.1371/journal.ppat.1002484 (2012).

143. Karginov, F. V. & Hannon, G. J. Remodeling of Ago2-mRNA interactions upon cellular stress reflects miRNA complementarity and correlates with altered translation rates. *Genes & development* **27,** 1624–1632; 10.1101/gad.215939.113 (2013).

144. Ren, M.-H., Chen, S., Wang, L.-G., Rui, W.-X. & Li, P. LINC00941 Promotes Progression of Non-Small Cell Lung Cancer by Sponging miR-877-3p to Regulate VEGFA Expression. *Frontiers in oncology* **11,** 650037; 10.3389/fonc.2021.650037 (2021).

145. Yan, X. *et al.* Mesenchymal Stem Cells Promote Hepatocarcinogenesis via lncRNA-MUF Interaction with ANXA2 and miR-34a. *Cancer research* **77,** 6704–6716; 10.1158/0008-5472.CAN-17-1915 (2017).

146. Shree, B., Tripathi, S. & Sharma, V. Transforming Growth Factor-Beta-Regulated LncRNA-MUF Promotes Invasion by Modulating the miR-34a Snail1 Axis in Glioblastoma Multiforme. *Frontiers in oncology* **11,** 788755; 10.3389/fonc.2021.788755 (2021).

147. Li, J.-H., Liu, S., Zhou, H., Qu, L.-H. & Yang, J.-H. starBase v2.0: decoding miRNA-ceRNA, miRNA-ncRNA and protein-RNA interaction networks from large-scale CLIP-Seq data. *Nucleic acids research* **42,** D92-7; 10.1093/nar/gkt1248 (2014).

148. Bandyopadhyay, S. & Mitra, R. TargetMiner: microRNA target prediction with systematic identification of tissue-specific negative examples. *Bioinformatics (Oxford, England)* **25,** 2625–2631; 10.1093/bioinformatics/btp503 (2009).

149. Mann, M., Wright, P. R. & Backofen, R. IntaRNA 2.0: enhanced and customizable prediction of RNA-RNA interactions. *Nucleic acids research* **45,** W435-W439; 10.1093/nar/gkx279 (2017).

150. Mückstein, U. *et al.* Thermodynamics of RNA-RNA binding. *Bioinformatics (Oxford, England)* **22,** 1177–1182; 10.1093/bioinformatics/btl024 (2006).

151. Gaidatzis, D., van Nimwegen, E., Hausser, J. & Zavolan, M. Inference of miRNA targets using evolutionary conservation and pathway analysis. *BMC bioinformatics* **8,** 69; 10.1186/1471-2105-8-69 (2007).

152. Liew, W. C. *et al.* Belinostat resolves skin barrier defects in atopic dermatitis by targeting the dysregulated miR-335:SOX6 axis. *The Journal of allergy and clinical immunology* **146,** 606-620.e12; 10.1016/j.jaci.2020.02.007 (2020).

153. Pantier, R., Mullin, N. P. & Chambers, I. A new twist to Sin3 complexes in pluripotent cells. *The EMBO journal* **36,** 2184–2186; 10.15252/embj.201797516 (2017).

154. Dubey, N. *et al.* The ESC/E(Z) complex, an effector of response to ovarian steroids, manifests an intrinsic difference in cells from women with premenstrual dysphoric disorder. *Molecular psychiatry* **22,** 1172–1184; 10.1038/mp.2016.229 (2017).

155. Zahid, H. *et al.* New Design Rules for Developing Potent Cell-Active Inhibitors of the Nucleosome Remodeling Factor (NURF) via BPTF Bromodomain Inhibition. *Journal of medicinal chemistry* **64,** 13902–13917; 10.1021/acs.jmedchem.1c01294 (2021).

156. Low, J. K. K. *et al.* The Nucleosome Remodeling and Deacetylase Complex Has an Asymmetric, Dynamic, and Modular Architecture. *Cell reports* **33,** 108450; 10.1016/j.celrep.2020.108450 (2020).

157. Kundaje, A. *et al.* Integrative analysis of 111 reference human epigenomes. *Nature* **518,** 317–330; 10.1038/nature14248 (2015).

158. Kim, T. W. *et al.* Ctbp2 Modulates NuRD-Mediated Deacetylation of H3K27 and Facilitates PRC2-Mediated H3K27me3 in Active Embryonic Stem Cell Genes During Exit from Pluripotency. *Stem cells (Dayton, Ohio)* **33,** 2442–2455; 10.1002/stem.2046 (2015).

159. Kim, K.-H. *et al.* EGR3 Is a Late Epidermal Differentiation Regulator that Establishes the Skin-Specific Gene Network. *The Journal of investigative dermatology* **139,** 615–625; 10.1016/j.jid.2018.09.019 (2019).

160. Zhang, J. *et al.* ATF3 -activated accelerating effect of LINC00941/lncIAPF on fibroblast-to-myofibroblast differentiation by blocking autophagy depending on ELAVL1/HuR in pulmonary fibrosis. *Autophagy,* 1–20; 10.1080/15548627.2022.2046448 (2022).

161. Wang, C.-G. *et al.* LncRNA KCNQ1OT1 promoted BMP2 expression to regulate osteogenic differentiation by sponging miRNA-214. *Experimental and molecular pathology* **107,** 77–84; 10.1016/j.yexmp.2019.01.012 (2019).

162. Wang, W. *et al.* MicroRNA-129 and -335 Promote Diabetic Wound Healing by Inhibiting Sp1-Mediated MMP-9 Expression. *Diabetes* **67,** 1627–1638; 10.2337/db17-1238 (2018).

163. Graf, J. & Kretz, M. From structure to function: Route to understanding lncRNA mechanism. *BioEssays : news and reviews in molecular, cellular and developmental biology* **42,** e2000027; 10.1002/bies.202000027 (2020).

164. Bowen, N. J., Fujita, N., Kajita, M. & Wade, P. A. Mi-2/NuRD: multiple complexes for many purposes. *Biochimica et biophysica acta* **1677,** 52–57; 10.1016/j.bbaexp.2003.10.010 (2004).

165. Zhang, Y. *et al.* Analysis of the NuRD subunits reveals a histone deacetylase core complex and a connection with DNA methylation. *Genes & development* **13,** 1924–1935; 10.1101/gad.13.15.1924 (1999).

166. Denslow, S. A. & Wade, P. A. The human Mi-2/NuRD complex and gene regulation. *Oncogene* **26,** 5433–5438; 10.1038/sj.onc.1210611 (2007).

167. Dege, C. & Hagman, J. Mi-2/NuRD chromatin remodeling complexes regulate B and T-lymphocyte development and function. *Immunological reviews* **261,** 126–140; 10.1111/imr.12209 (2014).

168. Torchy, M. P., Hamiche, A. & Klaholz, B. P. Structure and function insights into the NuRD chromatin remodeling complex. *Cellular and molecular life sciences : CMLS* **72,** 2491–2507; 10.1007/s00018-015-1880-8 (2015).

169. Kashiwagi, M., Morgan, B. A. & Georgopoulos, K. The chromatin remodeler Mi-2beta is required for establishment of the basal epidermis and normal differentiation of its progeny. *Development (Cambridge, England)* **134,** 1571–1582; 10.1242/dev.001750 (2007).

170. Lu, X. *et al.* Inactivation of NuRD component Mta2 causes abnormal T cell activation and lupus-like autoimmune disease in mice. *The Journal of biological chemistry* **283,** 13825–13833; 10.1074/jbc.M801275200 (2008).

171. Leboeuf, M. *et al.* Hdac1 and Hdac2 act redundantly to control p63 and p53 functions in epidermal progenitor cells. *Developmental cell* **19,** 807–818; 10.1016/j.devcel.2010.10.015 (2010).

172. Miccio, A. *et al.* NuRD mediates activating and repressive functions of GATA-1 and FOG-1 during blood development. *The EMBO journal* **29,** 442–456; 10.1038/emboj.2009.336 (2010).

173. Hu, G. & Wade, P. A. NuRD and pluripotency: a complex balancing act. *Cell stem cell* **10,** 497–503; 10.1016/j.stem.2012.04.011 (2012).

174. Pundhir, S. *et al.* The impact of SWI/SNF and NuRD inactivation on gene expression is tightly coupled with levels of RNA polymerase II occupancy at promoters. *Genome research* **33,** 332–345; 10.1101/gr.277089.122 (2023).

175. Bernstein, B. E. *et al.* A bivalent chromatin structure marks key developmental genes in embryonic stem cells. *Cell* **125,** 315–326; 10.1016/j.cell.2006.02.041 (2006).

176. Kinkley, S. *et al.* reChIP-seq reveals widespread bivalency of H3K4me3 and H3K27me3 in CD4(+) memory T cells. *Nature communications* **7,** 12514; 10.1038/ncomms12514 (2016).

177. Mikkelsen, T. S. *et al.* Genome-wide maps of chromatin state in pluripotent and lineage-committed cells. *Nature* **448,** 553–560; 10.1038/nature06008 (2007).

178. Barrero, M. J. *et al.* Macrohistone variants preserve cell identity by preventing the gain of H3K4me2 during reprogramming to pluripotency. *Cell reports* **3,** 1005–1011; 10.1016/j.celrep.2013.02.029 (2013).

179. Voigt, P., Tee, W.-W. & Reinberg, D. A double take on bivalent promoters. *Genes & development* **27,** 1318–1338; 10.1101/gad.219626.113 (2013).

180. Harikumar, A. & Meshorer, E. Chromatin remodeling and bivalent histone modifications in embryonic stem cells. *EMBO reports* **16,** 1609–1619; 10.15252/embr.201541011 (2015).

181. Kaji, K. *et al.* The NuRD component Mbd3 is required for pluripotency of embryonic stem cells. *Nature cell biology* **8,** 285–292; 10.1038/ncb1372 (2006).

182. Reynolds, N. *et al.* NuRD suppresses pluripotency gene expression to promote transcriptional heterogeneity and lineage commitment. *Cell stem cell* **10,** 583–594; 10.1016/j.stem.2012.02.020 (2012).

183. Oh, I. Y. *et al.* Regulation of the dynamic chromatin architecture of the epidermal differentiation complex is mediated by a c-Jun/AP-1-modulated enhancer. *The Journal of investigative dermatology* **134,** 2371–2380; 10.1038/jid.2014.44 (2014).

184. Ullah, I. *et al.* RNA inhibits dMi-2/CHD4 chromatin binding and nucleosome remodeling. *Cell reports* **39,** 110895; 10.1016/j.celrep.2022.110895 (2022).

185. Zhao, Z., Sentürk, N., Song, C. & Grummt, I. lncRNA PAPAS tethered to the rDNA enhancer recruits hypophosphorylated CHD4/NuRD to repress rRNA synthesis at elevated temperatures. *Genes & development* **32,** 836–848; 10.1101/gad.311688.118 (2018).

186. Piao, M., Sun, L. & Zhang, Q. C. RNA Regulations and Functions Decoded by Transcriptome-wide RNA Structure Probing. *Genomics, Proteomics & Bioinformatics* **15,** 267–278; 10.1016/j.gpb.2017.05.002 (2017).

187. Stevens, C. & La Thangue, N. B. The emerging role of E2F-1 in the DNA damage response and checkpoint control. *DNA Repair* **3,** 1071–1079; 10.1016/j.dnarep.2004.03.034 (2004).

188. Erb, P. *et al.* Role of apoptosis in basal cell and squamous cell carcinoma formation. *Immunology Letters* **100,** 68–72; 10.1016/j.imlet.2005.06.008 (2005).

189. Polager, S., Ofir, M. & Ginsberg, D. E2F1 regulates autophagy and the transcription of autophagy genes. *Oncogene* **27,** 4860–4864; 10.1038/onc.2008.117 (2008).

190. Panagiotis Zalmas, L. *et al.* DNA-damage response control of E2F7 and E2F8. *EMBO reports* **9,** 252–259; 10.1038/sj.embor.7401158 (2008).

191. Hazar-Rethinam, M., Endo-Munoz, L., Gannon, O. & Saunders, N. The role of the E2F transcription factor family in UV-induced apoptosis. *International journal of molecular sciences* **12,** 8947–8960; 10.3390/ijms12128947 (2011).

192. Di Stefano, L., Jensen, M. R. & Helin, K. E2F7, a novel E2F featuring DP-independent repression of a subset of E2F-regulated genes. *The EMBO journal* **22,** 6289–6298; 10.1093/emboj/cdg613 (2003).

193. Adams, M. R., Sears, R., Nuckolls, F., Leone, G. & Nevins, J. R. Complex transcriptional regulatory mechanisms control expression of the E2F3 locus. *Molecular and cellular biology* **20,** 3633–3639; 10.1128/MCB.20.10.3633-3639.2000 (2000).

194. Kent, L. N. & Leone, G. The broken cycle: E2F dysfunction in cancer. *Nature reviews. Cancer* **19,** 326–338; 10.1038/s41568-019-0143-7 (2019).

195. Iaquinta, P. J. & Lees, J. A. Life and death decisions by the E2F transcription factors. *Current Opinion in Cell Biology* **19,** 649–657; 10.1016/j.ceb.2007.10.006 (2007).

196. Logan, N. *et al.* E2F-8: an E2F family member with a similar organization of DNA-binding domains to E2F-7. *Oncogene* **24,** 5000–5004; 10.1038/sj.onc.1208703 (2005).

197. DeGregori, J. & Johnson, D. G. Distinct and Overlapping Roles for E2F Family Members in Transcription, Proliferation and Apoptosis. *Current molecular medicine* **6,** 739–748; 10.2174/1566524010606070739 (2006).

198. Leseva, M., Santostefano, K. E., Rosenbluth, A. L., Hamazaki, T. & Terada, N. E2f6-mediated repression of the meiotic Stag3 and Smc1β genes during early embryonic development requires Ezh2 and not the de novo methyltransferase Dnmt3b. *Epigenetics* **8,** 873–884; 10.4161/epi.25522 (2013).

199. Prezioso, C. & Orlando, V. Polycomb proteins in mammalian cell differentiation and plasticity. *FEBS letters* **585,** 2067–2077; 10.1016/j.febslet.2011.04.062 (2011).

200. Di Croce, L. & Helin, K. Transcriptional regulation by Polycomb group proteins. *Nature structural & molecular biology* **20,** 1147–1155; 10.1038/nsmb.2669 (2013).

201. Margueron, R. *et al.* Ezh1 and Ezh2 maintain repressive chromatin through different mechanisms. *Molecular cell* **32,** 503–518; 10.1016/j.molcel.2008.11.004 (2008).

202. Shen, X. *et al.* EZH1 mediates methylation on histone H3 lysine 27 and complements EZH2 in maintaining stem cell identity and executing pluripotency. *Molecular cell* **32,** 491–502; 10.1016/j.molcel.2008.10.016 (2008).

203. Wang, H. *et al.* Role of histone H2A ubiquitination in Polycomb silencing. *Nature* **431,** 873–878; 10.1038/nature02985 (2004).

204. Cao, R., Tsukada, Y.-I. & Zhang, Y. Role of Bmi-1 and Ring1A in H2A ubiquitylation and Hox gene silencing. *Molecular cell* **20,** 845–854; 10.1016/j.molcel.2005.12.002 (2005).

205. Bantignies, F. & Cavalli, G. Polycomb group proteins: repression in 3D. *Trends in Genetics* **27,** 454–464; 10.1016/j.tig.2011.06.008 (2011).

206. Kanhere, A. *et al.* Short RNAs are transcribed from repressed polycomb target genes and interact with polycomb repressive complex-2. *Molecular cell* **38,** 675–688; 10.1016/j.molcel.2010.03.019 (2010).

207. Brookes, E. *et al.* Polycomb associates genome-wide with a specific RNA polymerase II variant, and regulates metabolic genes in ESCs. *Cell stem cell* **10,** 157–170; 10.1016/j.stem.2011.12.017 (2012).

208. Gao, Z. *et al.* PCGF homologs, CBX proteins, and RYBP define functionally distinct PRC1 family complexes. *Molecular cell* **45,** 344–356; 10.1016/j.molcel.2012.01.002 (2012).

209. Tavares, L. *et al.* RYBP-PRC1 complexes mediate H2A ubiquitylation at polycomb target sites independently of PRC2 and H3K27me3. *Cell* **148,** 664–678; 10.1016/j.cell.2011.12.029 (2012).

210. Morey, L., Aloia, L., Cozzuto, L., Benitah, S. A. & Di Croce, L. RYBP and Cbx7 define specific biological functions of polycomb complexes in mouse embryonic stem cells. *Cell reports* **3,** 60–69; 10.1016/j.celrep.2012.11.026 (2013).

211. Farcas, A. M. *et al.* KDM2B links the Polycomb Repressive Complex 1 (PRC1) to recognition of CpG islands. *eLife* **1,** e00205; 10.7554/eLife.00205 (2012).

212. Wu, X., Johansen, J. V. & Helin, K. Fbxl10/Kdm2b recruits polycomb repressive complex 1 to CpG islands and regulates H2A ubiquitylation. *Molecular cell* **49,** 1134–1146; 10.1016/j.molcel.2013.01.016 (2013).

213. Blackledge, N. P. *et al.* PRC1 Catalytic Activity Is Central to Polycomb System Function. *Molecular cell* **77,** 857-874.e9; 10.1016/j.molcel.2019.12.001 (2020).

214. Tolhuis, B. *et al.* Genome-wide profiling of PRC1 and PRC2 Polycomb chromatin binding in Drosophila melanogaster. *Nature genetics* **38,** 694–699; 10.1038/ng1792 (2006).

215. Tanay, A., O'Donnell, A. H., Damelin, M. & Bestor, T. H. Hyperconserved CpG domains underlie Polycomb-binding sites. *Proceedings of the National Academy of Sciences of the United States of America* **104,** 5521–5526; 10.1073/pnas.0609746104 (2007).

216. Kim, H., Kang, K. & Kim, J. AEBP2 as a potential targeting protein for Polycomb Repression Complex PRC2. *Nucleic acids research* **37,** 2940–2950; 10.1093/nar/gkp149 (2009).

217. Landeira, D. *et al.* Jarid2 is a PRC2 component in embryonic stem cells required for multi-lineage differentiation and recruitment of PRC1 and RNA Polymerase II to developmental regulators. *Nature cell biology* **12,** 618–624; 10.1038/ncb2065 (2010).

218. Zhao, J., Sun, B. K., Erwin, J. A., Song, J.-J. & Lee, J. T. Polycomb proteins targeted by a short repeat RNA to the mouse X chromosome. *Science (New York, N.Y.)* **322,** 750–756; 10.1126/science.1163045 (2008).

219. Herranz, N. *et al.* Polycomb complex 2 is required for E-cadherin repression by the Snail1 transcription factor. *Molecular and cellular biology* **28,** 4772–4781; 10.1128/MCB.00323-08 (2008).

220. Dietrich, N. *et al.* REST-mediated recruitment of polycomb repressor complexes in mammalian cells. *PLoS genetics* **8,** e1002494; 10.1371/journal.pgen.1002494 (2012).

221. Morey, L. *et al.* MBD3, a component of the NuRD complex, facilitates chromatin alteration and deposition of epigenetic marks. *Molecular and cellular biology* **28,** 5912–5923; 10.1128/MCB.00467-08 (2008).

222. Reynolds, N. *et al.* NuRD-mediated deacetylation of H3K27 facilitates recruitment of Polycomb Repressive Complex 2 to direct gene repression. *The EMBO journal* **31,** 593–605; 10.1038/emboj.2011.431 (2012).

223. Ogawa, H., Ishiguro, K.-I., Gaubatz, S., Livingston, D. M. & Nakatani, Y. A complex with chromatin modifiers that occupies E2F- and Myc-responsive genes in G0 cells. *Science (New York, N.Y.)* **296,** 1132–1136; 10.1126/science.1069861 (2002).

224. Attwooll, C., Lazzerini Denchi, E. & Helin, K. The E2F family: specific functions and overlapping interests. *The EMBO journal* **23,** 4709–4716; 10.1038/sj.emboj.7600481 (2004).

225. Shirahama, Y. & Yamamoto, K. The E2F6 Transcription Factor is Associated with the Mammalian SUZ12-Containing Polycomb Complex. *The Kurume medical journal*; 10.2739/kurumemedj.MS674006 (2022).

226. Dahlet, T. *et al.* E2F6 initiates stable epigenetic silencing of germline genes during embryonic development. *Nature communications* **12,** 3582; 10.1038/s41467-021-23596-w (2021).

227. Mohn, F. *et al.* Lineage-specific polycomb targets and de novo DNA methylation define restriction and potential of neuronal progenitors. *Molecular cell* **30,** 755–766; 10.1016/j.molcel.2008.05.007 (2008).

228. Caretti, G., Di Padova, M., Micales, B., Lyons, G. E. & Sartorelli, V. The Polycomb Ezh2 methyltransferase regulates muscle gene expression and skeletal muscle differentiation. *Genes & development* **18,** 2627–2638; 10.1101/gad.1241904 (2004).

229. Lee, K. *et al.* Expression of Bmi-1 in epidermis enhances cell survival by altering cell cycle regulatory protein expression and inhibiting apoptosis. *The Journal of investigative dermatology* **128,** 9–17; 10.1038/sj.jid.5700949 (2008).

230. Ezhkova, E. *et al.* Ezh2 orchestrates gene expression for the stepwise differentiation of tissue-specific stem cells. *Cell* **136,** 1122–1135; 10.1016/j.cell.2008.12.043 (2009).

231. Sen, G. L., Webster, D. E., Barragan, D. I., Chang, H. Y. & Khavari, P. A. Control of differentiation in a self-renewing mammalian tissue by the histone demethylase JMJD3. *Genes & development* **22,** 1865–1870; 10.1101/gad.1673508 (2008).

232. Mejetta, S. *et al.* Jarid2 regulates mouse epidermal stem cell activation and differentiation. *The EMBO journal* **30,** 3635–3646; 10.1038/emboj.2011.265 (2011).

233. Luis, N. M. *et al.* Regulation of human epidermal stem cell proliferation and senescence requires polycomb- dependent and -independent functions of Cbx4. *Cell stem cell* **9,** 233–246; 10.1016/j.stem.2011.07.013 (2011).

234. Carbon, S. & Mungall, C. *Gene Ontology Data Archive* (2023), https://geneontology.org/

235. Andrews, S. *FastQC: a quality control tool for high throughput sequence data* (2010), https://www.bioinformatics.babraham.ac.uk/projects/fastqc/

236. Li, H. *et al.* The Sequence Alignment/Map format and SAMtools. *Bioinformatics (Oxford, England)* **25,** 2078–2079; 10.1093/bioinformatics/btp352 (2009).

237. Quinlan, A. R. & Hall, I. M. BEDTools: a flexible suite of utilities for comparing genomic features. *Bioinformatics (Oxford, England)* **26,** 841–842; 10.1093/bioinformatics/btq033 (2010).

238. Zhang, Z., Ma, X. & Zhang, M. Q. Bivalent-Like Chromatin Markers Are Predictive for Transcription Start Site Distribution in Human. *PloS one* **7,** e38112; 10.1371/journal.pone.0038112 (2012).

239. Liao, Y., Smyth, G. K. & Shi, W. featureCounts: an efficient general purpose program for assigning sequence reads to genomic features. *Bioinformatics (Oxford, England)* **30,** 923–930; 10.1093/bioinformatics/btt656 (2014).

240. Love, M. I., Huber, W. & Anders, S. Moderated estimation of fold change and dispersion for RNA-seq data with DESeq2. *Genome biology* **15,** 550; 10.1186/s13059-014-0550-8 (2014).

241. Di Tommaso, P. *et al.* Nextflow enables reproducible computational workflows. *Nature biotechnology* **35,** 316–319; 10.1038/nbt.3820 (2017).

242. Dobin, A. *et al.* STAR: ultrafast universal RNA-seq aligner. *Bioinformatics (Oxford, England)* **29,** 15–21; 10.1093/bioinformatics/bts635 (2013).

243. García-Alcalde, F. *et al.* Qualimap: evaluating next-generation sequencing alignment data. *Bioinformatics (Oxford, England)* **28,** 2678–2679; 10.1093/bioinformatics/bts503 (2012).

244. Broad Institute. *Picard toolkit* (2019), https://Broadinstitute.Github.Io/Picard/

245. Sayols, S., Scherzinger, D. & Klein, H. dupRadar: a Bioconductor package for the assessment of PCR artifacts in RNA-Seq data. *BMC bioinformatics* **17,** 428; 10.1186/s12859-016-1276-2 (2016).

246. Zhu, A., Ibrahim, J. G. & Love, M. I. Heavy-tailed prior distributions for sequence count data: removing the noise and preserving large differences. *Bioinformatics (Oxford, England)* **35,** 2084–2092; 10.1093/bioinformatics/bty895 (2019).

247. Ramírez, F. *et al.* deepTools2: a next generation web server for deep-sequencing data analysis. *Nucleic acids research* **44,** W160-5; 10.1093/nar/gkw257 (2016).

248. Hahne, F. & Ivanek, R. Visualizing Genomic Data Using Gviz and Bioconductor. *Methods in molecular biology (Clifton, N.J.)* **1418,** 335–351; 10.1007/978-1-4939-3578-9_16 (2016).

249. Yu, G., Wang, L.-G. & He, Q.-Y. ChIPseeker: an R/Bioconductor package for ChIP peak annotation, comparison and visualization. *Bioinformatics (Oxford, England)* **31,** 2382–2383; 10.1093/bioinformatics/btv145 (2015).

250. Wu, T. *et al.* clusterProfiler 4.0: A universal enrichment tool for interpreting omics data. *Innovation (Cambridge (Mass.))* **2,** 100141; 10.1016/j.xinn.2021.100141 (2021).

251. Encode Project consortium. An integrated encyclopedia of DNA elements in the human genome. *Nature* **489,** 57–74; 10.1038/nature11247 (2012).

252. Luo, Y. *et al.* New developments on the Encyclopedia of DNA Elements (ENCODE) data portal. *Nucleic acids research* **48,** D882-D889; 10.1093/nar/gkz1062 (2020).

253. Livak, K. J. & Schmittgen, T. D. Analysis of relative gene expression data using real-time quantitative PCR and the 2(-Delta C(T)) Method. *Methods (San Diego, Calif.)* **25,** 402–408; 10.1006/meth.2001.1262 (2001).

10 Acknowledgements

This thesis would never have come true without the help and support of so many people who have accompanied me on my way.

To begin with, I want to thank my supervisor Prof. Dr. Markus Kretz for the trust and the opportunity to do my PhD project in his laboratory. I really appreciate his tireless support, his optimism, and his enthusiasm throughout this project and beyond.

Many thanks to all members of the Kretz lab. Thank you, Fabi, for three years of complaining and feeling sad together but then moving on together. Thanks to Caro for her calming charisma on the one hand, and for the great passionate discussions on the other hand. Your open ear is worth its weight in gold. Additionally, I want to thank Danni for assisting in every situation and finding solutions to every problem inside and outside the lab. Many thanks also to Sonja and to Bianca for every advice you gave me when needed.

A big thank you also goes to Uwe Schwartz for data analysis and to Julia Wittur for critically reading this thesis.

Thanks to all members of the Biochemistry I institute, for your endless help and for creating a great working atmosphere. I am especially grateful for every member of the 11 a.m. lunch group meeting at 12:15 a.m., for many hours of entertaining discussions and cheerful breaks. I also appreciate Prof. Dr. Gunter Meisters support, especially at the end of my PhD project.

I would also like to thank my family from the bottom of my heart for their unconditional love throughout this journey. Thank you, mom, for listening, thank you dad for asking and thanks to my brother for simply doing nothing.

In this regard, I would also like to express my gratitude to Mrs. Barbara Hofmann for the best advice ever given to me.

Finally, I have to thank Steffen. I have probably not said it often enough during the last years, but thank you for being always there for me, thanks for caring and thanks for slowing me down when I needed a break. Your patience with me seems to have no limits.